

Investigations of Pyrrole-Imidazole Polyamide Effects on DNA Replication

Thesis by

Thomas Farid Martínez

In Partial Fulfillment of the Requirements

for the degree of

Doctor of Philosophy



CALIFORNIA INSTITUTE OF TECHNOLOGY

Pasadena, California

2016

(Defended June 18, 2015)

for Cesar.

Acknowledgments

The program that defines the parameters of our physical nature, our biology, is acquired from reproduction; our humanity, however, is born from the information we extract from our world. Based on the information we are given from the experience of countless lives before us and from sensory observations, and what we choose to believe, we learn how best to operate in our world. This information propagates and evolves through our interactions, both direct and indirect, with others. Thus, in expressing our unique humanity we are all models, whether we intend to be or not. Given the critical role of information in shaping our humanity, it is apparent that teaching and mentorship, which provide curated information, are extremely powerful means for shaping our world. Some individuals teach purposefully, and amongst those who have this intention some are better than others.

That some individuals are better teachers than others is not an indictment of any person. It is tantamount to a tautology. I make this point to express my incredulousness at my good fortune of having so many excellent mentors show up throughout my life at critical times. Though their individual styles were each unique and varied significantly, most of my mentors have been encouraging. They challenged and allowed me to continue asking for bigger mountains to climb, despite my penchant for biting off more than I could chew. It seems to me that in almost every case I can recall that my mentor chose to help me specifically, or at least more so than other pupils. Perhaps this interpretation is simply a reflection of their skill as teachers, making each student feel special, or my vanity. In any case, they did more than just offer guidance. They pinned their hopes and

expectations on me. I could feel this. I could sense their recognition of an opportunity in me, though I often had no idea what the opportunity was. I think that they believed at some level that training me would allow them to shape the world in ways they could not with their own hands. The interesting thing, though, is that it was not the guidance or training that usually impacted me the most, but the belief in myself born from their faith in me. This, too, is the power of teaching.

Not all of my mentors have resonated with me so strongly, though. Some mentors created such a strong dissonance with my own values that I found it impossible to ignore. I am grateful to them as well—just as grateful as I am to the mentors whom I understood immediately. Both positive and negative experiences contribute to self-discovery and development of one's value system. Therefore, the mentors whom I could not understand or agree with still played significant roles in my journey to become a person that I could respect. It is also true that some of the mentors whose teachings felt so alien to me I eventually learned to understand long after I had left their tutelage. These experiences have often stayed with me the most.

If I have had any success up to this point in my life, it is because of my mentors and the people I choose to keep close to my heart. My humanity is a reflection of their humanity, and theirs of mine.

Thomas F. Martínez
June 2015
Pasadena, CA

Abstract

Pyrrrole–Imidazole polyamides are programmable, cell-permeable small molecules that bind in the minor groove of double-stranded DNA sequence-specifically. Polyamide binding has been shown to alter the local helical structure of DNA, disrupt protein-DNA interactions, and modulate endogenous gene expression. Py–Im polyamides targeted to the androgen receptor-DNA interface have been observed to decrease expression of androgen-regulated genes, upregulate p53, and induce apoptosis in a hormone-sensitive prostate cancer cell line. Here we report that androgen response element (ARE)-targeted polyamides induced DNA replication stress in a hormone-insensitive prostate cancer cell line. The ATR checkpoint kinase was activated in response to this stress, causing phosphorylation of MCM2, and FANCD2 was monoubiquitinated. Surprisingly, little single-stranded DNA was exhibited, and the ATR targets RPA2 and Chk1 were not phosphorylated. We conclude that polyamide induces relatively low level replication stress, and suggest inhibition of the replicative helicase as a putative mechanism based on *in vitro* assays. We also demonstrate polyamide-induced inhibition of DNA replication in cell free extracts from *X. laevis* oocytes. In this system, inhibition of chromatin decondensation is observed, preventing DNA replication initiation. Finally, we show that Py-Im polyamides targeted to the ARE and ETS binding sequence downregulate AR- and ERG-driven signaling in a prostate cancer cell line harboring the TMPRSS2-ERG fusion. In a mouse xenograft model, ARE-targeted polyamide treatment reduced growth of the tumor.

Table of Contents

	Page
Acknowledgments.	iv
Abstract.	vi
Table of Contents	vii
List of Figures and Tables.	x
Chapter 1: Introduction	
1.1 Deoxyribonucleic acid	2
1.2 Molecular recognition of DNA in nature	4
1.3 Pyrrole-imidazole polyamides	7
1.4 Biological activity of pyrrole-imidazole polyamides	11
1.5 Small molecule inhibitors of DNA replication.	14
1.6 Scope of this work	16
1.7 References.	18
Chapter 2: Replication Stress by Py–Im Polyamides Induces a Non-canonical ATR- dependent Checkpoint Response	
Abstract	25
2.1 Introduction.	26
2.2. Results.	28
2.3 Discussion.	47
2.4 Materials and Methods	53
2.5 Acknowledgments.	65
2.6 References.	66

Chapter 3: Py-Im Polyamides Inhibit DNA Replication in Cell-Free Extracts

from *X. laevis* Oocytes

Abstract	73
3.1 Introduction	74
3.2 Results	76
3.3 Discussion	85
3.4 Materials and Methods	88
3.5 Acknowledgments	90
3.6 References	91

Chapter 4: DNA-binding Py-Im Polyamides Targeted to the AR-ERG Signaling Axis

in VCaP Prostate Cancer Cells

Abstract	94
4.1 Introduction	95
4.2 Results	97
4.3 Discussion	108
4.4 Materials and Methods	113
4.5 Acknowledgments	120
4.6 References	121

Appendix A: Investigations of anti-BrdU Antibody Staining of Py-Im Polyamide

Treated Cells

A.1 Background	126
A.2 Results	127

A.3 Conclusions.	143
A.4 Acknowledgments.	144
A.5 References.	145

List of Figures and Tables

	Page
Chapter 1	
Figure 1.1 Structure of DNA and hydrogen bonding patterns of Watson-Crick base pairs	2
Figure 1.2 Structures of transcription factor:DNA complexes	4
Figure 1.3 Chemical structures of DNA-binding small molecule natural products	5
Figure 1.4 Structures of distamycin A bound to DNA	7
Figure 1.5 Molecular recognition of DNA by Py-Im polyamides	9
Figure 1.6 Py-Im polyamide binding alters the structure of DNA	10
Figure 1.7 Examples of polyamide biological activities in tissue culture and animal studies	12
Table 1.1 Structures and putative mechanisms of a library of small molecule DNA replication inhibitors	16
Chapter 2	
Figure 2.1 Polyamides cause accumulation of S-phase cells and PCNA foci	29
Table 2.1 Summary of cytotoxicity IC ₅₀ values of polyamides 1 and 2 prostate cancer cell lines	30
Figure 2.2 Polyamides induce apoptosis in DU145 cells	31
Figure 2.3 Polyamides induce ATR activation without extensive ssDNA formation	33

Figure 2.4	Effects of small molecule PI3-kinase inhibitors on polyamide-induced S-phase accumulation	35
Figure 2.5	High concentration polyamide treatment does not does not inhibit aphidicolin-induced Chk1 phosphorylation.	37
Figure 2.6	Polyamides do not induce phosphorylation of Chk1, RPA2, or Chk2 or observable DNA breaks.	38
Figure 2.7	Polyamides induce phosphorylation of MCM2 and FANCD2 monoubiquitination	40
Figure 2.8	Effects of ATM- and ATR-specific small molecule inhibitors on polyamide-induced MCM2 S108 phosphorylation and FANCD2 monoubiquitination	42
Figure 2.9	FANCD2 increases cell survival after exposure to polyamide 1	43
Figure 2.10	Knockdown of FANCD2 by siRNA does not prevent the accumulation of DU145 cells in S-phase in response to polyamide treatment	44
Figure 2.11	Py-Im Polyamides stabilize duplex DNA regardless of match site position in the duplex.	45
Figure 2.12	Polyamide 1 inhibits T7 gp4A helicase activity	46
Figure 2.13	Polyamide 1 inhibits helicase activity of <i>S. cerevisiae</i> Dna2 nuclease dead but helicase active mutant (yDna2-K677R)	48
Figure 2.14	Putative model of Py-Im polyamide-induced replication stress and subsequent ATR-dependent checkpoint response	50
Figure 2.15	Dose-dependent increase in hydroxyurea (HU)-induced Chk1 S345 phosphorylation	52

Chapter 3

Figure 3.1	Polyamide 1 inhibits DNA replication in <i>Xenopus</i> oocyte extracts. . . .	77
Figure 3.2	Py-Im Polyamides targeted to different DNA sequences equally inhibit DNA replication in <i>Xenopus</i> oocyte extracts.	79
Figure 3.3	Polyamide 1 does not inhibit loading of pre-RC factors or activate ATR checkpoint signaling	80
Figure 3.4	Polyamide 1 inhibits decondensation of sperm chromatin	82
Figure 3.5	Polyamide 1 inhibits DNA replication when dosed after DNA decondensation step	84
Figure 3.6	Methods of synchronizing mammalian cells at different stages of the cell cycle	88

Chapter 4

Figure 4.1	Diagrams of targeting AR- and ERG-DNA interfaces by Py-Im polyamides.	96
Table 4.1	Analysis of DNA thermal stabilization by binding of Py-Im polyamides	97
Figure 4.2	Representative expression data for VCaP cells treated with AR1 and AR2 followed by DHT-induction	98
Table 4.2	Gene expression data for VCaP cells treated with AR1 and AR2 followed by induction with DHT.	99
Figure 4.3	Representative expression data for VCaP cells treated with ETS1-3 .	100
Table 4.3	Gene expression data for VCaP cells treated with ETS-targeting and AR-targeting polyamides	101

Figure 4.4	AR1 and AR2 are cytotoxic in VCaP cells	102
Figure 4.5	Nuclear uptake of FITC-analog polyamides in VCaP cells after 24 h	103
Figure 4.6	Nuclear uptake of FITC-analog polyamides in VCaP cells after 48 h	104
Figure 4.7	Analysis of DNA damage by neutral comet assay.	105
Figure 4.8	Py-Im polyamides mediate ERG-driven expression in PC3-ERG cells and reduce extant DNA damage	106
Figure 4.9	Gene expression data for PC3-ERG cells treated with ETS-targeting and AR-targeting polyamides	107
Figure 4.10	AR2 inhibits HUVEC tube formation <i>in vitro</i>	108
Figure 4.11	AR1 but not ETS3 reduces the growth of VCaP tumors in SCID mice	109
Figure 4.12	Chemical structures of Py-Im polyamides studied	114
Figure 4.13	Primer sequences for qPCR analysis	117
Appendix A		
Figure A.1	Ball-and-stick representations of Py-Im polyamides used in this study	127
Figure A.2	MoBU-1 immunocytochemistry shows punctate staining in DU145 cells treated with BrdU followed by polyamide 1	128
Figure A.3	MoBU-1 stains polyamide 1 treated DU145 cells in the absence of BrdU	130
Figure A.4	MoBU-1 stains polyamide 1 treated DU145 cells when fixed with	

MeOH:AcOH or 2% formaldehyde	132
Figure A.5 MoBU-1 staining in response to a small library of polyamides	134
Figure A.6 Z-stack of MoBU-1 stained DU145 cells treated with polyamide 1 or 5	135
Figure A.7 Staining of polyamide treated cells is dependent upon MoBU-1	136
Figure A.8 MoBU-1 staining in DU145 cells treated with Py-Im polyamides after fixation with formaldehyde	138
Figure A.9 Anti-BrdU antibody ZBU30 but not ICR1 stains polyamide- treated DU145 cells	139
Figure A.10 Electrophoretic mobility shift assay (EMSA) of MoBU-1 and polyamide 1 :DNA	141

Chapter 1

Introduction

1.1 Deoxyribonucleic acid

In 1944, Oswald Avery, Colin MacLeod, and Maclyn McCarty discovered that deoxyribonucleic acid (DNA) is the chemical that makes up genes, the molecular unit of heredity (1). Then in 1953, the structure of DNA was solved, revealing it to be a double-stranded, anti-parallel, right-handed, double-helical polymer (Figure 1.1A) (2,3). Each DNA strand is composed of four monomers called nucleotides: deoxyadenosine (A), deoxythymidine (T), deoxycytidine (C), and deoxyguanosine (G), which are connected to one another by phosphodiester bonds with the deoxyribose sugar (Figure 1.1B). The two

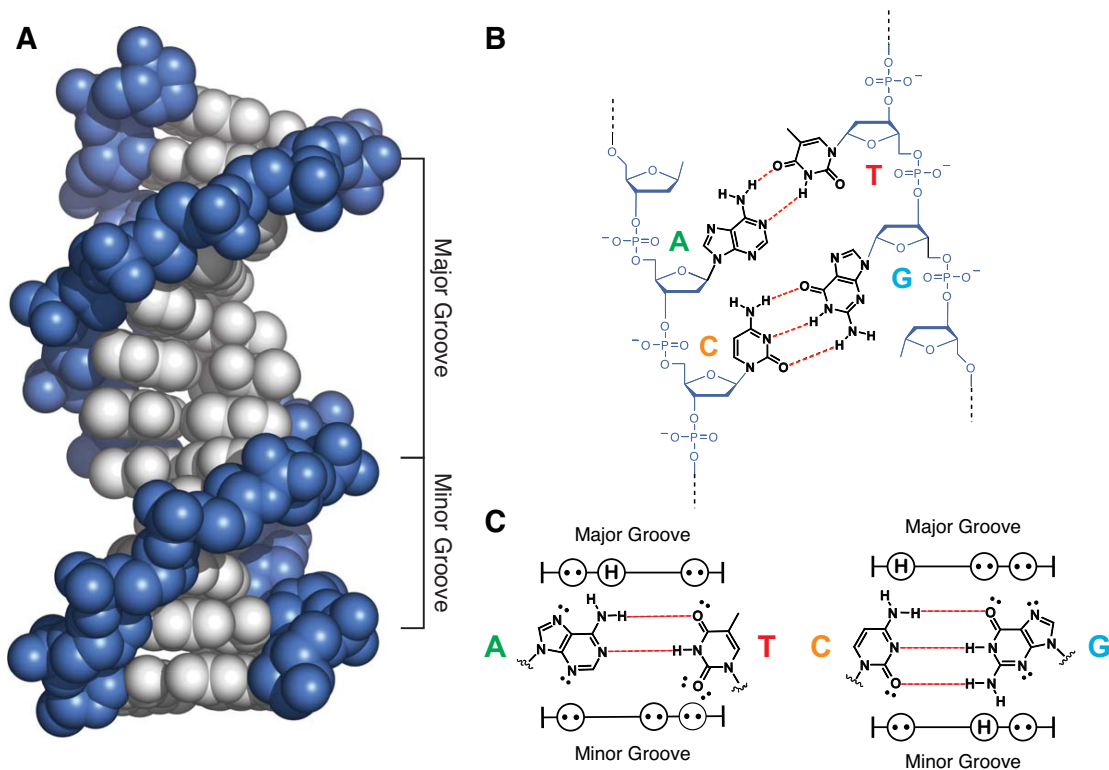


Figure 1.1 Structure of DNA and hydrogen bonding patterns of Watson-Crick base pairs. (A) Structure of B-form DNA (PDB 1BNA) (4). (B) Chemical structures duplex DNA showing all four bases. Adenine (A) is bonded to thymine (T) and cytosine (C) is bonded to guanine (G). Dashed lines indicate hydrogen bonds. (C) Major and minor groove hydrogen bonding patterns of the four Watson-Crick base pairs. Circles with dots represent lone pairs (hydrogen bond acceptor), and circles with an H represent hydrogen atoms from an exocyclic amine (hydrogen bond donor).

strands are held together by hydrogen bonds formed between the nitrogenous bases, which lie perpendicular to the helical axis. The structure of DNA also demonstrated the pairing rules between the bases of the two strands, namely A pairs with T and C pairs with G. These rules result in four possible base pairs, called Watson-Crick base pairs. Two hydrogen bonds can be formed between A and T, while three can form between C and G. The structure of DNA shown in Figure 1.1A is of B-form DNA which is believed to be the predominant form in cells. In this form of DNA, the asymmetric spacing of the strands caused by the nitrogenous bases creates major and minor grooves. The pattern of hydrogen bond donors and acceptors on the exocyclic portions of the bases allows for molecular recognition of all four base pairs in the two different grooves (Figure 1.1C), which is critical for all DNA functions.

DNA is vital to all life on Earth, and since the early discoveries of the 1940s and 1950s much effort has been put toward characterizing all of its functions. The central function of DNA was believed to be storing and coding the information for transcription of messenger RNA (mRNA) from genes that are then translated into the proteins needed for cellular processes. This is the so-called central dogma of molecular biology. Therefore, if one knew all of the genes within an organism's genome one could produce a list of all of the important factors. A milestone in this endeavor was the sequencing of the human genome in 2001 (5). Current estimates suggest that there are about 19,000 protein-coding genes encoded in the ~3 billion base pair human genome (6). Though, this number seems low relative to other less complex organisms, there is added information due to alternative splicing of exons. DNA also encodes for ~15,000 long non-coding RNAs,

which are believed to have regulatory functions (7). In addition, short peptides called short open reading frame encoded polypeptides (SEPs) are being discovered in higher order eukaryotes that are expressed from RNA transcripts previously thought to be non-coding (8). Clearly, after more than 70 years we still have much to learn about DNA. Continuing to learn about DNA's chemical properties and biological functions has been critical to understanding life and the origin of disease, as many diseases can be traced to aberrations in the genome. With enough knowledge, one may be able to develop chemical tools to combat a variety of diseases through targeting of the DNA.

1.2 Molecular recognition of DNA in nature

Transcription of DNA into RNA is one of the most critical processes in the cell. Transcription factors (TFs) are proteins that reversibly bind to DNA and regulate transcription by participating in the recruitment or blocking of RNA polymerase. TFs bind to specific sequences of DNA non-covalently through interactions with the nitrogenous bases in the minor groove, the major groove, or a combination of both.

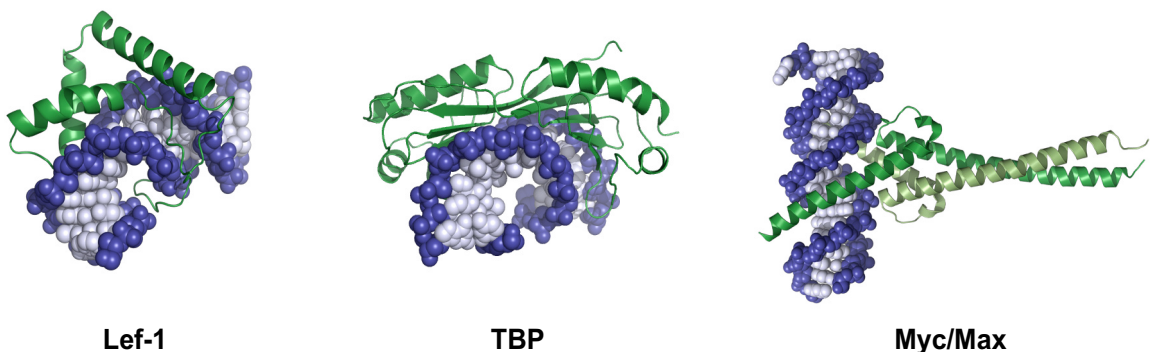


Figure 1.2 Structures of transcription factor:DNA complexes. Lef-1 (PDB 2LEF) (12), TBP (PDB 1TGH) (13), Myc/Max (PDB 1NKP) (14).

Through interactions with DNA as well as interactions with other proteins either directly or allosterically through DNA, TFs are able to achieve high binding affinities to DNA (9-11). TFs have a variety DNA-binding domain motifs, representing different strategies nature has evolved for molecular recognition of DNA. Such examples include the minor groove-binding high mobility group domain found in Lef-1, the minor groove-binding TATA binding protein, and the major groove-binding basic helix-loop-helix leucine zipper domain found in the Myc/MAX heterodimer (Figure 1.2) (12-14). In addition to their critical role in transcription, TFs offer insight into how sequence-selective recognition of DNA can be achieved by artificially engineered factors or synthetic molecules.

Another class of biomolecules that can reversibly bind to specific sequences of DNA is small molecule natural products. Like TFs, these small molecules are also able to

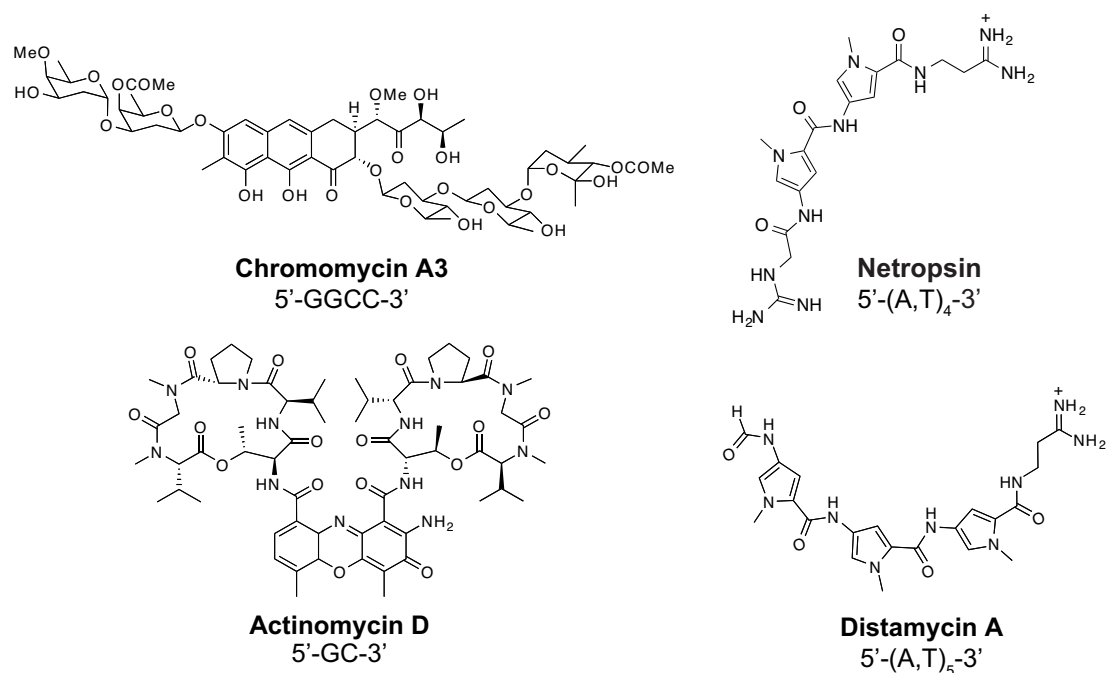


Figure 1.3 Chemical structures of DNA-binding small molecule natural products.

bind to DNA by various modes including intercalation, minor groove binding, major groove binding, and combinations thereof (15). Examples of DNA-binding natural products include the intercalator actinomycin D, and the minor groove binders chromomycin A3, netropsin, and distamycin A (Figure 1.3). Actinomycin D selects for 5'-GC-3' sequences, while chromomycin selects for 5'-GGCC-3'. Both netropsin and distamycin bind specifically to A/T tracts.

DNA-binding natural products are often antibiotics synthesized by microorganisms in order to kill or inhibit the growth of competing organisms of a different species, and some have also been effective as anticancer agents (15,16). These DNA-binding molecules often inhibit critical DNA-dependent processes such as transcription and DNA replication. For example, actinomycin has been shown to inhibit both transcription and replication (17,18). Distamycin A has been shown to disrupt a variety of DNA-dependent processes as well through inhibition of RNA polymerase, DNA polymerase, topoisomerases I and II, and helicases (19-21).

DNA binding by distamycin is a particularly interesting example of molecular recognition, as the crescent-shaped molecule can bind the DNA minor groove in either a 1:1 or 2:1 stoichiometry (Figure 1.4). In the 2:1 complex, two molecules of distamycin are stacked in an anti-parallel fashion such that the N-methylpyrrole units are across from each other, which results in significant widening of the minor groove compared to the 1:1 complex (22-24). In both 1:1 and 2:1 configurations, distamycin binds preferentially to A•T base pairs; however, it was suggested that replacement of N-methylpyrrole with N-

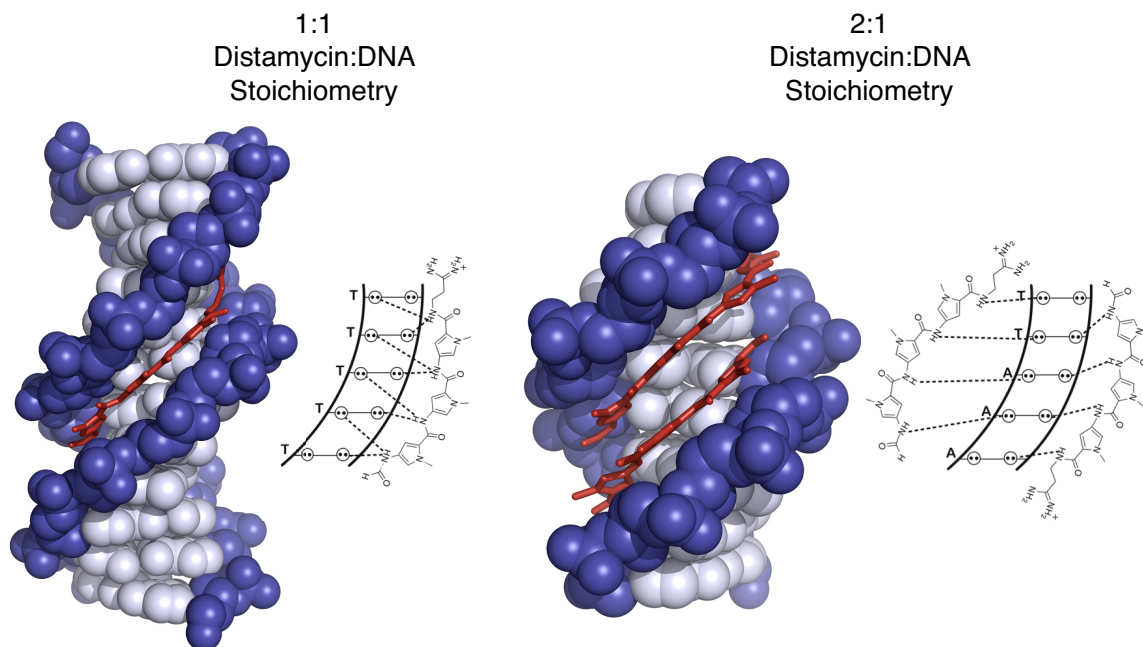


Figure 1.4 Structures of distamycin A bound to DNA. (A) Structure of 1:1 complex of distamycin with DNA (PDB 2DND) and a schematic of distamycin binding to the minor groove in the 1:1 mode. (B) 2:1 antiparallel complex of distamycin with DNA (PDB 378D) and a schematic of distamycin binding to the minor groove in the 2:1 mode.

methylimidazole would allow for recognition of G•C base pairs in the floor of the minor groove (25). Drawing inspiration from nature to synthesize small molecules capable of sequence-specific recognition of DNA could provide an effective means of combating disease states through the modulation of transcription.

1.3 Pyrrole-Imidazole polyamides

The initial observation of the 2:1 distamycin binding configuration to DNA led to the development of a new class of synthetic small molecules called pyrrole-imidazole (Py-Im) polyamides that are capable of recognizing all four Watson-Crick base pairs and bind to DNA with affinities comparable to DNA-binding proteins (26,27). Recognition of all four base pairs was achieved by modifying distamycin to incorporate N-

methylimidazole and 3-hydroxy-1-methylpyrrole (Hp) heterocycles. The side-by-side pairing of these monomers in the minor groove governs which base is preferentially recognized (Figure 1.5). An Im/Py pair preferentially recognizes a G•C base pair over C•G, A•T, and T•A, while Py/Im recognizes C•G. This preference exists due to the relief of the steric hindrance between the hydrogen at the C3 position of pyrrole and the guanine exocyclic amine provided by the substitution of imidazole. Hp/Py preferentially recognizes a T•A base pair over A•T, C•G, and G•C, while Py/Hp recognizes A•T. Specificity for T•A over A•T is likely due to steric accommodation of the exocyclic hydroxyl group on Hp. Another heterocycle that has been used to distinguish T•A over A•T is 3-chlorothiophene when paired across a Py (28). As with the 2:1 distamycin configuration, Py/Py pairs recognize A•T and T•A base pairs over G•C and C•G.

Many other modifications to the distamycin framework have also been made to improve properties such as affinity, specificity, solubility, and cellular/nuclear uptake. In the current generation of Py-Im polyamides, γ -diaminobutyric acid (γ -DABA) is used to link two chains of polyamides to help orient the molecule in a hairpin configuration when bound to DNA (Figure 1.5). This hairpin configuration mimics the 2:1 anti-parallel distamycin stacking and increases affinity to DNA significantly, in part due to reduced entropic penalty (29). In addition, linking two polyamide chains allows for two different sequences of Py and Im to be arranged on the top and bottom strands, as opposed to having the same strand stack against itself in a 2:1 fashion. The chiral alpha amine on γ -DABA also increases affinity to DNA and shows preferential binding to A•T and T•A base pairs (30). Polyamide chains have also been linked by (*R*)-3,4-diaminobutyric acid,

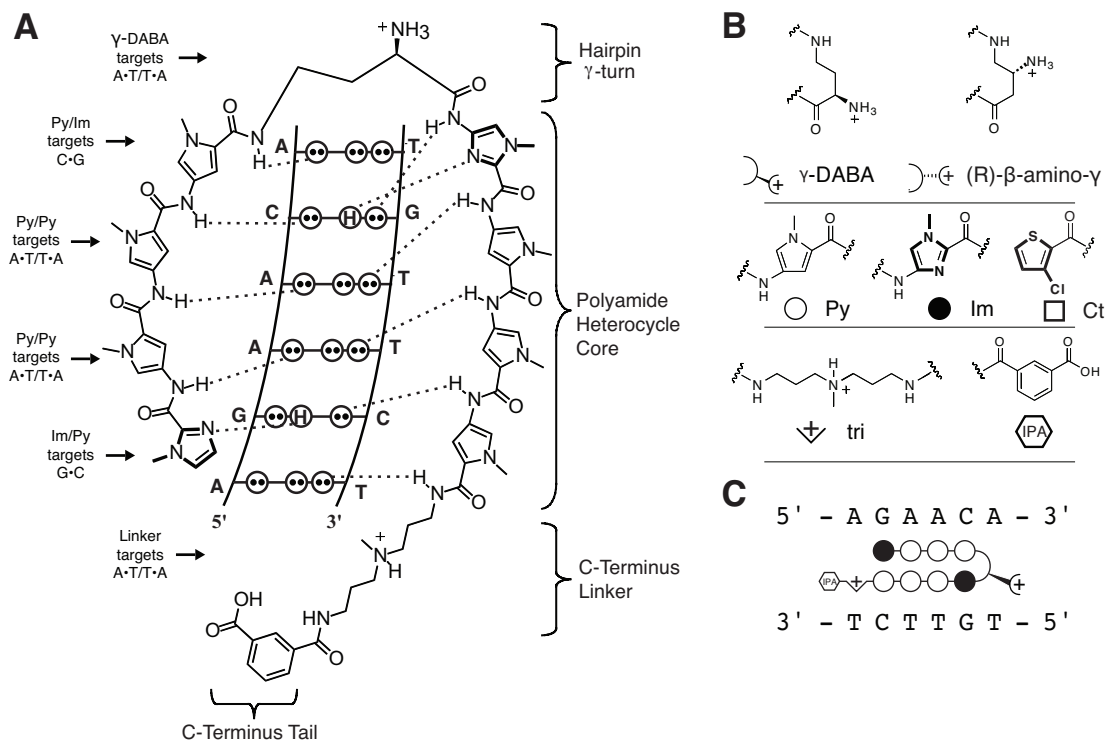


Figure 1.5 Molecular recognition of DNA by Py-Im polyamides. **(A)** Schematic of Py-Im polyamide targeted to 5'-WGWWCW-3' binding to the minor groove. **(B)** Chemical structures of monomers found in polyamides and their ball-and-stick representations. Abbreviation for each monomer is also listed. **(C)** Ball-and-stick representation of the Py-Im polyamide in **(A)** bound to its cognate DNA sequence.

which also show improvements to affinity (30,31). Another feature of current generation Py-Im polyamides is the conjugation of isophthalic acid to the C-terminus linked by 3,3'-diamino-N-methyldipropylamine. This C-terminus tail aids in the uptake of polyamides into live cells (32). Uptake into the nucleus of live cells was demonstrated by conjugating fluorescein to the C-terminus linker (33). The 3,3'-diamino-N-methyldipropylamine C-terminus linker also shows preferential binding for A•T and T•A base pairs. Therefore, currently used eight-ring hairpin Py-Im polyamides are capable of recognizing a specific six base pair sequence.

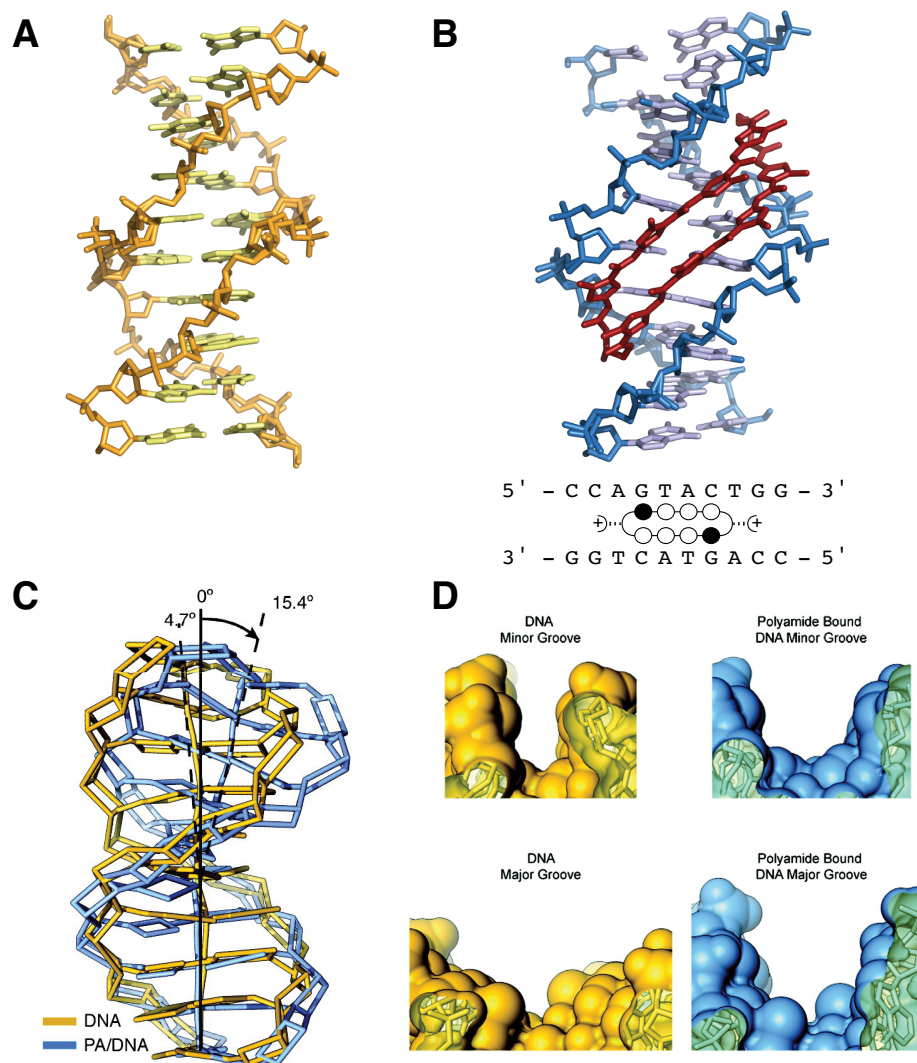


Figure 1.6 Py-Im polyamide binding alters the structure of DNA. (A) Native DNA crystal structure at 0.98 Å resolution (PDB 1D8G) (B) DNA/polyamide co-crystal structure at 0.95 Å resolution (PDB 3OMJ), ball-and-stick model of polyamide bound to DNA (C) Significant DNA bending is observed for polyamide-bound DNA (blue) versus unbound DNA (yellow). (D) Top: comparison of the minor-groove width for DNA in the absence of polyamide (yellow) and in the presence of bound polyamide (blue). Bottom: Comparison of the major-groove widths.

Features of the current generation Py-Im polyamide and its effects on DNA can be observed in the crystal structure of a macrocyclic eight-ring Py-Im polyamide bound to DNA (Figure 1.6) (34). Polyamide binding induces widening of the minor groove and narrowing of the major groove, as observed in the distamycin 2:1 structure (Figure 1.4),

as well as bending of the helix. This structure demonstrates how polyamides can act allosterically to inhibit binding of transcription factors and other DNA-binding proteins (34). Structural studies have also shown that polyamides can bind to DNA in a reconstituted nucleosomal core particle (35), suggesting that they are capable of binding to chromatin. The unique properties of these cell-permeable, sequence-specific, high affinity DNA-binding small molecules make them an attractive candidate for modulation of dysregulated gene expression in disease states.

1.4 Biological activity of pyrrole-imidazole polyamides

Py-Im polyamides have been used successfully to modulate gene expression in many cell culture models of disease. In human glioblastoma cells U251, for example, polyamides targeted to the HIF-1:DNA interface were shown to downregulate HIF-1-driven genes such as *vegf* (Figure 1.7A) (36). In total, 69 out of 297 induced transcripts were affected at least twofold by polyamide treatment in this cell line, and ~1500 total transcripts were affected. Polyamide treatment was also shown to reduce occupancy of HIF-1 at the promoter binding site at some, but not all, genes, suggesting that polyamides may inhibit binding of HIF-1 to DNA as observed *in vitro* (37). Similar results were observed in human prostate cancer cells LNCaP using a polyamide targeted to the androgen response element (ARE) in order to disrupt androgen receptor (AR):DNA binding (Figure 1.7B) (38). More recently, next generation sequencing has been employed to analyze all of the genes affected by a polyamide targeted to the NF- κ B:DNA interface in human non-small cell lung cancer A549 (39). By RNA-seq, polyamide

treatment was shown to downregulate 182 transcripts out of 650 induced transcripts, and in total the expression of ~1200 transcripts were affected.

Evidence that Py-Im polyamides are biologically active and potent in cell culture led to the investigations of polyamide effects in human tumor xenografts grown in mice. The first milestone was the demonstration that polyamides are able to circulate in a healthy mouse and have favorable pharmacokinetics (Figure 1.7C) (40-42). Py-Im polyamides were also shown to accumulate into tumors and modulate gene expression, as observed in cell culture (43-45). Interestingly, investigations of polyamide biodistribution

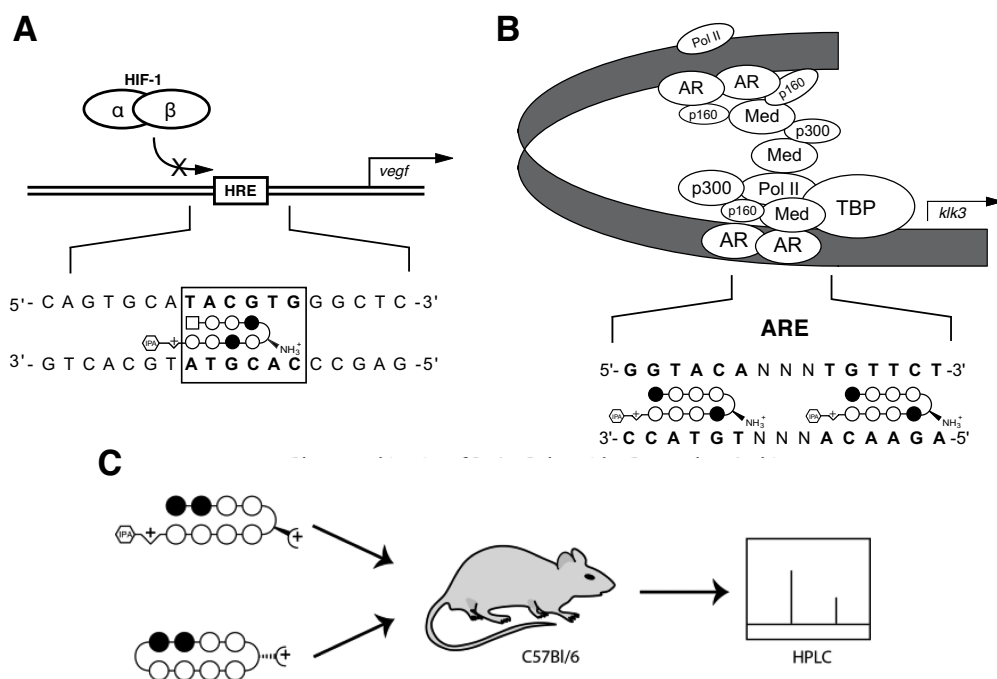


Figure 1.7 Examples of polyamide biological activities in tissue culture and animal studies. (A) A Py-Im polyamide targeted to the HIF response element (HRE) was able to downregulate *vegf* expression and reduce occupancy of HIF-1 at the *vegf* promoter (36). (B) A Py-Im polyamide targeted to the androgen response element (ARE) was able to downregulate *klk3* expression and reduce occupancy of AR at the *klk3* promoter and enhancer (38). (C) Py-Im polyamides injected into C57BL/6 mice were able to circulate for hours in the blood. Polyamide plasma levels varied with the architecture of the molecules (40).

in healthy mice showed measurable polyamide levels in all tissues except brain (46). Importantly, ARE-targeted polyamides were able to reduce the growth of human prostate cancer xenografts with favorable animal toxicity profiles (47,48).

The early success of animal experiments suggests that Py-Im polyamides could one day be an effective therapeutic for the treatment of human cancers. Before that point, however, it will be important to understand the mechanism of action of polyamides and any potential side effects. The abundance of transcripts affected by polyamide treatment that were not induced or directly driven by the TF of interest raised the question as to whether polyamide effects may be exerted by a non-specific mechanism rather than specific disruption of the TF:DNA interface to modulate gene expression. In addition, Py-Im polyamides targeted to different sequences have been found to induce cytotoxicity in a given cell line, despite affecting different genes and signaling pathways (39,44,49). Non-specific inhibition of DNA-dependent processes, such as transcription and replication, by other small molecule DNA-binders spoke to this concern as well (15,18). Non-specific inhibition of transcription was explored recently in LNCaP cells using ARE-targeted polyamides (47). In this study, polyamide treatment caused upregulation of p53 and PARP cleavage, suggesting induction of apoptosis. This was accompanied by degradation of the RNA polymerase (pol) II large subunit RPB1, which can occur when transcription is stalled. RNA pol II was also found to have reduced occupancy at transcription start sites. These results suggested that polyamide bound DNA may inhibit transcription by blocking RNA pol II, which leads to apoptosis. Inhibition of RNA pol II has also been shown with distamycin and actinomycin (50,51).

Another potential mechanism investigated to explain the non-specific effects of polyamides was inhibition of topoisomerases (52). Topoisomerases are enzymes that bind to DNA and introduce single- or double-strand breaks in DNA to relieve helical torsion that occurs during DNA replication and transcription (53). Many natural products exert their toxic effects through inhibition of topoisomerases (15). *In vitro* experiments showed that ARE-targeted polyamides inhibit Top2 α -catalyzed relaxation of a super-coiled plasmid *in vitro*, and that the likely mechanism is through inhibition of Top2 α binding to DNA. Knockdown of Top2 α in hormone-insensitive prostate cancer cells also conferred resistance to polyamide treatment. Inhibition of RNA Pol II elongation and inhibition of topoisomerase DNA binding are two potential mechanisms of non-specific polyamide effects and cytotoxicity, but there are other critical DNA-dependent processes to explore as well.

1.5 Small Molecule Inhibitors of DNA replication

Previous studies suggested that while Py-Im polyamides are effective modulators of gene expression and potent inhibitors of cell growth, their mechanism of action might not occur by specific inhibition of TF:DNA binding. Another process potentially inhibited by polyamides that can explain non-specific effects is DNA replication. DNA replication is the process by which the genome is copied prior to cell division. Like transcription, it involves that action of numerous proteins, many of which interact with DNA to form a complex called the replisome (54). Some of the proteins in the replisome are the DNA polymerases, the replicative helicase, the sliding clamp processivity factor,

primase, and single-stranded binding protein. Inhibition of any of these factors will disrupt DNA replication. Even prior to replication initiation, inhibition of any of the factors that are needed to begin DNA replication will prevent the process from moving forward. Damage to the DNA template itself by DNA base adducts can also prevent translocation of the replisome.

Numerous natural products and synthetic small molecules are capable of inhibiting DNA replication through a variety of mechanisms (Table 1.1). Aphidicolin binds directly to DNA polymerase to inhibit replication fork progression (55). Hydroxyurea and gemcitabine inhibit ribonucleotide reductase, which depletes the nucleotide pool needed for DNA synthesis (56,57). NSC 19630 inhibits Werner helicase, which is important in DNA repair (59). T2AA prevents binding of PCNA, the DNA polymerase processivity factor, to DNA polymerase (60). ET-743 alkylates DNA, which then forms a double-stranded break when encountered during replication (61). Comparison of Py-Im polyamide effects on the cell cycle and DNA replication to those of these small molecules can provide insight into the non-specific effects of polyamides.

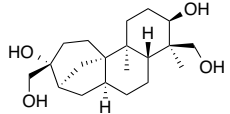
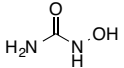
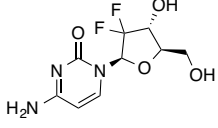
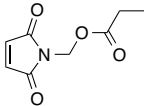
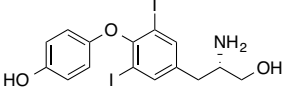
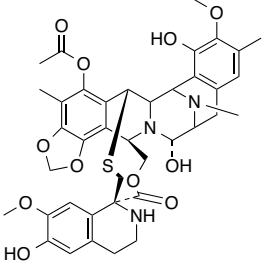
Inhibitor	Mechanism of Action
 <p>Aphidicolin</p>	Inhibits B-family DNA polymerases by binding near the nucleotide binding site
 <p>Hydroxyurea</p>	Inhibits ribonucleotide reductase by quenching the tyrosyl radical through a 1-electron transfer
 <p>Gemcitabine</p>	Inhibits ribonucleotide reductase through loss of tyrosyl radical or covalent reaction with alpha subunit; can also be incorporated into DNA
 <p>NSC 19630</p>	Inhibits WRN helicase
 <p>T2AA</p>	Inhibits of interaction of PCNA with PIP-box domain on DNA polymerase
 <p>ET-743</p>	Binds to minor groove of DNA and alkylates guanine at N2; adducts lead to replication-dependent double strand breaks

Table 1.1 Structures and putative mechanisms of a library of small molecule DNA replication inhibitors (55-61).

1.6 Scope of this work

The work presented in this thesis is primarily focused on elucidating the effects of Py-Im polyamides on DNA replication, and explores how mammalian cells respond to the unique stress exerted by these molecules. In Chapter 2, we present data demonstrating that androgen response element (ARE)-targeted polyamides inhibit DNA replication in

hormone insensitive prostate cancer cells. Cells respond to inhibited DNA replication by activating the ATR checkpoint signaling pathway. However, only part of the downstream signaling events observed in response to stress induced by other small molecules were activated in polyamide-treated cells. We conclude that the replication stress induced by polyamides in this cell line is low relative to other characterized inhibitors. Experiments testing polyamide effects *in vitro* suggest that polyamides may function by inhibiting the replicative helicase. In Chapter 3, we attempt to study the mechanism of polyamide-induced DNA replication stress in closer detail by utilizing cell-free extracts made from *X. laevis* oocytes. In this system, DNA replication is inhibited by treatment with a variety of Py-Im polyamides targeted to different six base pair sequences. However, ATR signaling is not activated. Imaging of the DNA in activated extracts revealed that chromatin failed to properly decondense in response to polyamide treatment, preventing replication initiation. Chapter 4 reports the effects of Py-Im polyamides in a cell line model of prostate cancer harboring the TMPRSS2-ERG gene fusion. We show that polyamides targeted to the ARE in the TMPRSS2 promoter decrease ERG expression, and that polyamides targeted to the ERG recognition sequence decrease expression of ERG-driven genes. A polyamide targeted to the ARE was found to reduce growth of tumors engrafted to SCID mice.

1.7 References

1. Avery, O.T., Macleod, C.M. and McCarty, M. (1944) Studies on the Chemical Nature of the Substance Inducing Transformation of Pneumococcal Types : Induction of Transformation by a Desoxyribonucleic Acid Fraction Isolated from Pneumococcus Type Iii. *J Exp Med*, 79, 137-158.
2. Watson, J.D. and Crick, F.H. (1953) Genetical implications of the structure of deoxyribonucleic acid. *Nature*, 171, 964-967.
3. Watson, J.D. and Crick, F.H. (1953) Molecular structure of nucleic acids; a structure for deoxyribose nucleic acid. *Nature*, 171, 737-738.
4. Drew, H.R., Wing, R.M., Takano, T., Broka, C., Tanaka, S., Itakura, K. and Dickerson, R.E. (1981) Structure of a B-DNA dodecamer: conformation and dynamics. *Proc Natl Acad Sci U S A*, 78, 2179-2183.
5. Lander, E.S., Linton, L.M., Birren, B., Nusbaum, C., Zody, M.C., Baldwin, J., Devon, K., Dewar, K., Doyle, M., FitzHugh, W. *et al.* (2001) Initial sequencing and analysis of the human genome. *Nature*, 409, 860-921.
6. Ezkurdia, I., Juan, D., Rodriguez, J.M., Frankish, A., Diekhans, M., Harrow, J., Vazquez, J., Valencia, A. and Tress, M.L. (2014) Multiple evidence strands suggest that there may be as few as 19,000 human protein-coding genes. *Hum Mol Genet*, 23, 5866-5878.
7. Harrow, J., Frankish, A., Gonzalez, J.M., Tapanari, E., Diekhans, M., Kokocinski, F., Aken, B.L., Barrell, D., Zadissa, A., Searle, S. *et al.* (2012) GENCODE: the reference human genome annotation for The ENCODE Project. *Genome Res*, 22, 1760-1774.
8. Chu, Q., Ma, J. and Saghatelian, A. (2015) Identification and characterization of sORF-encoded polypeptides. *Crit Rev Biochem Mol Biol*, 50, 134-141.
9. Nalefski, E.A., Nebelitsky, E., Lloyd, J.A. and Gullans, S.R. (2006) Single-molecule detection of transcription factor binding to DNA in real time: specificity, equilibrium, and kinetic parameters. *Biochemistry*, 45, 13794-13806.
10. Panne, D., Maniatis, T. and Harrison, S.C. (2007) An atomic model of the interferon-beta enhanceosome. *Cell*, 129, 1111-1123.
11. Naar, A.M., Lemon, B.D. and Tjian, R. (2001) Transcriptional coactivator complexes. *Annu Rev Biochem*, 70, 475-501.
12. Love, J.J., Li, X., Case, D.A., Giese, K., Grosschedl, R. and Wright, P.E. (1995) Structural basis for DNA bending by the architectural transcription factor LEF-1. *Nature*, 376, 791-795.

13. Juo, Z.S., Chiu, T.K., Leiberman, P.M., Baikalov, I., Berk, A.J. and Dickerson, R.E. (1996) How proteins recognize the TATA box. *J Mol Biol*, 261, 239-254.
14. Nair, S.K. and Burley, S.K. (2003) X-ray structures of Myc-Max and Mad-Max recognizing DNA. Molecular bases of regulation by proto-oncogenic transcription factors. *Cell*, 112, 193-205.
15. Tse, W.C. and Boger, D.L. (2004) Sequence-selective DNA recognition: natural products and nature's lessons. *Chem Biol*, 11, 1607-1617.
16. Gurova, K. (2009) New hopes from old drugs: revisiting DNA-binding small molecules as anticancer agents. *Future Oncol*, 5, 1685-1704.
17. Bensaude, O. (2011) Inhibiting eukaryotic transcription: Which compound to choose? How to evaluate its activity? *Transcription*, 2, 103-108.
18. Horikawa, S., Sakata, K., Uchiumi, F., Hatanaka, M. and Tsukada, K. (1987) Effect of actinomycin D on DNA replication and c-myc expression during rat liver regeneration. *Biochem Biophys Res Commun*, 144, 1049-1054.
19. Zimmer, C., Puschendorf, B., Grunicke, H., Chandra, P. and Venner, H. (1971) Influence of netropsin and distamycin A on the secondary structure and template activity of DNA. *Eur J Biochem*, 21, 269-278.
20. Beerman, T.A., McHugh, M.M., Sigmund, R., Lown, J.W., Rao, K.E. and Bathini, Y. (1992) Effects of analogs of the DNA minor groove binder Hoechst 33258 on topoisomerase II and I mediated activities. *Biochim Biophys Acta*, 1131, 53-61.
21. Brosh, R.M., Jr., Karow, J.K., White, E.J., Shaw, N.D., Hickson, I.D. and Bohr, V.A. (2000) Potent inhibition of werner and bloom helicases by DNA minor groove binding drugs. *Nucleic Acids Res*, 28, 2420-2430.
22. Coll, M., Frederick, C.A., Wang, A.H. and Rich, A. (1987) A bifurcated hydrogen-bonded conformation in the d(A.T) base pairs of the DNA dodecamer d(CGCAAATTTGCG) and its complex with distamycin. *Proc Natl Acad Sci U S A*, 84, 8385-8389.
23. Mitra, S.N., Wahl, M.C. and Sundaralingam, M. (1999) Structure of the side-by-side binding of distamycin to d(GTATATAC)₂. *Acta Crystallogr D Biol Crystallogr*, 55, 602-609.
24. Pelton, J.G. and Wemmer, D.E. (1989) Structural characterization of a 2:1 distamycin A.d(CGCAAATTGGC) complex by two-dimensional NMR. *Proc Natl Acad Sci U S A*, 86, 5723-5727.

25. Kopka, M.L., Yoon, C., Goodsell, D., Pjura, P. and Dickerson, R.E. (1985) The molecular origin of DNA-drug specificity in netropsin and distamycin. *Proc Natl Acad Sci U S A*, 82, 1376-1380.
26. White, S., Szewczyk, J.W., Turner, J.M., Baird, E.E. and Dervan, P.B. (1998) Recognition of the four Watson-Crick base pairs in the DNA minor groove by synthetic ligands. *Nature*, 391, 468-471.
27. Hsu, C.F., Phillips, J.W., Trauger, J.W., Farkas, M.E., Belitsky, J.M., Heckel, A., Olenyuk, B.Z., Puckett, J.W., Wang, C.C. and Dervan, P.B. (2007) Completion of a Programmable DNA-Binding Small Molecule Library. *Tetrahedron*, 63, 6146-6151.
28. Foister, S., Marques, M.A., Doss, R.M. and Dervan, P.B. (2003) Shape selective recognition of T.A base pairs by hairpin polyamides containing N-terminal 3-methoxy (and 3-chloro) thiophene residues. *Bioorg Med Chem*, 11, 4333-4340.
29. Herman, D.M., Turner, J.M., Baird, E.E. and Dervan, P.B. (1999) Cycle polyamide motif for recognition of the minor groove of DNA. *J Am Chem Soc*, 121, 1121-1129.
30. Farkas, M.E., Li, B.C., Dose, C. and Dervan, P.B. (2009) DNA sequence selectivity of hairpin polyamide turn units. *Bioorg Med Chem Lett*, 19, 3919-3923.
31. Dose, C., Farkas, M.E., Chenoweth, D.M. and Dervan, P.B. (2008) Next generation hairpin polyamides with (R)-3,4-diaminobutyric acid turn unit. *J Am Chem Soc*, 130, 6859-6866.
32. Nickols, N.G., Jacobs, C.S., Farkas, M.E. and Dervan, P.B. (2007) Improved nuclear localization of DNA-binding polyamides. *Nucleic Acids Res*, 35, 363-370.
33. Best, T.P., Edelson, B.S., Nickols, N.G. and Dervan, P.B. (2003) Nuclear localization of pyrrole-imidazole polyamide-fluorescein conjugates in cell culture. *Proc Natl Acad Sci U S A*, 100, 12063-12068.
34. Chenoweth, D.M. and Dervan, P.B. (2010) Structural basis for cyclic Py-Im polyamide allosteric inhibition of nuclear receptor binding. *J Am Chem Soc*, 132, 14521-14529.
35. Suto, R.K., Edayathumangalam, R.S., White, C.L., Melander, C., Gottesfeld, J.M., Dervan, P.B. and Luger, K. (2003) Crystal structures of nucleosome core particles in complex with minor groove DNA-binding ligands. *J Mol Biol*, 326, 371-380.
36. Nickols, N.G., Jacobs, C.S., Farkas, M.E. and Dervan, P.B. (2007) Modulating hypoxia-inducible transcription by disrupting the HIF-1-DNA interface. *ACS Chem Biol*, 2, 561-571.

37. Olenyuk, B.Z., Zhang, G.J., Klco, J.M., Nickols, N.G., Kaelin, W.G., Jr. and Dervan, P.B. (2004) Inhibition of vascular endothelial growth factor with a sequence-specific hypoxia response element antagonist. *Proc Natl Acad Sci U S A*, 101, 16768-16773.
38. Nickols, N.G. and Dervan, P.B. (2007) Suppression of androgen receptor-mediated gene expression by a sequence-specific DNA-binding polyamide. *Proc Natl Acad Sci U S A*, 104, 10418-10423.
39. Raskatov, J.A., Meier, J.L., Puckett, J.W., Yang, F., Ramakrishnan, P. and Dervan, P.B. (2012) Modulation of NF-kappaB-dependent gene transcription using programmable DNA minor groove binders. *Proc Natl Acad Sci U S A*, 109, 1023-1028.
40. Raskatov, J.A., Hargrove, A.E., So, A.Y. and Dervan, P.B. (2012) Pharmacokinetics of Py-Im polyamides depend on architecture: cyclic versus linear. *J Am Chem Soc*, 134, 7995-7999.
41. Harki, D.A., Satyamurthy, N., Stout, D.B., Phelps, M.E. and Dervan, P.B. (2008) In vivo imaging of pyrrole-imidazole polyamides with positron emission tomography. *Proc Natl Acad Sci U S A*, 105, 13039-13044.
42. Synold, T.W., Xi, B., Wu, J., Yen, Y., Li, B.C., Yang, F., Phillips, J.W., Nickols, N.G. and Dervan, P.B. (2012) Single-dose pharmacokinetic and toxicity analysis of pyrrole-imidazole polyamides in mice. *Cancer Chemother Pharmacol*, 70, 617-625.
43. Raskatov, J.A., Nickols, N.G., Hargrove, A.E., Marinov, G.K., Wold, B. and Dervan, P.B. (2012) Gene expression changes in a tumor xenograft by a pyrrole-imidazole polyamide. *Proc Natl Acad Sci U S A*, 109, 16041-16045.
44. Nickols, N.G., Szablowski, J.O., Hargrove, A.E., Li, B.C., Raskatov, J.A. and Dervan, P.B. (2013) Activity of a Py-Im polyamide targeted to the estrogen response element. *Mol Cancer Ther*, 12, 675-684.
45. Raskatov, J.A., Puckett, J.W. and Dervan, P.B. (2014) A C-14 labeled Py-Im polyamide localizes to a subcutaneous prostate cancer tumor. *Bioorg Med Chem*, 22, 4371-4375.
46. Raskatov, J.A., Szablowski, J.O. and Dervan, P.B. (2014) Tumor xenograft uptake of a pyrrole-imidazole (Py-Im) polyamide varies as a function of cell line grafted. *J Med Chem*, 57, 8471-8476.
47. Yang, F., Nickols, N.G., Li, B.C., Marinov, G.K., Said, J.W. and Dervan, P.B. (2013) Antitumor activity of a pyrrole-imidazole polyamide. *Proc Natl Acad Sci U S A*, 110, 1863-1868.

48. Yang, F., Nickols, N.G., Li, B.C., Szablowski, J.O., Hamilton, S.R., Meier, J.L., Wang, C.M. and Dervan, P.B. (2013) Animal toxicity of hairpin pyrrole-imidazole polyamides varies with the turn unit. *J Med Chem*, 56, 7449-7457.
49. Muzikar, K.A., Nickols, N.G. and Dervan, P.B. (2009) Repression of DNA-binding dependent glucocorticoid receptor-mediated gene expression. *Proc Natl Acad Sci U S A*, 106, 16598-16603.
50. Mote, J., Ghanouni, P. and Reines, D. (1994) A DNA Minor Groove-Binding Ligand Both Potentiates and Arrests Transcription by Rna-Polymerase-Ii - Elongation-Factor Sii Enables Readthrough at Arrest Sites. *Journal of Molecular Biology*, 236, 725-737.
51. Sobell, H.M. (1985) Actinomycin and DNA-Transcription. *P Natl Acad Sci USA*, 82, 5328-5331.
52. Phillips, J.W. (2011). PhD Thesis, California Institute of Technology.
53. Durand-Dubief, M., Svensson, J.P., Persson, J. and Ekwall, K. (2011) Topoisomerases, chromatin and transcription termination. *Transcription*, 2, 66-70.
54. Masai, H., Matsumoto, S., You, Z.Y., Yoshizawa-Sugata, N. and Oda, M. (2010) Eukaryotic Chromosome DNA Replication: Where, When and How? *Annual Review of Biochemistry*, Vol 79, 79, 89-130.
55. Baranovskiy, A.G., Babayeva, N.D., Suwa, Y., Gu, J., Pavlov, Y.I. and Tahirov, T.H. (2014) Structural basis for inhibition of DNA replication by aphidicolin. *Nucleic Acids Res*, 42, 14013-14021.
56. Lassmann, G., Thelander, L. and Graslund, A. (1992) EPR stopped-flow studies of the reaction of the tyrosyl radical of protein R2 from ribonucleotide reductase with hydroxyurea. *Biochem Biophys Res Commun*, 188, 879-887.
57. Artin, E., Wang, J., Lohman, G.J.S., Yokoyama, K., Yu, G.X., Griffin, R.G., Bar, G. and Stubbe, J. (2009) Insight into the Mechanism of Inactivation of Ribonucleotide Reductase by Gemcitabine 5 '-Diphosphate in the Presence or Absence of Reductant. *Biochemistry*, 48, 11622-11629.
58. Gowda, A.S.P., Polizzi, J.M., Eckert, K.A. and Spratt, T.E. (2010) Incorporation of Gemcitabine and Cytarabine into DNA by DNA Polymerase beta and Ligase III/XRCC1. *Biochemistry*, 49, 4833-4840.
59. Aggarwal, M., Sommers, J.A., Shoemaker, R.H. and Brosh, R.M. (2011) Inhibition of helicase activity by a small molecule impairs Werner syndrome helicase (WRN) function in the cellular response to DNA damage or replication stress. *P Natl Acad Sci USA*, 108, 1525-1530.

60. Punchihewa, C., Inoue, A., Hishiki, A., Fujikawa, Y., Connelly, M., Evison, B., Shao, Y.M., Heath, R., Kuraoka, I., Rodrigues, P. *et al.* (2012) Identification of Small Molecule Proliferating Cell Nuclear Antigen (PCNA) Inhibitor That Disrupts Interactions with PIP-box Proteins and Inhibits DNA Replication. *Journal of Biological Chemistry*, 287, 14289-14300.
61. Soares, D.G., Escargueil, A.E., Poindessous, V., Sarasin, A., de Gramont, A., Bonatto, D., Henriques, J.A.P. and Larsen, A.K. (2007) Replication and homologous recombination repair regulate DNA double-strand break formation by the antitumor alkylator ecteinascidin 743. *P Natl Acad Sci USA*, 104, 13062-13067.

Chapter 2

Replication Stress by Py-Im Polyamides

Induces a Non-canonical ATR-dependent Checkpoint Response

The text of this chapter was taken in part from a manuscript co-authored with John W. Phillips, Kenneth K. Karanja, Piotr Polazcek, Chieh-Mei Wang, Benjamin C. Li, Judith L. Campbell, and Peter B. Dervan (California Institute of Technology)

(Martinez, T.F., Phillips, J.W., Karanja, K.K., Polazcek, P., Wang, C.M., Li, B.C., Campbell, J.L. and Dervan, P.B. (2014) Replication stress by Py-Im polyamides induces a non-canonical ATR-dependent checkpoint response. *Nucleic Acids Res*, 42, 11546-11559.)

Abstract

Pyrrrole-imidazole polyamides targeted to the androgen response element were cytotoxic in multiple cell lines, independent of intact androgen receptor signaling. Polyamide treatment induced accumulation of S-phase cells and of PCNA replication/repair foci. Activation of a cell cycle checkpoint response was evidenced by autophosphorylation of ATR, the S-phase checkpoint kinase, and by recruitment of ATR and the ATR activators RPA, 9-1-1, and Rad17 to chromatin. Surprisingly, ATR activation was accompanied by only a slight increase in single-stranded DNA, and the ATR targets RPA2 and Chk1, a cell cycle checkpoint kinase, were not phosphorylated. However, ATR activation resulted in phosphorylation of the replicative helicase subunit MCM2, an ATR effector. Polyamide treatment also induced accumulation of monoubiquitinated FANCD2, which is recruited to stalled replication forks and interacts transiently with phospho-MCM2. This suggests that polyamides induce replication stress that ATR can counteract independently of Chk1 and that the FA/BRCA pathway may also be involved in the response to polyamides. In biochemical assays, polyamides inhibit DNA helicases, providing a plausible mechanism for S-phase inhibition.

2.1 Introduction

Many DNA-binding small molecules can challenge a cell's ability to accurately replicate its DNA. Tolerance to various forms of replication stress is possible with the aid of stress sensors and mediators that activate DNA repair and cell cycle pathways, collectively called the DNA damage response (DDR) (1). The master regulators of the DDR are ATR and ATM, two PI3 protein kinase family members which respond to stalled replication forks and DNA breaks. ATR and ATM phosphorylate many substrates to stabilize the DNA replication fork and activate cell cycle checkpoints. The checkpoints slow cell cycle progression and allow time for the cell to respond to stress before entry into mitosis (2). During S-phase, ATR is recruited to sites of stalled replication by RPA-bound single-stranded DNA (ssDNA) in the presence of DNA damage. ATR is activated by a complex of many proteins and phosphorylates a number of targets, among which Chk1, a cell cycle checkpoint kinase, is best understood (3,4). ATM is similarly recruited to sites of double stranded breaks (DSBs) by the Mre11-Rad50-NBS1 (MRN) complex, where it can phosphorylate Chk2, another cell cycle checkpoint kinase, and the histone variant H2AX (5). However, how the DDR reacts to specific types of stresses, what downstream signaling events are necessary, and what physical structures are sensed are still under investigation (6). Furthermore, there are many levels of crosstalk between ATM and ATR and many targets beyond the checkpoint kinases, Chk1 and Chk2, which adds to the complexity (4). We have studied the checkpoint response activated by DNA minor groove binding pyrrole-imidazole (Py-Im) polyamides to discover what response polyamides elicit.

Py-Im polyamides are programmable small molecules that bind in the minor groove of double-stranded DNA with affinities and specificities comparable to DNA-binding proteins (7,8). Binding of the polyamides alters the local helical structure of DNA (9). Eight-ring hairpin polyamides are cell-permeable and localize to the nucleus in live cells (10). Py-Im Polyamides are derived from the natural products distamycin A and netropsin (11). Distamycin A is cytotoxic at relatively high concentrations (12), and inhibits the activity of RNA polymerase, DNA polymerase, topoisomerases I and II, and helicases (13-15). Previously, we showed that hairpin Py-Im polyamides designed to bind the androgen response element (ARE) decrease the expression of prostate cancer related genes, inhibit RNA polymerase activity, upregulate p53, and induce apoptosis (16,17). Curiously, no evidence of DNA breaks, which usually occurs upon treatment with DNA damaging agents such as doxorubicin, was observed. However, effects on replication remain to be investigated.

Here we report that hairpin Py-Im polyamides targeted to the ARE cause replication stress, resulting in an accumulation of S-phase cells. Furthermore, the polyamide-induced checkpoint response activates ATR and downstream phosphorylation of the mini-chromosome maintenance complex (MCMs), but not the downstream ATR effector kinase Chk1. The checkpoint response also results in monoubiquitination of the Fanconi anemia/Breast cancer (FA/BRCA) gateway protein FANCD2. The checkpoint is activated despite low levels of ssDNA formation and the absence of observable DNA breaks. We also show that polyamides are potent inhibitors of helicase unwinding *in vitro*, suggesting a model in which polyamides preclude fork progression through DNA-

binding. These results demonstrate that polyamides are capable of imposing replication stress and can activate both a non-canonical Chk1-independent ATR-checkpoint response and the FA/BRCA pathway, resulting in S-phase delay.

2.2 Results

Py-Im polyamides cause accumulation of S-phase cells and PCNA foci.

Hairpin Py-Im Polyamides **1** and **2** were designed to target the ARE (5'-GGTACANNNTGTTCT-3' (18)) and antagonize gene expression changes driven by the androgen receptor (AR) in the prostate cancer cell line, LNCaP (Figure 1A and B) (16,19). In LNCaP cells, AR signaling plays a critical role in cell proliferation (20), and therefore disruption of AR-dependent signaling may contribute to cell death. However, disruption of other DNA-dependent processes such as RNA pol II transcription elongation may also cause cell death. To investigate the effects of polyamides outside of AR-dependent transcription, we first compared the cytotoxicity of polyamides **1** and **2** in three different prostate cancer cell lines, LNCaP, LNAR, and DU145, which express high, normal, and low levels of AR, respectively. Polyamides **1** and **2** displayed dose-dependent cytotoxicity at 72 and 96 h as measured by sulfarhodamine B staining (Table 2.1). Polyamide **2** had approximately ten-fold higher potency than polyamide **1**, which is consistent with its greater potency against AR-driven gene expression (19). Importantly, the IC₅₀ values were similar in all cell lines regardless of AR status, suggesting that the observed cytotoxicity occurred via an AR-independent mechanism. In DU145 cells, expression of an AR-driven reporter is insensitive to androgen treatment and AR is

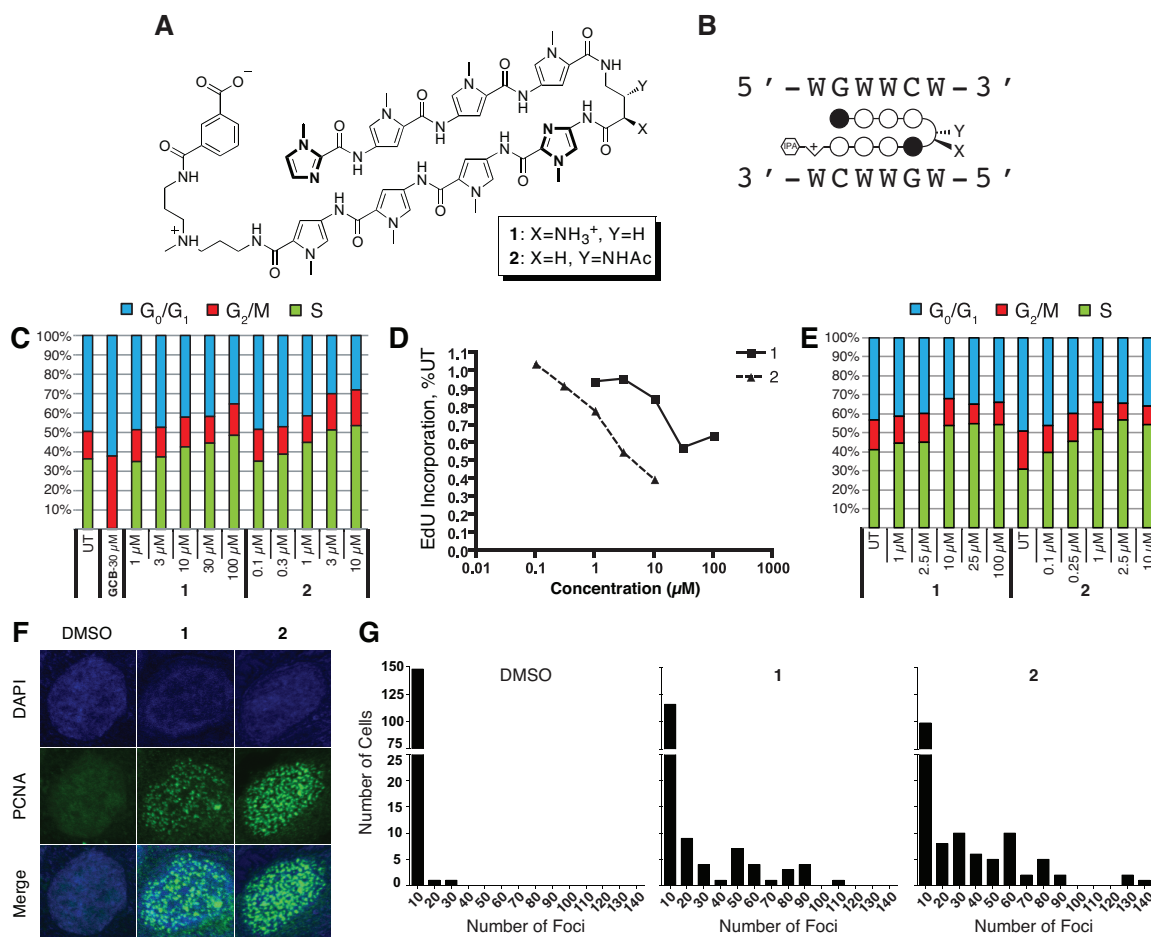


Figure 2.1 Polyamides cause accumulation of S-phase cells and PCNA foci. **(A)** Chemical structure Py-Im polyamides used in this study. **(B)** Ball-and-stick representation of the polyamides. Open circles represent N-methylpyrrole residues, filled circles represent N-methylimidazoles. The hexagon represents the isophthalic acid moiety. Polyamides **1** and **2** are specific for the same 5'-WGWWCW-3' DNA sequence, where W=A or T. **(C)** Cell cycle distribution of DU145 cells untreated (UT) or treated with gemcitabine (GCB), polyamide **1**, or polyamide **2** for 24 h as measured by two-color flow cytometric evaluation of EdU pulse-labeled cells stained for DNA content with 7AAD. **(D)** Dose-dependent decrease in average EdU incorporation indicative of slowed DNA synthesis in response to polyamide treatment. **(E)** Cell cycle distribution of DU145 cells untreated or treated with polyamide **1** or **2** for 48 h as measured by single-color flow cytometric evaluation of propidium iodide stained cells. **(F)** Representative images of immunofluorescent detection of PCNA in DU145 cells. Treatment with either 10 μM polyamide **1** or 1 μM **2** for 36 h causes more cells to contain significant punctate staining of PCNA. **(G)** PCNA foci counts for each cell are plotted in a histogram with bin sizes of 10 foci for each condition. 150 cells over three replicates were counted for each condition. Kruskal-Wallis test reports $P < 0.0001$ for **1** versus DMSO and **2** versus DMSO.

minimally expressed (21). Therefore, DU145 cells provide an environment to investigate the effects of polyamides **1** and **2** independent of AR-signaling.

Next, we examined the effects of polyamides **1** and **2** on the cell cycle in DU145 cells. We pulse-labeled exponentially growing and asynchronous DU145 cells with ethynyldeoxyuridine (EdU) after 24 h of polyamide treatment. Both polyamides produced a dose-dependent increase in the percentage of cells in S-phase, with a corresponding drop in the percentage of G0/G1 cells (Figure 1C). Although more cells were in S-phase, the average intensity of EdU staining decreased, suggesting that the treated cells were replicating their DNA more slowly and thus cells spent longer in S-phase (Figure 1D). Similar results were also obtained using traditional one-color flow cytometry to determine the cell cycle distribution after 48 h of polyamide treatment (Figure 1E).

We then determined whether replication/repair foci accumulated in the treated cells using PCNA immunofluorescence (22,23). We chose treatment conditions to allow for maximal effect on the cells before any significant decrease in viability or activation of

		Cytotoxicity IC ₅₀ values (μM)			
Cell line	AR	1		2	
		72h	96h	72h	96h
LNAR	+++	40±10	36±14	3±1	1.5±0.2
LNCaP	+	18±4	7±3	1.8±0.9	0.6±0.2
DU145	-	14±4	8±4	1.5±0.5	0.76±0.06

Table 2.1 Summary of cytotoxicity IC₅₀ values of polyamides **1** and **2** prostate cancer cell lines. Cell lines expressing different levels of AR were studied: AR-overexpressing (+++, LNAR), AR-expressing (+, LNCaP), and AR-negative (-, DU145) cancer cell lines. Cells were treated continuously with polyamides for 72 or 96 h before fixation and staining. Values represent the mean ± S.D. of three replicates.

apoptosis, as measured by mitochondrial reduction activity and caspase 3/7 activation (Figure 2.2). Nearly all DMSO treated cells showed 0-2 foci per cell, while polyamide treatment resulted in a significant increase in cells with greater than 20 foci (Figure 1F and G). Interestingly, some of the polyamide-treated cells but none of the DMSO-treated cells showed more than 50 foci. Observation of cells with such high incidence of foci suggests that polyamides cause prolonged stalling of replication forks and the recruitment of repair machinery (22).

Py-Im Polyamide treatment induces ATR activation.

S-phase accumulation subsequent to treatment with a DNA-binding compound was suggestive of checkpoint activation in response to replication stress. We therefore

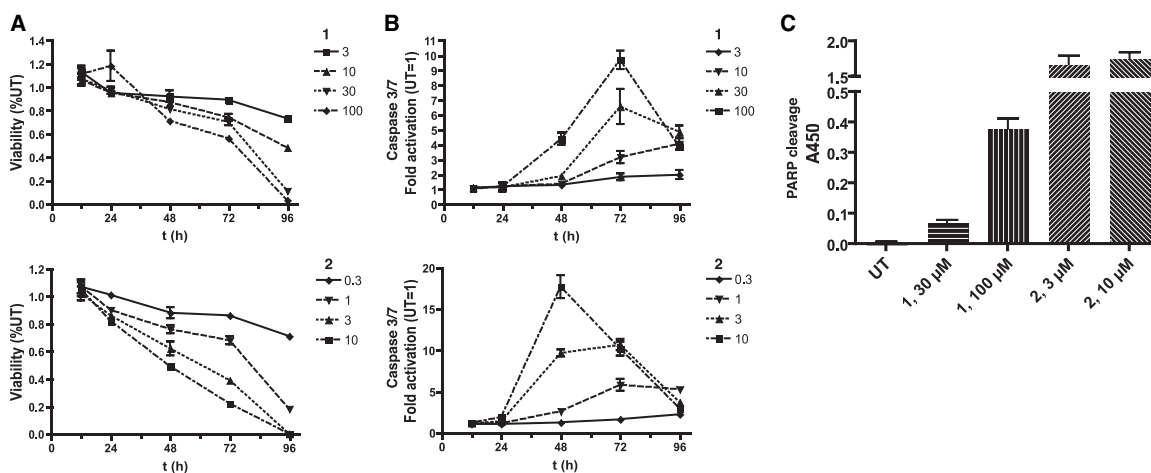


Figure 2.2 Polyamides induce apoptosis in DU145 cells. (A) Cell viability assay. Cells were treated in quadruplicate with polyamide 1 (top) or polyamide 2 (bottom) for range of concentrations (μM) for up to 96 h and then assayed for bioreductive capacity with WST-1 reagent. The data are normalized to the untreated condition. (B) Caspase 3/7 activity assay. Cells were treated in triplicate with polyamide 1 (top) or polyamide 2 (bottom) for the indicated time and then homogenized in guanidinium lysis buffer containing a pro-luminescent Caspase 3/7 substrate. The data are normalized to the untreated condition. (C) ELISA for cleaved PARP formation. Cells were treated with polyamides for 72 h. before assaying the lysates by sandwich ELISA using an HRP-conjugated secondary antibody and a chromogenic substrate. The data are presented as the background-corrected absorbance values at 450 nm. Error bars represent the mean ± S.D. of experiments conducted in triplicate or quadruplicate.

probed for activation of the master regulator kinases, ATR and ATM. We assayed ATR activation by immunoblotting for T1989 phosphorylation, an autophosphorylation site that has been implicated in ATR activation and a robust checkpoint response (24,25). Cells treated with polyamide **1** or **2** showed a slight increase in ATR T1989 phosphorylation relative to DMSO treated cells (Figure 2.3A). However, cells treated with hydroxyurea (HU), which causes nucleotide depletion, showed greater ATR T1989 phosphorylation compared to polyamide-treated cells suggesting a weaker activation of ATR by polyamides. NU6027, which inhibits cellular ATR but not ATM, did not abrogate T1989 phosphorylation under polyamide treatment (26). While polyamide treatment appeared to activate ATR, polyamides did not induce ATM S1981 phosphorylation, an autophosphorylation site that has been associated with ATM activation and stabilization at DSBs (Figure 2.3B) (27).

The weak phosphorylation of ATR suggested that polyamide treatment might result in limited ssDNA formation (4). To directly probe for ssDNA accumulation, we preincubated cells with the thymidine analog, 5-chloro-2'-deoxyuridine (CldU), and then treated with polyamide or HU. After treatment, we fixed the cells and immunostained using an anti-CldU antibody, which reacts with CldU exposed in ssDNA but not dsDNA. About 25% of cells on average showed >10 CldU foci after treatment with HU, while only about 3% and 1% of cells showed >10 CldU foci after 12 h treatment with high concentrations of polyamide **1** or **2** (Figure 2.3C and D). When treated with lower concentrations of polyamide **1** or **2** for 36 h post-CldU incubation, about 8% and 9% cells were positive for CldU foci. However, among the positive cells present under polyamide

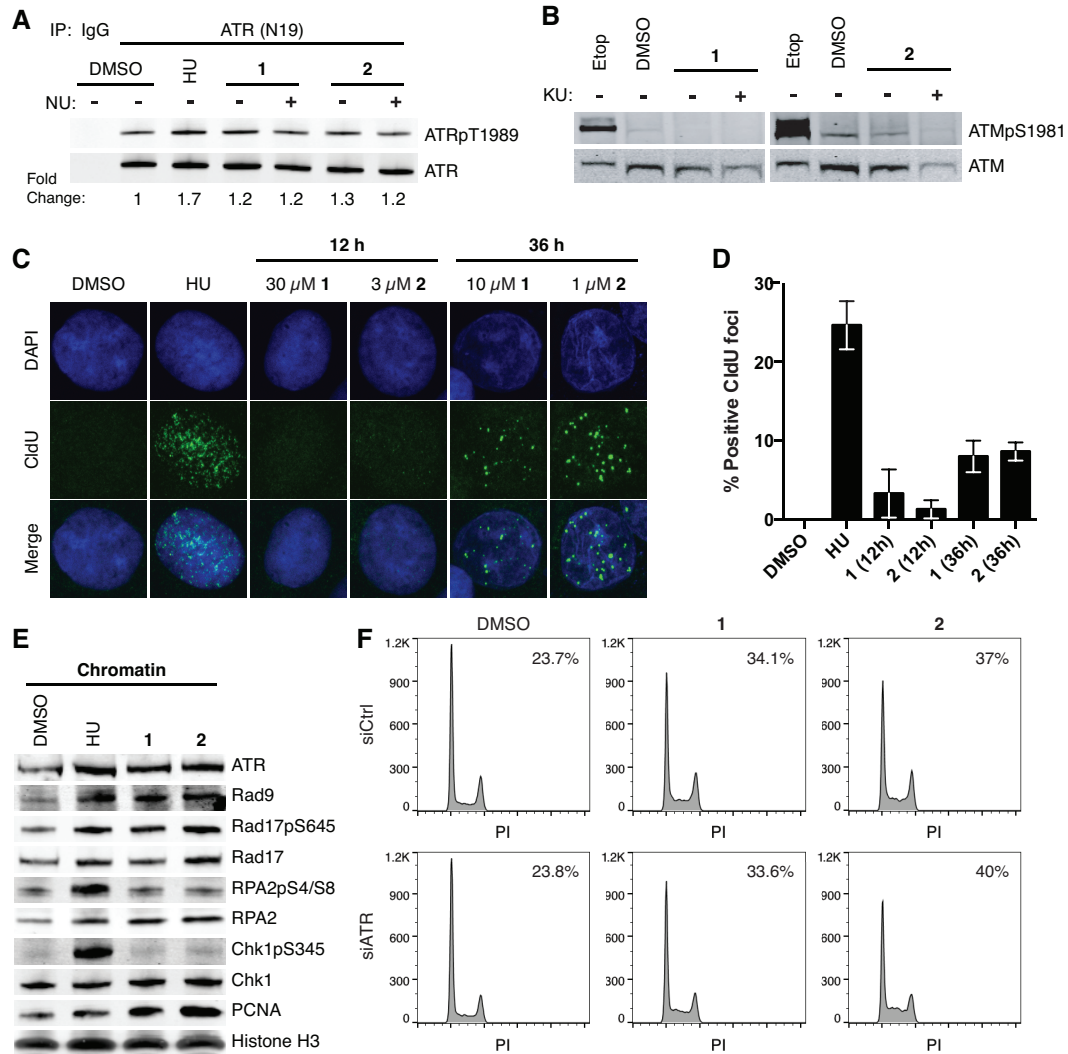


Figure 2.3 Polyamides induce ATR activation without extensive ssDNA formation. (A) Immunoblot of ATRpT1989 and ATR following IP of ATR in DU145 whole cell lysates treated with 4 mM hydroxyurea (HU) for 2 h, and DMSO, 10 μ M polyamide 1, or 1 μ M polyamide 2 in the presence or absence of 10 μ M NU6027 (NU, ATR inhibitor) for 36 h. (B) Immunoblots of ATMpS1981 and ATM after treatment with 30 μ M etoposide (Etop) for 30 min, and DMSO, 10 μ M polyamide 1, or 1 μ M polyamide 2 in the presence or absence of 10 μ M KU55933 (KU, ATM inhibitor) for 36 h. (C) Representative images of ssDNA formation via CldU immunofluorescence under non-denaturing conditions are shown for cells after treatment with 4 mM HU for 2 h, DMSO, 30 μ M polyamide 1, or 3 μ M polyamide 2 for 12 h, and 10 μ M polyamide 1 or 1 μ M polyamide 2 for 36 h. (D) Bar graphs of the mean and standard deviation of percent CldU positive cells (>10 foci/cell). 150 cells over three replicates were counted for each condition. (E) Immunoblots of ATR and checkpoint related factors loaded onto chromatin upon treatment with 10 mM HU for 2 h, and DMSO, 10 μ M polyamide 1, or 1 μ M polyamide 2 for 36 h. (F) DNA histograms of propidium iodide (PI) stained DU145 cells after treatment with negative control or ATR-targeting siRNA for 48 h followed by treatment with DMSO, 10 μ M polyamide 1, or 1 μ M polyamide 2 for 36 h. The percentage of cells in S-phase is included at the top right of each graph.

treatment the number of CldU foci was substantially lower than in HU treated cells. Thus, the degree of ssDNA formation in polyamide treated cells was also lower than in HU treated cells, consistent with the lower levels of T1989 phosphorylation observed.

To confirm ATR activation, we determined if ATR and mediators of the ATR response accumulate on chromatin after polyamide treatment. Polyamide treatment resulted in ATR loading onto chromatin (Figure 2.3E). Interestingly, although we had observed a lower level of ATR phosphorylation in polyamide treated cells than in HU treated cells (Figure 2.3A), similar amounts of ATR were loaded onto chromatin following each treatment. Polyamide treatment also induced loading of RPA, the Rad9-Rad1-Hus1 (9-1-1) complex, which is integral to ATR checkpoint signaling, and Rad17, which is part of the clamp loader that facilitates 9-1-1 loading, to similar levels as did HU. Rad17 S645, a target for ATR phosphorylation that is necessary for G2 checkpoint activation (28), was phosphorylated in the presence of polyamide, indicating that ATR was activated. Polyamide treatment also induced higher PCNA loading on chromatin, which is consistent with the high incidence of PCNA foci formation (Figure 2.1D). Despite the lack of extensive ssDNA formation, ATR as well as its mediators are recruited to chromatin and ATR is active after polyamide treatment.

Py-Im Polyamide-induced S-phase delay is not abrogated by ATR knockdown.

To determine whether the activation of ATR had physiological consequences, we monitored the effect of siRNA knockdown of ATR on accumulation of polyamide treated cells in S-phase. The percentage of S-phase cells was the same in cells treated with either

siRNA against ATR or negative control siRNA prior to treatment with polyamide **1** or **2** (Figure 2.3F). This suggests that ATR activity is not contributing to S-phase accumulation. When caffeine, a PI3 kinase inhibitor with preference for ATR over ATM, was added to cells in addition to polyamide **1** or **2**, the S-phase population was reduced compared to cells treated only with polyamide; however, caffeine treatment also reduces the basal level of S-phase cells and may account for this decrease (Figure 2.4). Similarly, when the ATR inhibitor NU6027 was added to cells the S-phase population was reduced under both the basal and polyamide-treated conditions.

Although ATM S1981 was not phosphorylated in response to polyamide treatment, ATM autophosphorylation sites other than S1981 have been implicated in its activation and function in the cell cycle checkpoint (29). Therefore the effects of ATM inhibition were also monitored. KU55933, a selective inhibitor of ATM, did not diminish the polyamide induced S-phase accumulation (Figure 2.4) (30).

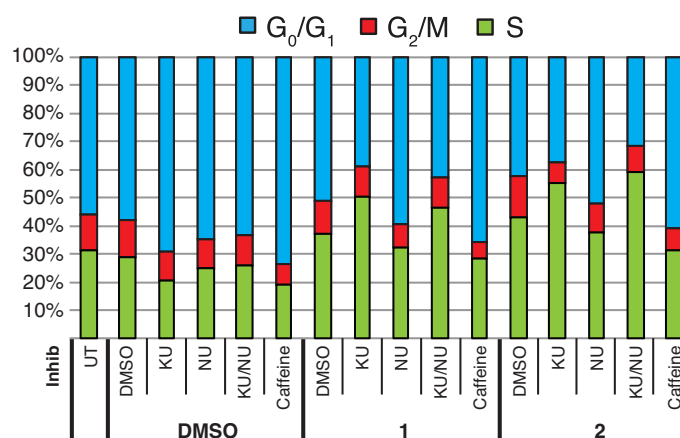


Figure 2.4 Effects of small molecule PI3-kinase inhibitors on polyamide-induced S-phase accumulation. Cell cycle distribution of DU145 cells after 36 h treatment with DMSO, 10 μ M polyamide **1**, or 1 μ M polyamide **2** in the presence of 2 mM caffeine, 10 μ M KU55933 (KU, ATM inhibitor), or 10 μ M NU6027 (NU, ATR inhibitor) as measured by single-color flow cytometric evaluation of propidium iodide stained cells. When both KU and NU were added together with DMSO or polyamide, only 4 μ M of each inhibitor was used to reduce toxicity.

Py-Im Polyamide treatment does not induce Chk1, RPA2, or Chk2 phosphorylation.

The ATR-mediated checkpoint response can be propagated by a variety of downstream effectors. Chk1, the best studied of the ATR effectors, signals cell cycle delay after activation by ATR via phosphorylation at S345. Surprisingly, Chk1 S345 was not phosphorylated after treatment with polyamide (Figure 2.3E). Chk1 S345 phosphorylation is dependent upon RPA2 hyperphosphorylation at sites S4 and S8, which occurs following DSBs from collapsed replication forks (31). Polyamide treatment also did not induce phosphorylation of RPA2 S4/S8. To ensure that we were not missing a transient activation of Chk1 or RPA2, we assayed for their phosphorylation across multiple time points. In addition, we monitored other known Chk1 and RPA2 phosphorylation sites including Chk1 S317 and S296 and RPA2 S33. Chk1 S317 is another target for phosphorylation by ATR in response to replication stress, and Chk1 S296 is an autophosphorylation site that is important for its function (32). RPA2 S33 phosphorylation by ATR under replication stress protects cells by stimulating DNA synthesis and facilitates S4/S8 phosphorylation by DNA-PKcs (31,33). After 12, 18, 36, and 72 h of treatment with polyamide **1** or **2** neither Chk1 nor RPA2 were phosphorylated at any of the sites monitored (A). To test the possibility that polyamide **1** and **2** may somehow inhibit ATR from phosphorylating Chk1, DU145 cells were treated with both polyamide **1** or **2** and aphidicolin, a DNA polymerase inhibitor that induces Chk1 S345 phosphorylation. The polyamides did not inhibit aphidicolin-induced Chk1 S345 phosphorylation (Figure 2.5A and B).

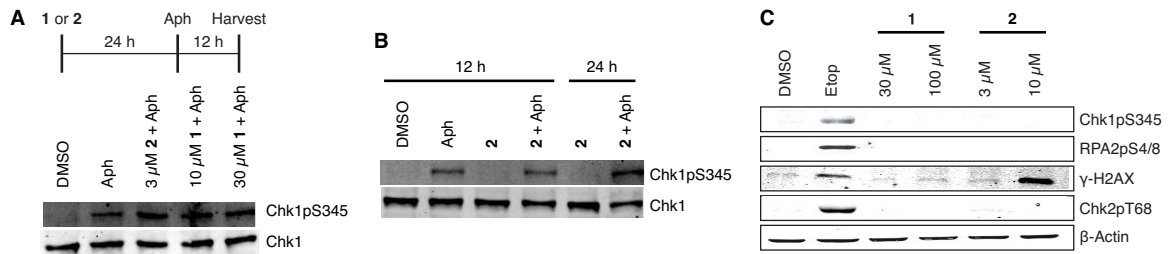


Figure 2.5 High concentration polyamide treatment does not inhibit aphidicolin-induced Chk1 phosphorylation. (A) Immunoblot of Chk1pS345 after the treatment with polyamides followed by aphidicolin. DU145 cells were treated with DMSO, 10 μ M polyamide 1, or 1 μ M polyamide 2 followed by the addition of 10 μ g/mL aphidicolin (Aph) after 24 h. Cells were harvested after 36 h total incubation. (B) Immunoblot of Chk1pS345 after simultaneous treatment of DMSO or 3 μ M polyamide 2 plus 10 μ g/mL aph for 12 or 24 h. (C) Immunoblot of S-phase checkpoint and DNA damage response proteins, Chk1pS345, RPA2pS4/8, Chk2pT68, and γ -H2AX in DU145 cells after 18 h treatment with DMSO, 30 μ M etoposide, polyamide 1, or polyamide 2 at the indicated concentrations.

The absence of Chk1 or RPA2 phosphorylation led us to investigate phosphorylation of Chk2, another cell cycle checkpoint kinase, and H2AX, a histone variant that is phosphorylated rapidly upon DNA damage, as possible downstream checkpoint mediators. ATM predominantly phosphorylates Chk2 T68, though there is evidence for phosphorylation of Chk2 by ATR following cisplatin treatment (34,35). Similarly, ATM or ATR can phosphorylate H2AX S139 in response to different types of replication stress (36). Consistent with the absence of ATM S1981 phosphorylation after polyamide treatment, polyamides failed to induce Chk2 T68 phosphorylation (Figure 2.6A). H2AX and RPA2 S4/S8 phosphorylation were slightly elevated after 72 h treatment of 1 μ M polyamide 2, and may be suggestive of DNA damage. However, H2AX can be phosphorylated under non-damaging stress (37). It is also worth noting that these phosphorylation events may be triggered by apoptosis, which occurs after 72 h treatment with polyamide 2 (Figure 2.2). Finally, we also studied the effect of high

concentration polyamide treatment for 18 h and similar results were observed (Figure 2.5C).

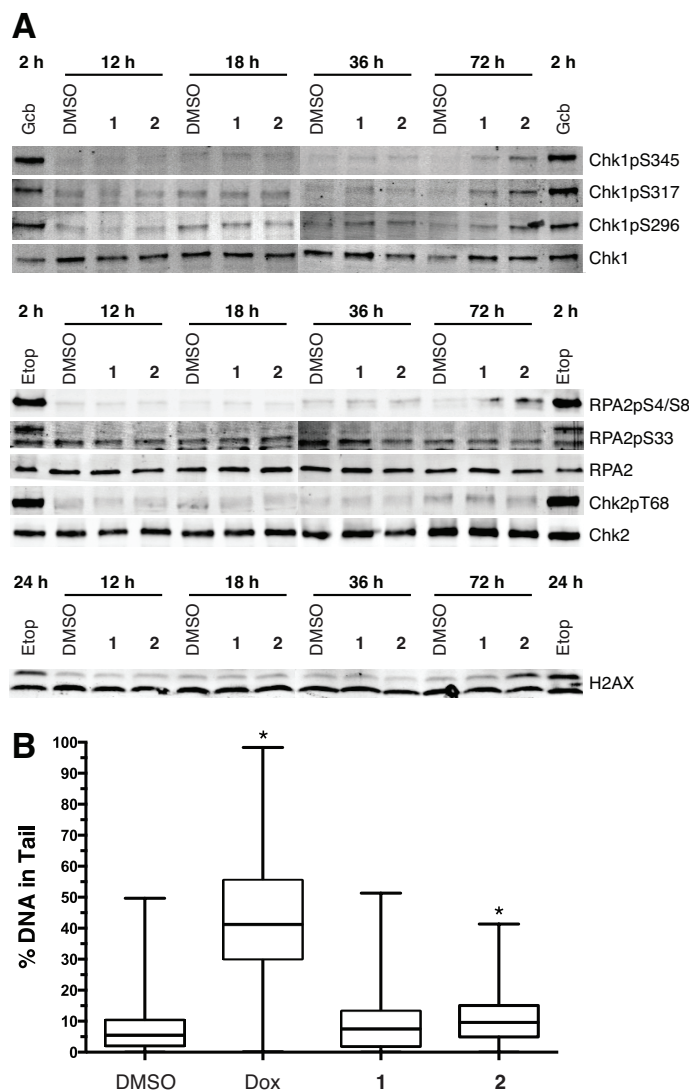


Figure 2.6 Polyamides do not induce phosphorylation of Chk1, RPA2, or Chk2 or observable DNA breaks. (A) Immunoblots of phosphorylated Chk1 at S345, S317, and S296; RPA2 S4/S8 and S33; Chk2 T68; and H2AX S139 after 12, 18, 36, and 72 h treatment with DMSO, 10 μM polyamide 1, 1 μM polyamide 2, or treatment with 30 μM gemcitabine (Gcb) for 2 h or 30 μM etoposide (Etop) for 2 h and 24 h in whole cell lysates. (B) Single cell alkaline gel electrophoretic analysis DU145 cells treated with 1 μM doxorubicin (Dox) for 24 h, and DMSO, 10 μM polyamide 1, or 1 μM polyamide 2 for 36 h. Boxes show the median percentage of DNA in the comet tail and are bounded by 25th and 75th percentile while whiskers represent the min and max percentile. 400 cells from two biological replicates were counted for each condition. Mann Whitney test reports $P < 0.0001$ for Dox and 2, and is indicated by *.

Py-Im polyamide treatment does not induce DNA breakage.

The absence of ATM, Chk2, and RPA2 phosphorylation suggested that polyamide-induced replication stress does not lead to gross breakage of DNA. To study DNA breakage directly, we treated cells with polyamides and then analyzed them by single cell alkaline gel electrophoresis (Figure 2.6B). Migration of the DNA from the centroid into the ‘comet tail’ is proportional to the amount of single- and double-strand breakage that has occurred. Cells treated with doxorubicin, a known DNA-damaging agent, were used as a positive control and showed a median value of 41% of total DNA in the tail. Polyamide-treated cells, however, were similar to the DMSO control with median %DNA in tail values of 8 and 10 for polyamides **1** and **2**, respectively, compared to 6% for DMSO. The lack of extensive DNA breakage correlates with the absence of ATM-Chk2 activation.

Py-Im Polyamide treatment induces MCM2 phosphorylation and monoubiquitination of FANCD2, a major gatekeeper of the FA/BRCA Repair Pathway.

Since Chk1, Chk2, and RPA2 were not phosphorylated, our results suggested that ATR phosphorylates targets intrinsic to the replication fork to regulate S-phase progression. MCM2 is a component of the replicative helicase and is required for both initiation and elongation phases of DNA replication. MCM2 S108 is phosphorylated by ATR and ATM in response to stalled replication and DSBs (38). This phosphorylation is thought to be an attempt by the cells to promote the firing of local dormant replication origins via Plk1 in order to ensure complete replication (39). We monitored MCM2 phosphorylation for response to polyamide-induced replication stress. Treatment with

polyamide **1** or **2** resulted in a time-dependent increase of MCM2 S108 phosphorylation (Figure 2.7A). The level of MCM2 phosphorylation observed after 36 h polyamide treatment was similar to that observed after 2 h HU treatment. Polyamide-induced

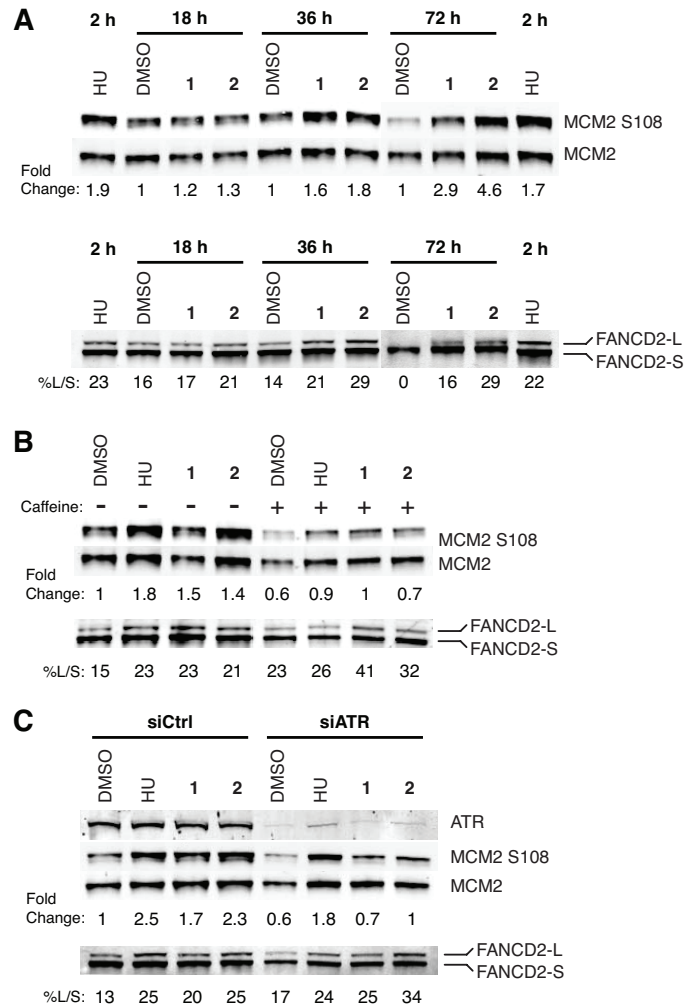


Figure 2.7 Polyamides induce phosphorylation of MCM2 and FANCD2 monoubiquitination. **(A)** MCM2 S108 phosphorylation and FANCD2 monoubiquitination levels were measured in DU145 cells treated with 4 mM HU for 2 h, and DMSO, 10 μ M polyamide **1** or 1 μ M polyamide **2** over a time course of 18, 36, and 72 h. Monoubiquitination was estimated by normalizing the band intensity of the large molecular weight monoubiquitinated FANCD2 band (FANCD2-L) to the low molecular weight non-ubiquitinated FANCD2 band (FANCD2-S). **(B)** MCM2 S108 phosphorylation and FANCD2-Ub levels were measured in cells treated with 4 mM HU for 2 h, and DMSO, 10 μ M polyamide **1** or 1 μ M polyamide **2** for 36 h with or without the addition of 2 mM caffeine. **(C)** MCM2 S108 phosphorylation and FANCD2-Ub levels were measured in cells treated with negative control or ATR-targeting siRNA for 48 h prior to the addition of 4 mM HU for 2 h, and DMSO, 10 μ M polyamide **1** or 1 μ M polyamide **2** for 36 h.

MCM2 S108 phosphorylation was also inhibited by co-treatment with caffeine (Figure 2.7B). To determine the contribution of ATR to MCM2 phosphorylation, ATR was knocked down using siRNA prior to polyamide treatment, and similar levels of inhibition were observed as under caffeine treatment (Figure 2.7C). We also investigated the contributions of ATR and ATM to MCM2 phosphorylation using the small molecule kinase inhibitors NU6027 and KU55933. Both inhibitors reduced MCM2 phosphorylation levels induced by HU or polyamide, with a stronger effect from NU6027 (Figure 2.8A). Together, these observations suggest that ATR is the predominant mediator of polyamide-induced MCM2 phosphorylation.

Recently, the FA/BRCA pathway protein FANCD2 was implicated in a general replisome surveillance mechanism (40). In response to replication stress, FANCD2 undergoes ATR-dependent monoubiquitination (41), which is critical for prolonged localization to chromatin at stalled replication forks (40,42). FANCD2 functions to protect stalled forks from degradation (42) and physically interacts with phosphorylated MCM2 (40), though interaction with MCM2 is not dependent upon monoubiquitination. This led us to search for polyamide-induced monoubiquitination of FANCD2 as a marker of FA/BRCA pathway activation. Treatment with polyamide **1** or **2** caused a time-dependent increase in monoubiquitinated FANCD2 (FANCD2-Ub) (Figure 2.7A). FANCD2-Ub was present in vehicle treated samples, which is perhaps a consequence of DU145 cells' endogenous genomic instability. Surprisingly, inhibition of ATR through the use of caffeine or siRNA both failed to decrease the level of polyamide-induced FANCD2-Ub (Figure 2.7B and C). In addition, the ATR inhibitor NU6027 increased the

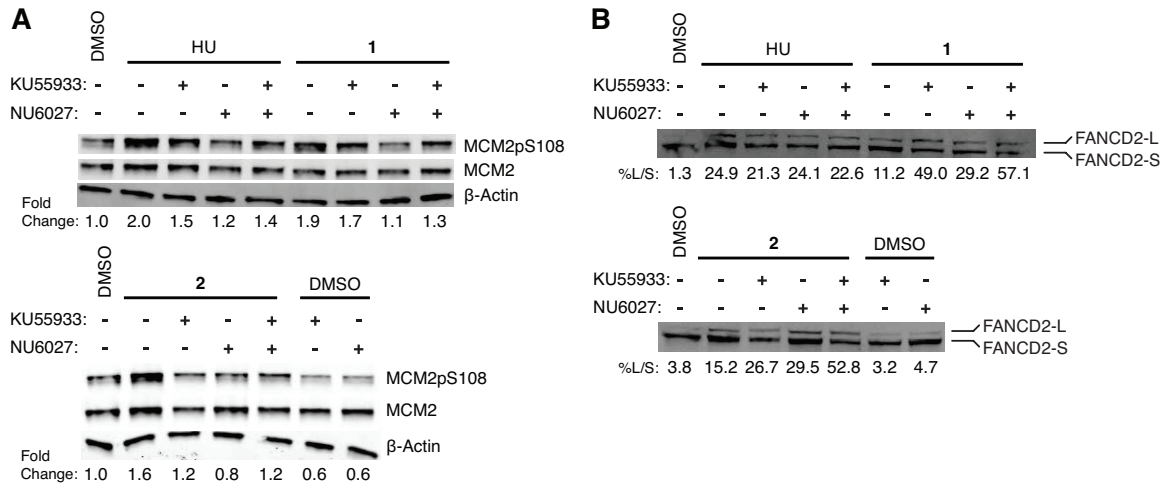


Figure 2.8 Effects of ATM- and ATR-specific small molecule inhibitors on polyamide-induced MCM2 S108 phosphorylation and FANCD2 monoubiquitination. **(A)** MCM2 S108 phosphorylation levels were measured in DU145 cells treated with 4 mM HU for 2 h, and DMSO, 10 μ M polyamide **1** or 1 μ M polyamide **2** for 36 h in addition to 10 μ M KU55933 (KU, ATM inhibitor), 10 μ M NU6027 (NU, ATR inhibitor), or both KU and NU. Only 4 μ M KU and 4 μ M NU were used when both inhibitors were added together to reduce toxicity. **(B)** FANCD2-Ub levels were measured in selective kinase inhibitor-containing lysates. Monoubiquitination was estimated by normalizing the band intensity of the large molecular weight monoubiquitinated FANCD2 band (FANCD2-L) to the low molecular weight non-ubiquitinated FANCD2 band (FANCD2-S).

fraction of FANCD2-Ub in response to polyamide treatment (Figure 2.8B). These results may be unique to DU145 cells, as ATR knockdown by siRNA has been shown to abrogate FANCD2 ubiquitination in the presence of high levels of replication fork damage caused by 12 h treatment of HU or mitomycin C (MMC) in U2OS cells (43). The ATM inhibitor KU55933 similarly increased FANCD2-Ub levels when co-treated with polyamides, though this result is consistent with previous studies (Figure 2.8B) (44).

Next, we confirmed the functional role of FANCD2 in resisting the toxic effects of polyamides in a model outside of prostate cancer. The FANCD2 deficient fibroblast cell line PD20 complemented with an empty vector exhibited greater sensitivity to

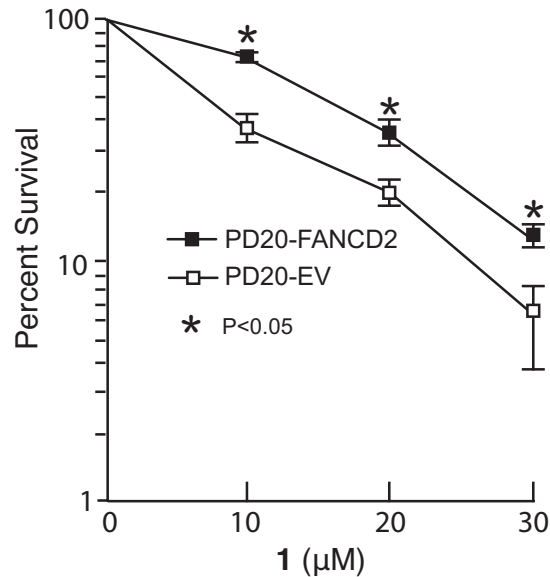


Figure 2.9 FANCD2 increases cell survival after exposure to polyamide **1**. PD20 cells complemented with empty vector (PD20-EV) or FANCD2 (PD20-FANCD2) were treated with the indicated concentrations of polyamide **1** for 36h and assayed for survival after 14 days. Error bars indicate mean \pm SEM for n=3 independent experiments. Unpaired T-tests were performed at *P<0.05.

polyamide treatment than PD20 cells complemented with a FANCD2-expressing vector (Figure 2.9). Together, these data support the conclusion that MCM2 and FANCD2 participate in the response to polyamide-induced replication stress in addition to ATR.

We also tested whether FANCD2 participated in the S-phase accumulation observed in response to polyamide treatment. Similar to Figure 2.3F, we tested whether knockdown of FANCD2 by siRNA prior to the addition of polyamides **1** or **2** would prevent cells from accumulating in S-phase (Figure 2.10). Knockdown of FANCD2 did not prevent cells from accumulating in S-phase, therefore suggesting that its role in the stress response is not necessarily to activate the intra-S-phase checkpoint to prevent cells from entering G2.

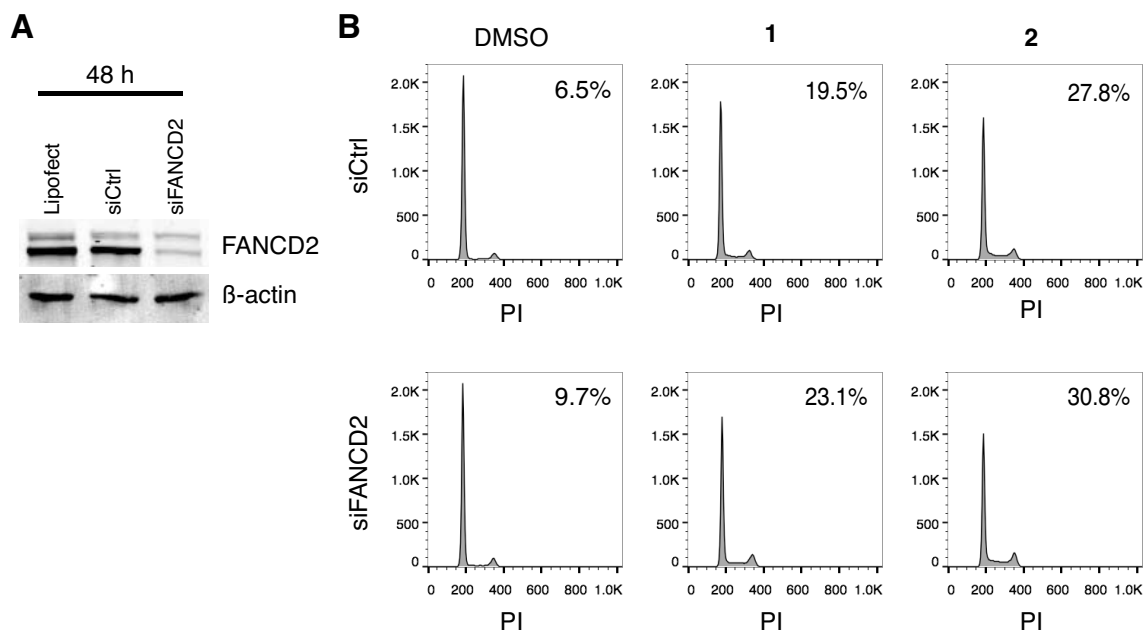


Figure 2.10 Knockdown of FANCD2 by siRNA does not prevent the accumulation of DU145 cells in S-phase in response to polyamide treatment. **(A)** Immunoblot depicting the knockdown of FANCD2 by treatment with 25 nM siRNA for 48 h. **(B)** DNA histograms of propidium iodide (PI) stained DU145 cells after treatment with negative control or ATR-targeting siRNA for 48 h followed by treatment with DMSO, 10 μ M polyamide **1**, or 1 μ M polyamide **2** for 36 h. The percentage of cells in S-phase is included at the top right of each graph.

Polyamide 1 inhibits T7 gp4A helicase activities in vitro.

The results from cell culture experiments suggested a model in which polyamides stall replication forks without causing extensive ssDNA or DNA breaks and that the ATR and the FA/BRCA pathways are activated. The high affinity DNA-binding properties of polyamides coupled with limited ssDNA formation suggested that polyamides might inhibit unwinding of the replication fork. To test this hypothesis, we determined the ability of polyamide **1** to inhibit DNA helicases *in vitro*. We first studied a strong replicative, hexameric helicase similar to the MCM2-7 complex. Testing both polyamides was deemed unnecessary for this particular study, as both polyamides **1** and **2** have comparable binding affinities *in vitro*, as shown by a duplex DNA thermal stabilization assay (Figure 2.11). We used T7 gp4A, the well-studied T7 phage homohexameric

replicative helicase (45). We followed unwinding of a forked duplex DNA substrate containing either a single match site or no match sites for polyamide **1** by gel electrophoresis (45). Helicase inhibition was measured by the percent of unwound substrate relative to the mock treated sample. Incubating polyamide **1** with the substrate containing the match site resulted in effective inhibition of gp4A helicase activity ($IC_{50} \sim 5\text{nM}$) (Figure 2.12A, top). The polyamide was still able to inhibit gp4A helicase activity on the mismatch substrate but required significantly higher concentrations of polyamide ($IC_{50} \sim 335\text{ nM}$), owing to the sequence specificity of polyamides (Figure 2.12A, bottom). Similar results were also obtained when using a different class of helicase, *S. cerevisiae* Dna2 (Figure 2.13). These results suggest that the polyamide is not directly interacting with the helicases but acts through DNA binding.

The sequence specific non-covalent binding nature of polyamides led us to hypothesize that helicase inhibition would not only be stronger at a given concentration when comparing the match to the mismatch substrate but that the enzyme would also show slower unwinding kinetics given the polyamide's longer dwell time at a match site.

A			B			C		
5' -TCGC AGAACA GCGA-3'			5' -GT AGAACA GCGACC-3'			5' -C AGAACA GCAGTCG-3'		
3' -AGCG TCTTGT CGCT-5'			3' -CA TCTTGT CGCTGG-5'			3' -G TCTTGT CGTCAGC-5'		
$T_m = 61.7 (\pm 0.4) ^\circ\text{C}$			$T_m = 61.4 (\pm 0.3) ^\circ\text{C}$			$T_m = 61.3 (\pm 0.5) ^\circ\text{C}$		
	$T_m (^{\circ}\text{C})$	$\Delta T_m (^{\circ}\text{C})$		$T_m (^{\circ}\text{C})$	$\Delta T_m (^{\circ}\text{C})$		$T_m (^{\circ}\text{C})$	$\Delta T_m (^{\circ}\text{C})$
1	76.7(± 0.1)	14.9	1	74.8(± 0.1)	13.3	1	73.5(± 0.4)	12.1
2	76.2(± 0.2)	14.4	2	74.4(± 0.2)	12.9	2	74.2(± 0.3)	12.8

Figure 2.11 Py-Im Polyamides stabilize duplex DNA regardless of match site position in the duplex. DMSO or 4 μM polyamide was incubated with 2 μM 14 bp duplex DNA containing only a single 5'-WGWWCW-3' binding site positioned either 4 bps (A), 2 bps (B), or 1 bp (C) from the edge and a melting curve was measured using DNA hyperchromicity (46). The average melting temperature and standard deviation were calculated from four replicates.

when allowed to incubate longer (Figure 2.12C, right). These data support helicase inhibition as one explanation for how polyamides cause replication stress.

2.3 Discussion

In the present study we determine that hairpin Py-Im polyamides designed to target the AR:DNA interface are cytotoxic and cause replication stress in androgen-insensitive DU145 cells. Polyamide-induced replication stress causes the accumulation of S-phase cells and PCNA foci, decreased replication, and triggers chromatin loading and activation of ATR. The ssDNA-binding protein subunit, RPA2, and the downstream effector kinase, Chk1, were not phosphorylated in response to polyamide treatment, even at high concentrations and after long incubations. ATR did, however, phosphorylate the MCM helicase subunit, MCM2. In addition, the phospho-MCM2 binding partner and FA/BRCA family member, FANCD2, was monoubiquitinated following polyamide treatment. ATR activation also led to phosphorylation of Rad17, the major subunit of the checkpoint clamp loader. In sum, the polyamide-induced checkpoint response, like that induced by nucleotide depletion, requires the general replisome surveillance pathway involving FANCD2, but does not also require the canonical Chk1 pathway that nucleotide depletion activates to mitigate the stress. Consistent with the DNA helix altering and duplex stabilization properties of polyamides, we showed that polyamides inhibit a hexameric replicative helicase *in vitro* and postulate a model in which non-covalently binding polyamides intermittently preclude replisome progression, resulting in a limited ATR checkpoint response (Figure 2.14A).

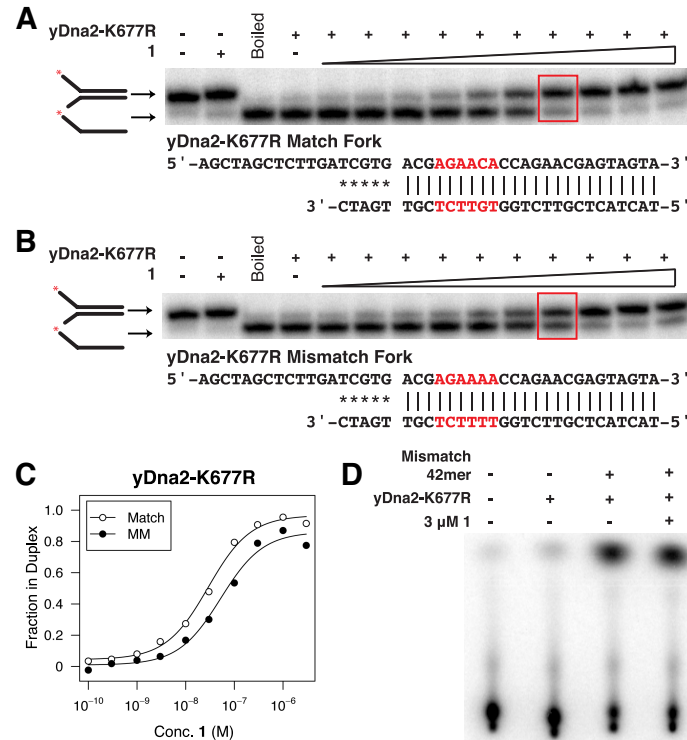


Figure 2.13 Polyamide **1** inhibits helicase activity of *S. cerevisiae* Dna2 nuclease dead but helicase active mutant (yDna2-K677R). Inhibition of yDna2-K677R by polyamide **1** was tested using a forked DNA duplex containing either one match-binding site (**A**) or no match-binding site (**B**). 32 P is represented in the cartoon of the substrate by the red asterisk. Polyamide **1** was added in increasing concentrations (lanes 4-14): 100 pM, 300 pM, 1 nM, 3 nM, 10 nM, 30 nM, 100 nM, 300 nM, 1 μ M, 3 μ M. (**C**) Graphical representation of yDna2-K677R inhibition curves. (**D**) 3 μ M polyamide **1** was incubated with the single-stranded mismatch DNA oligomer and yDna2-K677R to assess whether polyamide **1** can inhibit yDna2-K677R ATPase activity.

When activated at a stalled replication fork, ATR is critical for protection of the forks from collapse. ATR also suppresses the firing of dormant origins globally, presumably to prevent further replication-associated damage (6). Recently, Koundrioukoff *et al.* (47) reported that ATR could be activated in discrete stages. Low concentration aphidicolin treatment, which resulted in moderately reduced fork speeds, led to recruitment of ATR and ATR activators to chromatin as well as delayed mitotic entry but did not result in ssDNA accumulation or Chk1 phosphorylation. In addition, low concentrations of aphidicolin did not induce ATM or H2AX phosphorylation. Based

on the similarity in checkpoint response to polyamides, we propose that polyamides induce low level replication stress leading to ATR recruitment and cell cycle delay decoupled from Chk1 activity.

Although the previous work established that activation of the ATR checkpoint response might occur in the absence of downstream Chk1 activation, it did not identify the mediators of fork protection. Our findings implicate ATR-dependent phosphorylation of MCM2 and FA/BRCA pathway activation, as evidenced by monoubiquitination of FANCD2. ATR-mediated MCM2 phosphorylation has previously been shown to recruit Plk1 to stalled forks, which may allow origin firing near the stall for completion of replication (39). FANCD2 has been shown to bind nascent DNA at sites of replication stalling due to nucleotide depletion and, importantly, restrains replisome progression to minimize ssDNA accumulation (40,48). FANCD2 bound to nascent DNA interacts transiently but directly with the MCMs, including phosphorylated MCM2, though this interaction does not depend on monoubiquitination of FANCD2 (40). However, this interaction was shown to depend on ATR activity. It is interesting that polyamide-induced FANCD2 monoubiquitination in DU145 cells was not inhibited upon knockdown of ATR. The current model of FA/BRCA pathway activation, based on studies in U2OS osteosarcoma cells, DT40 chicken B cells, and *in vitro* assays, links ATR to downstream FANCD2 monoubiquitination through the phosphorylation of FANCI, a FANCD2 paralog, in the presence of catastrophic interstrand crosslinking damage or long term treatment with HU (41,43,49). It is possible that replication stress may trigger FANCI phosphorylation by a kinase other than ATR in DU145 cells, or that

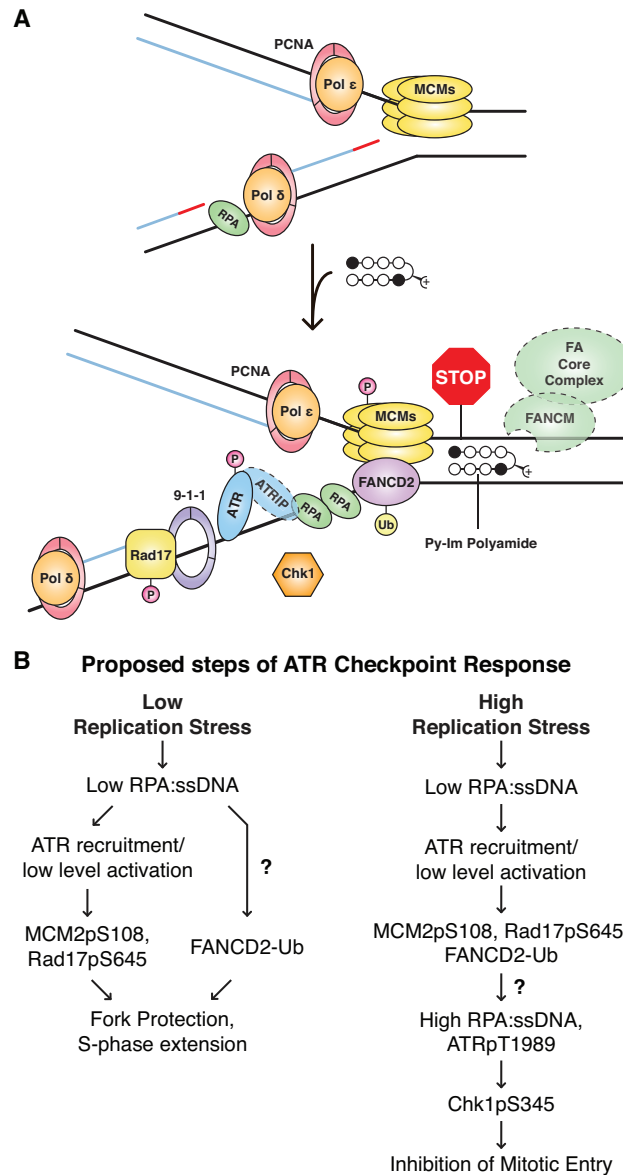


Figure 2.14 Putative model of Py-Im polyamide-induced replication stress and subsequent ATR-dependent checkpoint response. **(A)** Polyamides bind transiently at match sites throughout the genome, distorting the structure of the helix locally and precluding the progression of the replisome when encountering a fork. Stalled replication fork components that were not investigated directly (except polymerases) are outlined in dashed lines. **(B)** Proposed steps of ATR checkpoint response under low replication stress, such as polyamide treatment, or high replication stress, such as high concentration HU treatment. Our data supports the model for stepwise activation of ATR. First, ATR is recruited to chromatin and moderately phosphorylated, leading to MCM2 phosphorylation and Rad17 phosphorylation. FANCD2 is also monoubiquitinated and recruited to chromatin for fork protection. Then, if the stress is sufficiently high, such that replication forks are persistently stalled, ssDNA accumulation and higher ATR T1989 phosphorylation occur, followed by downstream phosphorylation of Chk1 by ATR. What triggers the switch leading to ssDNA accumulation and ATR-Chk1 activation is unclear.

FANCI is an ATR substrate under more severe forms of replication stress. However the FA/BRCA pathway is activated, our results suggest that the FA/BRCA pathway acts in concert with ATR-MCM2 signaling to stabilize replication forks in response to polyamide treatment. The lack of ATR-dependence on polyamide-induced S-phase accumulation is also notable, but consistent with published studies in U2OS cells treated with HU (43). Investigating the effects of knockdown of FA family genes on ssDNA formation and cell cycle phase distribution in polyamide-treated cells would be of interest for future studies.

In order to understand how ATR-MCM2 and FA/BRCA activation is related to ATR-Chk1 activation, we compared the checkpoint response induced by low replication stress, such as polyamide treatment, and high replication stress, such as high concentration HU treatment (Figure 2.15). Both treatments result in MCM2 phosphorylation and FANCD2 monoubiquitination (Figure 2.7), as well as recruitment of equivalent amounts of ATR and its mediators to chromatin (Figure 2.3E). However, polyamide treatment resulted in significantly lower levels of ssDNA formation (Figure 2.3C and D). Our data suggest that polyamide treatment either induces sufficient ssDNA for ATR recruitment, or perhaps triggers an alternative or cooperative mechanism to recruit ATR-ATRIP to DNA. The amount of ssDNA is also sufficient for partial ATR activation, as indicated by Rad17 phosphorylation. We hypothesize that only in the presence of higher levels of ssDNA is ATR fully activated and Chk1 phosphorylated, in keeping with the fact that Chk1 phosphorylation depends on the formation of long ssDNA gaps (50). Polyamide treatment also induced much lower levels of ATR T1989

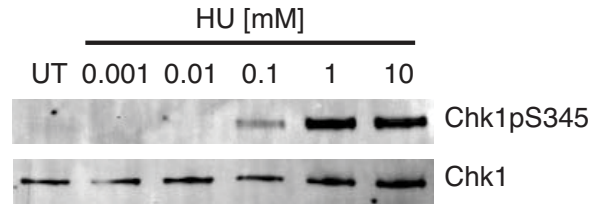


Figure 2.15 Dose-dependent increase in hydroxyurea (HU)-induced Chk1 S345 phosphorylation. Chk1 S345 phosphorylation was measured in DU145 cells treated with increasing doses of HU for 2 h. Chk1 S345 is maximally phosphorylated at 1 mM or higher HU.

phosphorylation than did HU treatment. This correlates as well with the lack of Chk1 phosphorylation, which requires robust ATR T1989 autophosphorylation (24,25), and is consistent with a model for quantitative regulation of ATR (25). ATR T1989 phosphorylation has actually been shown to be dispensable for ATR recruitment, Rad17 S645 phosphorylation, and recovery from transient replication stress (24,25). Based on these data, we conclude that ATR-MCM2 and FANCD2 signaling are sufficient to induce some fork protection. However, ATR-Chk1 cell cycle checkpoint activation requires ssDNA accumulation and extensive ATR T1989 phosphorylation, which is observed under higher replication stress (Figure 2.14B). While it is unclear what causes ssDNA accumulation and ATR-Chk1 activation, some possible causes are uncoupling of polymerase and helicase, accumulation of excess primers, or nascent DNA degradation.

A few studies have shown previously that the FA/BRCA pathway and the ATR-Chk1 pathway serve non-redundant functions and that their signaling mechanisms are separable. In human primary fibroblasts, Chk1 and FANCD2 both contribute to senescence induction but Chk1 is also responsible for persistent cell cycle arrest in response to psoralen treatment (51). Similarly, knockdown of FANCD2 but not Chk1 sensitizes HeLa cells to cisplatin treatment, despite activation of Chk1 (52). Supporting

the evidence for their different functions, it has been shown that the canonical ATR activators, Rad17 and TopBP1, are necessary for Chk1 phosphorylation but dispensable for FANCD2 monoubiquitination and FANCI phosphorylation in DT40 cells treated with MMC (53). Conversely, the FA core complex is necessary for FANCD2 monoubiquitination but is dispensable for Chk1 phosphorylation (53). Also, the interaction of FANCD2 with the MCMs is not dependent on Chk1 activity (40). Thus, the activation of the FA/BRCA pathway but not Chk1 in response to polyamide treatment appears to reflect a level of stress that does not require intervention by Chk1.

Hairpin Py-Im polyamide-induced replication stress causes what appears to be an intermediate state of ATR-dependent checkpoint response. We suggest that this is due to transient inhibition of replisome progression caused by the polyamide's unique high affinity non-covalent DNA-binding properties. This proposed mode of action distinguishes hairpin Py-Im polyamides from other replication inhibitors such as HU and aphidicolin, and will prove useful for further dissociating the S-phase, essential ATR functions from G2 checkpoint functions. Further delineation of the S-phase specific ATR mediators and effectors involved in protecting replication forks can be determined as distinct from or coordinated with those involved in cell cycle slowing.

2.4 Materials and Methods

Chemicals and reagents.

Hairpin Py-Im polyamides **1** and **2** were synthesized on solid phase Kaiser oxime resin using previously published protocols (54). Gemcitabine, etoposide, hydroxyurea,

and doxorubicin were purchased from Sigma-Aldrich, as were all other reagents unless otherwise noted.

Antibodies purchased from Santa Cruz Biotech were mouse anti-PCNA, anti-Chk1, anti-RPA2, anti-Rad17, anti-FANCD2, goat anti-ATR, and rat anti-BrdU (CldU cross-reactivity). Antibodies purchased from Bethyl were rabbit anti-H2AX, anti-MCM2, anti-MCM2pS108, and anti-RPA2pS4/S8. Antibodies purchased from Abcam were: rabbit anti-FANCD2, anti-MCM2pS108, anti-Rad9, anti-RPA2pS33, anti-Chk2, anti-H2AXpS139. Antibodies purchased from Cell Signaling Technologies were rabbit anti-ATMpS1981, anti-Rad17pS645, anti-Chk1pS345, anti-Chk1pS317, anti-Chk1pS296. Rabbit anti-Chk2pT68 was purchased from Millipore. Rabbit anti-ATM was purchased from Calbiochem. Rabbit anti-ATRpT1989 was a gift of Prof. Lee Zou.

Cell culture conditions.

LNCaP, LNAR, and DU145 cells were maintained in RPMI 1640 (Invitrogen) with 10% FBS (Irvine Scientific) at 37 °C under 5% CO₂. LNCaP and DU145 cells were purchased from ATCC (Manassas, VA). LNAR cells were a gift from C.L. Sawyers at Memorial Sloan-Kettering Cancer Center (NY, NY).

Cytotoxicity assay.

C₅₀ values for cytotoxicity were determined using a sulfarhodamine-based colorimetric assay for cellular protein content in 96-well microplates (55). LNCaP and LNAR cells were plated at 3,000 or 4,000 cells per well for the 72 h and 96 h time points,

respectively. DU145 cells were plated at 2,000 or 2,500 cells per well. Polyamides were added in 100 μ l RPMI 1640 supplemented with 10% FBS 24 h after plating. Quadruplicate wells were used for each concentration. Cells were fixed with 100 μ l 10% trichloroacetic acid solution, washed, stained, and dried as described. After solubilization of the bound dye in 10 mM Tris (pH 8), the absorbance was measured at 490 nm on a Victor microplate reader (PerkinElmer).

The cytotoxicity data are charted as a percentage of untreated controls, corrected for background absorbance. IC_{50} is defined as the concentration that inhibits 50% of control cell growth. These values were determined by non-linear least squares regression fit to $Y = A + (B-A)/(1+10^{((\text{Log } EC_{50}-X)*H})}$, where A =max, B =min, and H =Hill Slope. Three independent trials were averaged; stated IC_{50} values represent the mean and standard deviation. These calculations were performed using Prism 4 (GraphPad) software.

Caspase 3/7 activation assay.

DU145 cells were plated in 96-well microplates at 2,000-8,000 cells per well. As above, polyamides and controls were added 24 h after plating. Each timepoint was assayed in triplicate. At harvest, Caspase 3/7 activity was assessed using 100 μ l of Caspase-Glo reagent (Promega), which contains the proluminescent caspase substrate DEVD-aminoluciferin. Luminescence was measured after 30 min incubation at room temperature. Luminescence data are expressed as a fold difference from untreated controls as measured using a Victor microplate reader (PerkinElmer). The cell viability of

each treatment condition was monitored in a sister plate using a tetrazolium-based assay for mitochondrial bio-reductive capacity (56). 10 μ l WST-1 reagent (Roche) was added to each well and incubated at 37 °C for 30 min before measuring the absorbance at 450 nm. The WST-1 data are corrected for background absorbance and expressed as a percentage of untreated controls.

PARP cleavage assay.

400,000 DU145 cells were plated in 10 cm diameter dishes. Polyamides were added after 24 h and were allowed to incubate an additional 72 h. At harvest, cells were washed once with PBS then treated with 400 μ l ice-cold lysis buffer (20 mM Tris-HCl pH 7.5, 150 mM NaCl, 1 mM Na₂EDTA, 1 mM EGTA, 1% Triton, 2.5 mM sodium pyrophosphate, 2 mM β -glycerophosphate, 1 mM Na₃VO₄, 1 μ g/ml leupeptin, 1 mM PMSF) for 5 min at 5°C. The lysate was sonicated for 15 s and then centrifuged for 10 min at 20,000 x g at 5°C. The supernatant was retained. Protein concentrations were determined by Bradford assay (Bio-Rad) using bovine serum albumin (Bio-Rad) to create a standard curve. PARP cleavage was assayed by sandwich ELISA (Cell Signaling Technology) and performed according to the manufacturer's recommendations. 10 μ g total protein was loaded into each well of a microplate coated with anti-cleaved PARP (Asp214) mouse mAb and allowed to incubate overnight at 5°C. Rabbit anti-PARP mAb was then added, followed by anti-rabbit IgG conjugated to HRP. Triplicate wells were included for each condition, and the data are representative of both experimental replicates. The data are expressed as fold change from the untreated condition, showing the mean and standard deviation of each measurement.

Cell cycle analysis.

800,000 DU145 cells were plated in 10 cm diameter dishes for 24 h before treatment with polyamides for an additional 24 h. Cells were pulsed with 10 μ M EdU 30 min before harvest to estimate rate of DNA synthesis. Cells were trypsinized and pelleted at 300 x g with cell culture supernatant. Following overnight fixation in 70% ethanol, the cells were rehydrated in 1% BSA/PBS and processed with the Click-it EdU Alexa Fluor 488 Flow Cytometry assay kit (Invitrogen) using half the recommended A488 reagent. After overnight treatment with 0.2 mg/ml RNase A in 1% BSA/PBS, the cells were stained for DNA content with 7-aminoactinomycin D and analyzed on a FACSCalibur (Becton-Dickinson) instrument. The data were analyzed using FlowJo v9.5.3 (TreeStar) and are representative of two trials. Monoparametric, propidium iodide, flow cytometry was also used to evaluate the effect of polyamides **1** and **2** on cell cycle distribution. DU145 cells were treated with 1-100 μ M of polyamide **1** or 0.1-10 μ M of polyamide **2** for 48 h. The effect of PI3 kinases on cell cycle distribution was measured by treating DU145 cells with 10 μ M polyamide **1** or 1 μ M polyamide **2** as well as 2 mM caffeine, 4 or 10 μ M NU6027 (Calbiochem) and 4 or 10 μ M KU55933 (Calbiochem) for 36 h. Data were analyzed using FlowJo and fitted to the Watson (Pragmatic) model. The data are representative of two trials.

Knockdown of ATR and FANCD2 by siRNA.

ATR was knocked down for cell cycle analysis and immunoblot experiments using 20 nM Silencer Select siRNA against ATR (Ambion, s536) and RNAiMAX

lipofectamine (Life Technologies) according to the manufacturer's protocol. 20 nM Silencer Select Negative Control #1 (Ambion) was used as a control. FANCD2 was knocked down using 25 nM Dharmacon SMARTpool, siGENOME Human FANCD2 (2177). 25 nM siGENOME Non-Targeting Pool #1 was used as a control. Briefly, the siRNA was incubated for 48 h, with a media swap after the first 24 h, prior to the addition of 10 μ M polyamide **1** or 1 μ M polyamide **2** for an additional 36 h. Efficiency of knockdown was determined by western blot.

PCNA (Proliferating Cell Nuclear Antigen) immunocytochemistry.

PCNA immunocytochemistry experiments were performed as in (23). Briefly, DU145 cells were plated in 4-well glass chamber slides (Lab-Tek) at 70,000 cells per well. Polyamide **1** was added at a final concentration of 10 μ M and polyamide **2** at a final concentration of 1 μ M with 0.2% DMSO. After fixation, permeabilization, and blocking, cells were incubated with mouse PCNA mAb at a 1:500 dilution at 4°C overnight. Cells were then washed, followed by incubation with Alexa Fluor 488-conjugated donkey anti-mouse IgG (Life Technologies) at a 1:400 dilution at room temperature for 2 h. Cells were washed and mounted with Prolong Gold Anti-Fade reagent with DAPI (Life Technologies). Images were obtained using a Zeiss LSM 510 Meta NLO with Coherent Chameleon and a Plan-Apochromat 63x 1.4-numerical aperture oil immersion objective lens and processed using the LSM Browser software package. Foci were counted using the open source Python software, FociCounter (<http://focicounter.sourceforge.net/>). Parameters were kept constant across all conditions for a particular replicate, but differed slightly over the three replicates to account for differences in staining. Cells that were

likely positive but sufficiently out of focus so as to not produce distinct foci were not counted. Kruskal-Wallis test was performed using Prism 4 (Graphpad) software.

Assessment of phosphorylation of proteins by immunoblot.

800,000 DU145 cells were plated in 10 cm diameter dishes and allowed to adhere for 24 h before treatment with 0.1% DMSO, polyamide **1**, or polyamide **2** for the indicated time. Cells were lysed in TBS-Tx buffer (50 mM Tris-HCl pH 7.4, 150 mM NaCl, 1 mM EDTA, 1% Triton X-100) containing fresh protease inhibitors (Roche), 1 mM PMSF, phosphatase inhibitors, and 10 mM N-ethylmaleimide. The samples were quantified by Bradford assay, denatured by boiling in Laemmli buffer, and total protein was separated by SDS-PAGE on 4-15% gradient polyacrylamide gels (Bio-rad). After transfer to the nitrocellulose (Bio-rad) or PVDF (Millipore) membrane and blocking with Odyssey Blocking Buffer (Li-Cor), primary antibodies were incubated overnight at 4°C. Donkey anti-rabbit, Donkey anti-mouse, or donkey anti-goat 800CW IR dye-conjugated secondary antibody (Li-Cor) was added and the bands were visualized on an Odyssey infrared imager (Li-Cor). For assessment of MCM2 and FANCD2 modification, plates treated with either DMSO, polyamide **1**, polyamide **2**, or polyamide plus 2 mM caffeine, 10 μ M KU55933 (KU, ATM inhibitor), or 10 μ M NU6027 (NU, ATR inhibitor) were added together and harvested at the indicated times. For hydroxyurea (HU) treatment, cells were incubated with the indicated inhibitor for 34 h prior to the addition of HU for the final 2 h before harvesting at 36 h. ATR immunoprecipitation was performed using pre-cleared Protein G agarose beads (Pierce) and either normal goat IgG or ATR (N19)

antibodies (Santa Cruz) overnight at 4°C. All immunoblots and accompanying quantifications are representative of at least two biological replicates.

Chromatin fractionation assay.

2 x 10⁶ DU145 cells were plated in 15 cm diameter dishes and allowed to adhere for 24 h, followed by treatment with 0.1% DMSO, 10 μM polyamide **1**, 1 μM polyamide **2**, or 10 mM HU for indicated times. Chromatin fractions were prepared according to published protocols(57). Briefly, cells were harvested, washed with PBS, and resuspended with 400 μL buffer A (10 mM HEPES pH 7.9, 10 mM KCl, 1.5 mM MgCl₂, 0.34M sucrose, 10% glycerol, 1 mM DTT, and fresh protease and phosphatase inhibitors). Triton X-100 was added to a final concentration of 0.1% and incubated on ice for 5 min followed by centrifugation at 1,300 x g for 4 min to pellet the nuclei. Nuclei were washed with buffer A and then lysed with 400 μL buffer B (3 mM EDTA, 0.2 mM EGTA, 1 mM DTT) for 10 min on ice. Chromatin was pelleted by centrifugation at 1,700 x g for 4 min. Isolated chromatin was washed once with buffer B and spun down at 10,000 x g for 1 min. The supernatant is completely removed and the chromatin pellet was resuspended in 300 μL SDS sample buffer and sheared for 20 s at 25% amplitude with a microtip adapter. Samples were then incubated at 80°C and analyzed by SDS-PAGE and immunoblot.

5-chloro-2'-deoxyuridine immunocytochemistry.

20,000 or 50,000 DU145 cells were plated in 4-well glass chamber slides and allowed to adhere for 24 h. Cells were incubated with 50 μM CldU for 48 h then the

media was swapped and polyamide added. Following polyamide treatment, cells were washed, fixed with 2% formaldehyde (Ted Pella), and permeabilized with 0.2% Triton X-100. Following permeabilization, cells were blocked with 3% goat serum with 0.1% Triton for 45 min at room temperature. After blocking, cells were washed with 0.1% Triton and then incubated with rat anti-BrdU antibody (ICR1) at a concentration of 10 $\mu\text{g}/\text{mL}$ in 3% goat serum for 30 min at 37°C. After washes, cells were incubated with chicken anti-rat Alexa488 antibody at a concentration of 4 $\mu\text{g}/\text{mL}$. Finally, cells were washed, mounted, and then imaged as in PCNA staining above. Cells were scored as positive for ssDNA if >10 foci were counted. 150 cells were counted per condition over three biological replicates.

Single cell alkaline gel electrophoresis.

The apparatus and reagent kit were purchased from Trevigen. The assay was performed according to the manufacturer's recommendations. Briefly, 800,000 DU145 cells were plated in 10 cm diameter dishes for 24 h before treatment with polyamides for an additional 36 h. Cells were harvested by trypsinization and washed once with cold PBS before being suspended in 37°C low-melting point agarose at 1×10^5 cells/ml. An aliquot of the suspension was placed on a 37°C glass slide and allowed to cool for 30 min. The slides were bathed in lysis buffer for 30 min followed by a 30 min treatment with alkaline unwinding buffer (200 mM NaOH, 1 mM EDTA) at 5°C. The slides were subjected to electrophoresis at 21V in a prechilled apparatus and fresh unwinding buffer for 30 min. The slides were washed twice in water and once in 70% ethanol, then dried for 30 min. at 37 °C. Dried slides were stained with 1X SYBR Gold in TE buffer for 30

min at room temperature, and excess dye was removed by blotting. Slides were dried and stored at room temperature with desiccant. Comets were visualized using a Zeiss LSM 510 Meta NLO confocal microscope with a 5x objective (Zeiss) and scored using Comet Assay IV image analysis software (Perceptive). A random sampling of 400 cells from two biological replicates were analyzed for each condition. The data are displayed as a box and whisker diagram showing median and middle quartiles with whiskers at the min and max.

T7 gp4A helicase assays.

Helicase assays using T7 gp4A (BioHelix) were performed as published in (45). First, 40 pmol of a 75mer oligonucleotide was labeled with [γ - 32 P]ATP (MP Biomedicals) using T4 polynucleotide kinase (NEB) and annealed to 80 pmol of a 95mer oligonucleotide with 56 complementary bases to form a forked substrate in STE buffer (100 mM NaCl, 10 mM Tris-HCl, 1 mM EDTA). The forked substrate was purified by extraction from a 10% non-denaturing acrylamide gel. To assess polyamide effects on gp4A helicase activity, the forked substrate (1:1000 dilution final) was incubated in a 10 μ l volume with increasing concentrations of polyamide **1** (DMSO solution, 5% final concentration) in 1x reaction buffer (BioHelix) for 1 h at room temperature prior to addition of gp4A at a final concentration 143 ng/ml (\sim 2.27 nM) and incubated at 30°C for 10 min. The mock treated helicase reaction contained 5% DMSO with no polyamide. Reactions were stopped with the addition of 5 μ l stop buffer (60 mM EDTA, 40% sucrose, 0.6% SDS, 0.25% bromphenol blue, and 0.25% xylene cyanole FF). Unwound labeled single-stranded 75mer was separated from the intact fork substrate on a pre-run

10% non-denaturing acrylamide gel at 200 V for 1 h. The gel was then placed on a PhosphorImager screen (Molecular Dynamics) overnight and imaged on a Storm Molecular Imager. Match 75mer: 5'-CGC CGG GTA CCG AGC TCG AAT TCA CTG GCC GTC GTT TTA CAA CGT CGT **GAA CTG** CCT₁₉-3'. Match 95mer: 5'-T₃₉GGC **AGT TCA** CGA CGT TGT AAA ACG ACG GCC AGT GAA TTC GAG CTC GGT ACC CGG CG-3'. Mismatch 75mer: 5'-CGC CGG GTA CCG AGC TCG AAT TCA CTG GCC GTC GTT TTA CAA CGT CGT **GAC ATG** CCT₁₉-3'. Mismatch 95mer: 5'-T₃₉GGC **ATG TCA** CGA CGT TGT AAA ACG ACG GCC AGT GAA TTC GAG CTC GGT ACC CGG CG-3'.

S. cerevisiae Dna2-K677R helicase assay.

S. cerevisiae K677R Dna2 (yDna2-K677R), lacking nuclease activity, was prepared and helicase assays were performed similarly to (58). First, 40 pmol of a 42mer oligonucleotide was labeled with [γ -³²P]ATP (MP Biomedicals) and annealed to 80 pmol of a 29mer oligonucleotide with 24 complementary bases to form a forked substrate in STE buffer. To assess polyamide effects on yDna2-K677R helicase activity, the forked substrate (1:2000 dilution final) was incubated in a 20 μ l volume with increasing concentrations of polyamide **1** (DMSO solution, 5% final concentration) in 1x reaction buffer (25 mM Tris-HCl (pH 7.5), 2 mM MgCl₂, 2 mM DTT, 0.25 mg/ml BSA, 2 mM ATP) for 1 h at room temperature prior to addition of 150 fmol yDna2-K667R and incubated at 37°C for 30 min. The mock treated helicase reaction contained 5% DMSO with no polyamide. Reactions were stopped with the addition of 5 μ l stop buffer. Unwound labeled single-stranded 42mer was separated from the intact fork substrate on a

pre-run 20% non-denaturing acrylamide gel run at 150 V for 3 h. The gel was then placed on a PhosphorImager screen overnight and imaged on a Storm Molecular Imager. Match 42mer: 5'-AGC TAG CTC TTG ATC GTG ACG **AGA ACA** CCA GAA CGA GTA GTA-3'. Match 29mer 5'-TAC TAC TCG TTC TGG **TGT TCT** CGT TGA TC-3'. Mismatch 42mer: 5'-AGC TAG CTC TTG ATC GTG ACG **AGA AAA** CCA GAA CGA GTA GTA-3'. Mismatch 29mer 5'-TAC TAC TCG TTC TGG **TTT TCT** CGT TGA TC-3'.

S. cerevisiae Dna2-K677R ATPase Assay.

The ATPase assay was run as in (58). Briefly, reactions containing 300 fmol of yDna2-K677R protein in 20 μ l of reaction buffer (40 mM Tris-HCl (pH 7.5), 5 mM MgCl₂, 25 mM NaCl, 1 mM DTT, 0.5 mg/ml BSA, 0.2 mM ATP, 10% glycerol, and 3 μ Ci of [γ -³²P]ATP) were supplemented with the mismatch 42mer plus DMSO or 3 μ M polyamide **1** and incubated at 30 °C for 1 h. The reactions were stopped by addition of EDTA. 0.8 μ l of each reaction was spotted onto a polyethyleneimine-cellulose TLC plate (Selecto Scientific) and developed in 0.5 M LiCl, 1 M formic acid solution. The radiolabelled products were detected by PhosphorImager.

Clonogenic assays.

Clonogenic assays were performed with FANCD2-deficient PD20 cells complemented with empty vector (PD20-EV) or FANCD2 (PD20-FANCD2). FANCD2 protein expression and phenotype rescue was previously confirmed (59). Briefly, 1000 cells per well were seeded in a 12 well plate and left to attach overnight. Polyamide **1** (0, 10, 20, 30 μ M) or polyamide **2** (0, 1, 2, 3 μ M) was added for 36 h. Polyamide-containing

media was exchanged for fresh media and cells were cultured for 14 days with media changed every 4 days. Visible colonies were fixed and stained with 1% crystal violet in methanol and enumerated. Three independent experiments were performed.

2.5 Acknowledgments

We thank Dr. Subhash Pokharel for *S. cerevisiae* Dna2-K677R, C. L. Sawyers (University of California, Los Angeles) for the LNAR cell line, and L. Zou for the ATRpT1989 antibody (Harvard Medical School). We thank members of the Dervan and Campbell laboratories for critical reading of the manuscript. We thank members of the Dunphy laboratory for helpful discussions. Mass spectrometry analyses were performed in the Mass Spectrometry Laboratory of the Division of Chemistry and Chemical Engineering at the California Institute of Technology. Imaging was performed at the Caltech Bioimaging Center in the Beckman Institute. Flow cytometry analyses were performed at the Caltech Flow Cytometry Cell Sorting Facility. We thank Rochelle Diamond for support and technical expertise in performing flow cytometry experiments. This work was supported by the National Institutes of Health [R01GM27681 and R01GM51747 to P.B.D., R01GM07866 to J.L.C.]; the Ellison Foundation [AG-SS-2143-08 to J.L.C.]; the Margaret Early Trust [to J.L.C.], the Army Research Office [09-1-0041 to J.L.C.]; T.F.M. is a recipient of a predoctoral fellowship [F31CA159896] from the National Institutes of Health.

2.6 References

1. Ciccia, A. and Elledge, S.J. (2010) The DNA Damage Response: Making It Safe to Play with Knives. *Mol. Cell*, 40, 179-204.
2. Branzei, D. and Foiani, M. (2008) Regulation of DNA repair throughout the cell cycle. *Nat. Rev. Mol. Cell Biol.*, 9, 297-308.
3. Olson, E., Nievera, C.J., Klimovich, V., Fanning, E. and Wu, X. (2006) RPA2 is a direct downstream target for ATR to regulate the S-phase checkpoint. *J. Biol. Chem.*, 281, 39517-39533.
4. Cimprich, K.A. and Cortez, D. (2008) ATR: an essential regulator of genome integrity. *Nat. Rev. Mol. Cell Biol.*, 9, 616-627.
5. Polo, S.E. and Jackson, S.P. (2011) Dynamics of DNA damage response proteins at DNA breaks: a focus on protein modifications. *Genes Dev.*, 25, 409-433.
6. Zeman, M.K. and Cimprich, K.A. (2014) Causes and consequences of replication stress. *Nat. Cell Biol.*, 16, 2-9.
7. Trauger, J.W., Baird, E.E. and Dervan, P.B. (1996) Recognition of DNA by designed ligands at subnanomolar concentrations. *Nature*, 382, 559-561.
8. White, S., Szewczyk, J.W., Turner, J.M., Baird, E.E. and Dervan, P.B. (1998) Recognition of the four Watson-Crick base pairs in the DNA minor groove by synthetic ligands. *Nature*, 391, 468-471.
9. Chenoweth, D.M. and Dervan, P.B. (2010) Structural basis for cyclic Py-Im polyamide allosteric inhibition of nuclear receptor binding. *J. Am. Chem. Soc.*, 132, 14521-14529.
10. Edelson, B.S., Best, T.P., Olenyuk, B., Nickols, N.G., Doss, R.M., Foister, S., Heckel, A. and Dervan, P.B. (2004) Influence of structural variation on nuclear localization of DNA-binding polyamide-fluorophore conjugates. *Nucleic Acids Res.*, 32, 2802-2818.
11. Luck, G., Zimmer, C., Reinert, K.E. and Arcamone, F. (1977) Specific interactions of distamycin A and its analogs with (A-T) rich and (G-C) rich duplex regions of DNA and deoxypolynucleotides. *Nucleic Acids Res.*, 4, 2655-2670.
12. Baraldi, P.G., Beria, I., Cozzi, P., Bianchi, N., Gambari, R. and Romagnoli, R. (2003) Synthesis and growth inhibition activity of alpha-bromoacrylic heterocyclic and benzoheterocyclic derivatives of distamycin A modified on the amidino moiety. *Bioorg. Med. Chem.*, 11, 965-975.

13. Zimmer, C., Puschendorf, B., Grunicke, H., Chandra, P. and Venner, H. (1971) Influence of netropsin and distamycin A on the secondary structure and template activity of DNA. *Eur. J. Biochem.*, 21, 269-278.
14. Beerman, T.A., McHugh, M.M., Sigmund, R., Lown, J.W., Rao, K.E. and Bathini, Y. (1992) Effects of analogs of the DNA minor groove binder Hoechst-33258 on Topoisomerase-II and Topoisomerase-I mediated activities. *Biochim. Biophys. Acta*, 1131, 53-61.
15. Brosh, R.M., Jr., Karow, J.K., White, E.J., Shaw, N.D., Hickson, I.D. and Bohr, V.A. (2000) Potent inhibition of werner and bloom helicases by DNA minor groove binding drugs. *Nucleic Acids Res.*, 28, 2420-2430.
16. Nickols, N.G. and Dervan, P.B. (2007) Suppression of androgen receptor-mediated gene expression by a sequence-specific DNA-binding polyamide. *Proc. Natl. Acad. Sci. USA*, 104, 10418-10423.
17. Yang, F., Nickols, N.G., Li, B.C., Marinov, G.K., Said, J.W. and Dervan, P.B. (2013) Antitumor activity of a pyrrole-imidazole polyamide. *Proc. Natl. Acad. Sci. USA*, 110, 1863-1868.
18. Roche, P.J., Hoare, S.A. and Parker, M.G. (1992) A consensus DNA-binding site for the androgen receptor. *Mol. Endocrinol.*, 6, 2229-2235.
19. Chenoweth, D.M., Harki, D.A., Phillips, J.W., Dose, C. and Dervan, P.B. (2009) Cyclic pyrrole-imidazole polyamides targeted to the androgen response element. *J. Am. Chem. Soc.*, 131, 7182-7188.
20. Xu, Y.Y., Chen, S.Y., Ross, K.N. and Balk, S.P. (2006) Androgens induce prostate cancer cell proliferation through mammalian target of rapamycin activation and post-transcriptional increases in cyclin D proteins. *Cancer Res.*, 66, 7783-7792.
21. Alimirah, F., Chen, J., Basrawala, Z., Xin, H. and Choubey, D. (2006) DU-145 and PC-3 human prostate cancer cell lines express androgen receptor: implications for the androgen receptor functions and regulation. *FEBS Lett.*, 580, 2294-2300.
22. Essers, J., Theil, A.F., Baldeyron, C., van Cappellen, W.A., Houtsmuller, A.B., Kanaar, R. and Vermeulen, W. (2005) Nuclear dynamics of PCNA in DNA replication and repair. *Mol. Cell. Biol.*, 25, 9350-9359.
23. Aggarwal, M., Sommers, J.A., Shoemaker, R.H. and Brosh, R.M., Jr. (2011) Inhibition of helicase activity by a small molecule impairs Werner syndrome helicase (WRN) function in the cellular response to DNA damage or replication stress. *Proc. Natl. Acad. Sci. USA*, 108, 1525-1530.

24. Nam, E.A., Zhao, R.X., Glick, G.G., Bansbach, C.E., Friedman, D.B. and Cortez, D. (2011) Thr-1989 Phosphorylation Is a Marker of Active Ataxia Telangiectasia-mutated and Rad3-related (ATR) Kinase. *J. Biol. Chem.*, 286, 28707-28714.
25. Liu, S.Z., Shiotani, B., Lahiri, M., Marechal, A., Tse, A., Leung, C.C.Y., Glover, J.N.M., Yang, X.H.H. and Zou, L. (2011) ATR Autophosphorylation as a Molecular Switch for Checkpoint Activation. *Mol. Cell*, 43, 192-202.
26. Peasland, A., Wang, L.Z., Rowling, E., Kyle, S., Chen, T., Hopkins, A., Cliby, W.A., Sarkaria, J., Beale, G., Edmondson, R.J. *et al.* (2011) Identification and evaluation of a potent novel ATR inhibitor, NU6027, in breast and ovarian cancer cell lines. *Br. J. Cancer*, 105, 372-381.
27. So, S.R., Davis, A.J. and Chen, D.J. (2009) Autophosphorylation at serine 1981 stabilizes ATM at DNA damage sites. *J. Cell Biol.*, 187, 977-990.
28. Bao, S.D., Tibbetts, R.S., Brumbaugh, K.M., Fang, Y.N., Richardson, D.A., Ali, A., Chen, S.M., Abraham, R.T. and Wang, X.F. (2001) ATR/ATM-mediated phosphorylation of human Rad17 is required for genotoxic stress responses. *Nature*, 411, 969-974.
29. Kozlov, S.V., Graham, M.E., Jakob, B., Tobias, F., Kijas, A.W., Tanuji, M., Chen, P., Robinson, P.J., Taucher-Scholz, G., Suzuki, K. *et al.* (2011) Autophosphorylation and ATM activation: additional sites add to the complexity. *J. Biol. Chem.*, 286, 9107-9119.
30. Hickson, I., Zhao, Y., Richardson, C.J., Green, S.J., Martin, N.M., Orr, A.I., Reaper, P.M., Jackson, S.P., Curtin, N.J. and Smith, G.C. (2004) Identification and characterization of a novel and specific inhibitor of the ataxia-telangiectasia mutated kinase ATM. *Cancer Res.*, 64, 9152-9159.
31. Liu, S.Q., Opiyo, S.O., Manthey, K., Glanzer, J.G., Ashley, A.K., Amerin, C., Troksa, K., Shrivastav, M., Nickoloff, J.A. and Oakley, G.G. (2012) Distinct roles for DNA-PK, ATM and ATR in RPA phosphorylation and checkpoint activation in response to replication stress. *Nucleic Acids Res.*, 40, 10780-10794.
32. Okita, N., Minato, S., Ohmi, E., Tanuma, S. and Higami, Y. (2012) DNA damage-induced CHK1 autophosphorylation at Ser296 is regulated by an intramolecular mechanism. *FEBS Lett.*, 586, 3974-3979.
33. Vassin, V.M., Anantha, R.W., Sokolova, E., Kanner, S. and Borowiec, J.A. (2009) Human RPA phosphorylation by ATR stimulates DNA synthesis and prevents ssDNA accumulation during DNA-replication stress. *J. Cell Sci.*, 122, 4070-4080.
34. Ward, I.M., Wu, X.L. and Chen, J.J. (2001) Threonine 68 of Chk2 is phosphorylated at sites of DNA strand breaks. *J. Biol. Chem.*, 276, 47755-47758.

35. Pabla, N., Huang, S., Mi, Q.S., Daniel, R. and Dong, Z. (2008) ATR-Chk2 signaling in p53 activation and DNA damage response during cisplatin-induced apoptosis. *J. Biol. Chem.*, 283, 6572-6583.
36. Sirbu, B.M., Couch, F.B., Feigerle, J.T., Bhaskara, S., Hiebert, S.W. and Cortez, D. (2011) Analysis of protein dynamics at active, stalled, and collapsed replication forks. *Genes Dev.*, 25, 1320-1327.
37. Fragkos, M., Jurvansuu, J. and Beard, P. (2009) H2AX Is Required for Cell Cycle Arrest via the p53/p21 Pathway. *Mol. Cell. Biol.*, 29, 2828-2840.
38. Yoo, H.Y., Shevchenko, A. and Dunphy, W.G. (2004) Mcm2 is a direct substrate of ATM and ATR during DNA damage and DNA replication checkpoint responses. *J. Biol. Chem.*, 279, 53353-53364.
39. Trenz, K., Errico, A. and Costanzo, V. (2008) Plx1 is required for chromosomal DNA replication under stressful conditions. *EMBO J.*, 27, 876-885.
40. Lossaint, G., Larroque, M., Ribeyre, C., Bec, N., Larroque, C., Decaillet, C., Gari, K. and Constantinou, A. (2013) FANCD2 binds MCM proteins and controls replisome function upon activation of s phase checkpoint signaling. *Mol. Cell*, 51, 678-690.
41. Shigechi, T., Tomida, J., Sato, K., Kobayashi, M., Eykelenboom, J.K., Pessina, F., Zhang, Y., Uchida, E., Ishiai, M., Lowndes, N.F. *et al.* (2012) ATR-ATRIP kinase complex triggers activation of the Fanconi anemia DNA repair pathway. *Cancer Res.*, 72, 1149-1156.
42. Schlacher, K., Wu, H. and Jasin, M. (2012) A distinct replication fork protection pathway connects Fanconi anemia tumor suppressors to RAD51-BRCA1/2. *Cancer Cell*, 22, 106-116.
43. Andreassen, P.R., D'Andrea, A.D. and Taniguchi, T. (2004) ATR couples FANCD2 monoubiquitination to the DNA-damage response. *Genes Dev.*, 18, 1958-1963.
44. Kennedy, R.D., Chen, C.C., Stuckert, P., Archila, E.M., De la Vega, M.A., Moreau, L.A., Shimamura, A. and D'Andrea, A.D. (2007) Fanconi anemia pathway-deficient tumor cells are hypersensitive to inhibition of ataxia telangiectasia mutated. *J. Clin. Invest.*, 117, 1440-1449.
45. Satapathy, A.K., Kulczyk, A.W., Ghosh, S., van Oijen, A.M. and Richardson, C.C. (2011) Coupling dTTP hydrolysis with DNA unwinding by the DNA helicase of bacteriophage T7. *J. Biol. Chem.*, 286, 34468-34478.
46. Dose, C., Farkas, M.E., Chenoweth, D.M. and Dervan, P.B. (2008) Next generation hairpin polyamides with (R)-3,4-diaminobutyric acid turn unit. *J. Am. Chem. Soc.*, 130, 6859-6866.

47. Koundrioukoff, S., Carignon, S., Techer, H., Letessier, A., Brison, O. and Debatisse, M. (2013) Stepwise Activation of the ATR Signaling Pathway upon Increasing Replication Stress Impacts Fragile Site Integrity. *PLoS Genet.*, 9, e1003643.
48. Sirbu, B.M., McDonald, W.H., Dungrawala, H., Badu-Nkansah, A., Kavanaugh, G.M., Chen, Y., Tabb, D.L. and Cortez, D. (2013) Identification of proteins at active, stalled, and collapsed replication forks using isolation of proteins on nascent DNA (iPOND) coupled with mass spectrometry. *J. Biol. Chem.*, 288, 31458-31467.
49. Ishiai, M., Kitao, H., Smogorzewska, A., Tomida, J., Kinomura, A., Uchida, E., Saberi, A., Kinoshita, E., Kinoshita-Kikuta, E., Koike, T. *et al.* (2008) FANCI phosphorylation functions as a molecular switch to turn on the Fanconi anemia pathway. *Nat. Struct. Mol. Biol.*, 15, 1138-1146.
50. MacDougall, C.A., Byun, T.S., Van, C., Yee, M.C. and Cimprich, K.A. (2007) The structural determinants of checkpoint activation. *Genes Dev.*, 21, 898-903.
51. Hovest, M.G., Krieg, T. and Herrmann, G. (2011) Differential roles for Chk1 and FANCD2 in ATR-mediated signalling for psoralen photoactivation-induced senescence. *Experimental dermatology*, 20, 883-889.
52. Wagner, J.M. and Karnitz, L.M. (2009) Cisplatin-Induced DNA Damage Activates Replication Checkpoint Signaling Components that Differentially Affect Tumor Cell Survival. *Mol. Pharmacol.*, 76, 208-214.
53. Tomida, J., Itaya, A., Shigechi, T., Unno, J., Uchida, E., Ikura, M., Masuda, Y., Matsuda, S., Adachi, J., Kobayashi, M. *et al.* (2013) A novel interplay between the Fanconi anemia core complex and ATR-ATRIP kinase during DNA cross-link repair. *Nucleic Acids Res.*, 41, 6930-6941.
54. Belitsky, J.M., Nguyen, D.H., Wurtz, N.R. and Dervan, P.B. (2002) Solid-phase synthesis of DNA binding polyamides on oxime resin. *Bioorg. Med. Chem.*, 10, 2767-2774.
55. Vichai, V. and Kirtikara, K. (2006) Sulforhodamine B colorimetric assay for cytotoxicity screening. *Nature protocols*, 1, 1112-1116.
56. Ishiyama, M., Shiga, M., Sasamoto, K., Mizoguchi, M. and He, P.G. (1993) A New Sulfonated Tetrazolium Salt That Produces a Highly Water-Soluble Formazan Dye. *Chem. Pharm. Bull. (Tokyo)*, 41, 1118-1122.
57. Zou, L., Cortez, D. and Elledge, S.J. (2002) Regulation of ATR substrate selection by Rad17-dependent loading of Rad9 complexes onto chromatin. *Genes Dev.*, 16, 198-208.

58. Fortini, B.K., Pokharel, S., Polaczek, P., Balakrishnan, L., Bambara, R.A. and Campbell, J.L. (2011) Characterization of the endonuclease and ATP-dependent flap endo/exonuclease of Dna2. *J. Biol. Chem.*, 286, 23763-23770.
59. Karanja, K.K., Cox, S.W., Duxin, J.P., Stewart, S.A. and Campbell, J.L. (2012) DNA2 and EXO1 in replication-coupled, homology-directed repair and in the interplay between HDR and the FA/BRCA network. *Cell cycle*, 11, 3983-3996.

Chapter 3

*Py-Im Polyamides Inhibit DNA Replication in Cell-Free Extracts from *X. laevis* Oocytes*

This research was conducted in collaboration with Joon Lee, William G. Dunphy, and Peter B. Dervan (California Institute of Technology).

Abstract

The effects of DNA-binding pyrrole-imidazole (Py-Im) polyamides on DNA replication in *Xenopus* oocyte cell-free extracts were investigated for the purpose of elucidating the mechanism of polyamide-induced replication stress. Inhibition of nucleotide incorporation was observed in this system in response to multiple polyamides targeting different 6 base pair DNA sequences, consistent with previous results found in mammalian cells. Disruption of the pre-replication complex (pre-RC) was probed as a potential cause of inhibition; however, the pre-RC factors Orc2 and MCM2 as well as helicase-associated Cdc45 were all recruited to chromatin in polyamide treated extracts. Activation of the ATR checkpoint was investigated for evidence of replication fork stalling, as observed in mammalian cells. Polyamide treatment did not result in phosphorylation of Chk1 or MCM2, suggesting that the ATR checkpoint was not activated and that an early step in the cell cycle was likely inhibited. Staining of sperm chromatin incubated in polyamide treated extracts revealed that chromatin decondensation was inhibited, preventing replication initiation. Comparison to other small molecule DNA binders suggests that inhibition of chromatin decondensation is likely due to impaired nuclear membrane formation. These results show that inhibition of chromatin decondensation should be studied as a possible effect of polyamides in mammalian cells, and that a different model system should be employed to study the effects of polyamides on active replication forks.

3.1 Introduction

The previous chapter detailed the evidence for polyamide-induced replication stress in an asynchronous population of DU145 human prostate carcinoma cells (1). This low-level stress was sufficient to activate ATR but not the downstream effector kinase Chk1. In order to investigate the generality of these effects more cell lines should be tested, as each cancer cell line harbors unique genetic alterations that can affect major signaling pathways. Another method for testing the generality of polyamide-induced replication stress is to test for polyamide effects *in vitro* using cell-free extracts that are capable of undergoing cell cycle progression including DNA replication and DNA damage response signaling. Cell extracts are beneficial because they can be easily synchronized and arrested, thus allowing the polyamide to be dosed before induction of the cell cycle in a controlled manner. Cell extracts also allow for direct comparison of different sequences of polyamides and accurate measurements of effective concentrations, given that there is no variability due to uptake across cell membranes. The cell extract system most frequently employed to study the cell cycle and DNA replication is from *Xenopus laevis* oocytes.

Oocyte extracts from *X. laevis*, the African clawed frog, are made by harvesting healthy eggs, packing them, and then crushing them by ultracentrifugation. After centrifugation, the middle layer containing the cytosol and membranes is then separated from the top layer containing lipids and the bottom layer containing the dark yolk and pigments (2). *Xenopus* oocyte extracts produced by this relatively low speed centrifugation are arrested at metaphase of meiosis II and will undergo nuclear membrane

formation and DNA replication upon the addition of demembrated sperm nuclei and exogenous calcium for release from cytosolic factor (CSF) arrest. The use of sperm chromatin provides a large concentrated and diverse sequence of DNA targets for the polyamide to interact with, similar to experiments in cell culture. Importantly, no transcription occurs during the first cell divisions, and therefore polyamide effects on transcription as opposed to processes related to DNA replication can be reasonably ruled out. These egg extracts contain a high concentration of the molecular machinery, regulatory factors, checkpoint proteins, and damage response proteins necessary to execute eukaryotic cell division. Egg extracts can be used to monitor the loading of specific replication factors to determine which specific step in replication is inhibited and monitor any DNA checkpoint signaling that might occur in response to replication stress. It also allows for individual factors to be easily depleted through the use of antibodies in order to probe for the functional roles of specific replication and stress response factors. Another important benefit of this system is the wealth of data on the effects of common replication inhibitors for comparison against polyamides. This was an issue previously, as the DU145 cell line is not commonly used to investigate DNA replication.

In this study we report that Py-Im polyamides inhibit nucleotide incorporation in frog egg extracts. We also show that inhibition of DNA replication is not the result of impaired loading of pre-replication complex (pre-RC) factors, and that polyamide treatment does not induce phosphorylation of either Chk1 or MCM2, which suggested a lack of ATR signaling activation. Finally we show that polyamides prevent proper decondensation of sperm chromatin, the DNA template in this system, causing inhibition

of DNA replication initiation. These results suggest that while DNA replication is inhibited in this model system, the mechanism is likely different from what we observed in DU145 given the difference in DNA checkpoint response signaling. However, the effect on chromatin decondensation is interesting, and represents another potential effect of polyamides in mammalian cells.

3.2 Results

Py-Im polyamides inhibit DNA replication in Xenopus egg extracts.

The most general method for testing replication inhibition by polyamides is to measure the extent of nucleotide incorporation in activated extracts. DNA replication was probed using alpha phosphate-substituted ^{32}P -dATP ($[\alpha\text{-}^{32}\text{P}]\text{-dATP}$). *Xenopus* oocyte extracts mixed with sperm chromatin were incubated with increasing concentrations of polyamide **1**, which targets the 6 base pair sequence 5'-WGWWCW-3'. Treatment with **1** resulted in decreased dATP incorporation, with full inhibition of nucleotide incorporation occurring between 1 and 2.5 μM . This result was consistent with observations in DU145 cells measuring the incorporation of EdU (Figure 3.1).

Using cell-free extracts also allows for direct comparison of polyamide targeted to different sequences. We therefore compared the effects of three different polyamides, as well as two other DNA-binding small molecule, actinomycin D and distamycin A, and the DNA polymerase alpha inhibitor aphidicolin. Polyamide **2** is targeted to the sequence 5'-WGGWCW-3' and polyamide **3** is targeted to 5'-WGGWWW-3'. The polyamides and distamycin were all dosed at 500 nM while aphidicolin and actinomycin were dosed

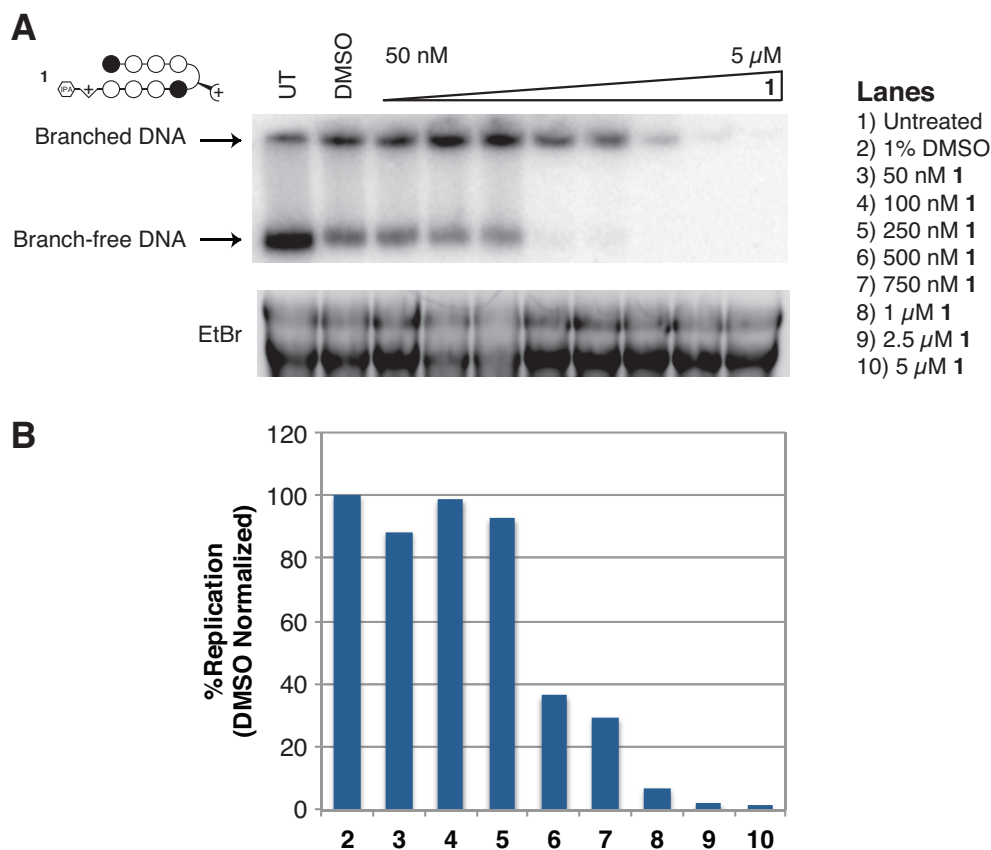


Figure 3.1 Polyamide **1** inhibits DNA replication in *Xenopus* oocyte extracts. **(A)** Frog egg extracts arrested at Meiosis II containing 3000 sperm nuclei/ μL were treated with increasing concentrations of **1** (50 nM – 5 μM) just prior to release from CSF arrest by 0.4 mM CaCl_2 . After 100 min, an aliquot of each sample was run out on an agarose gel, which was then dried and visualized on a storage phosphor screen. Total DNA content in the extracts was estimated by ethidium bromide staining of the gel. Polyamide **1** is shown by ball-and-stick representation. It targets the 6 bp sequence 5'-WGWWCW-3'. **(B)** The percent of DNA replication completed was estimated by measuring the band intensity for the entire lane and shown in the bar graphs in the bottom panel. The IC_{50} was \sim 500 nM, and maximal inhibition was observed at 2.5 μM . Data is representative of two replicates.

at 10 ng/ μL . Significant inhibition of nucleotide incorporation was observed for all compounds tested with the exception of distamycin, which showed only weak inhibition (Figure 3.2). Weaker inhibition by distamycin is consistent with the lower binding affinity of distamycin to DNA compared to Py-Im polyamides.

Py-Im polyamide treatment does not inhibit loading of pre-Replication Complex factors.

The previous results showed that DNA replication is inhibited in *Xenopus* egg extracts. Next, we wanted to investigate which step might be inhibited. We first tested whether treatment with Py-Im polyamides affects loading of the pre-replication complex, which consists of Cdt1, Cdc6, and the origin recognition complex (ORC) as well as the MCM2-7 helicase. The ORC proteins, composed of Orc1-6, in addition to Cdt1 and Cdc6 are responsible for loading two MCM2-7 hexameric helicases onto the DNA prior to replication (3). In order to test whether polyamides inhibit loading of the pre-RC onto DNA, the replicated oocyte extract was fractionated, and purified chromatin was collected. Next, the proteins were separated by SDS-PAGE and immunoblots were run against representative pre-RC factors, Orc2 and MCM2. We also probed for Cdc45, which is another component of the replicative helicase with the MCMs. In addition, we probed for RPA70, which is the large subunit of the single stranded DNA (ssDNA)-binding protein replication protein A (RPA) and accumulates on chromatin under replication stress.

For this experiment, we included a non-activated control (lane 1), which lacked both calcium and sperm chromatin. These conditions showed no significant detection of Orc2, MCM2, Cdc45, or RPA (Figure 3.3A) as expected. Two positive controls, which inhibit the loading of different pre-RC factors, were also tested for comparison. Geminin negatively regulates the cell cycle by inhibition of Cdt1, thus preventing loading of the MCMs (4). Geminin-treated extracts showed loading of Orc2, but not MCM2 or associated Cdc45 (lane 6). The protein p27, which inhibits cyclin E-CDK2, thus

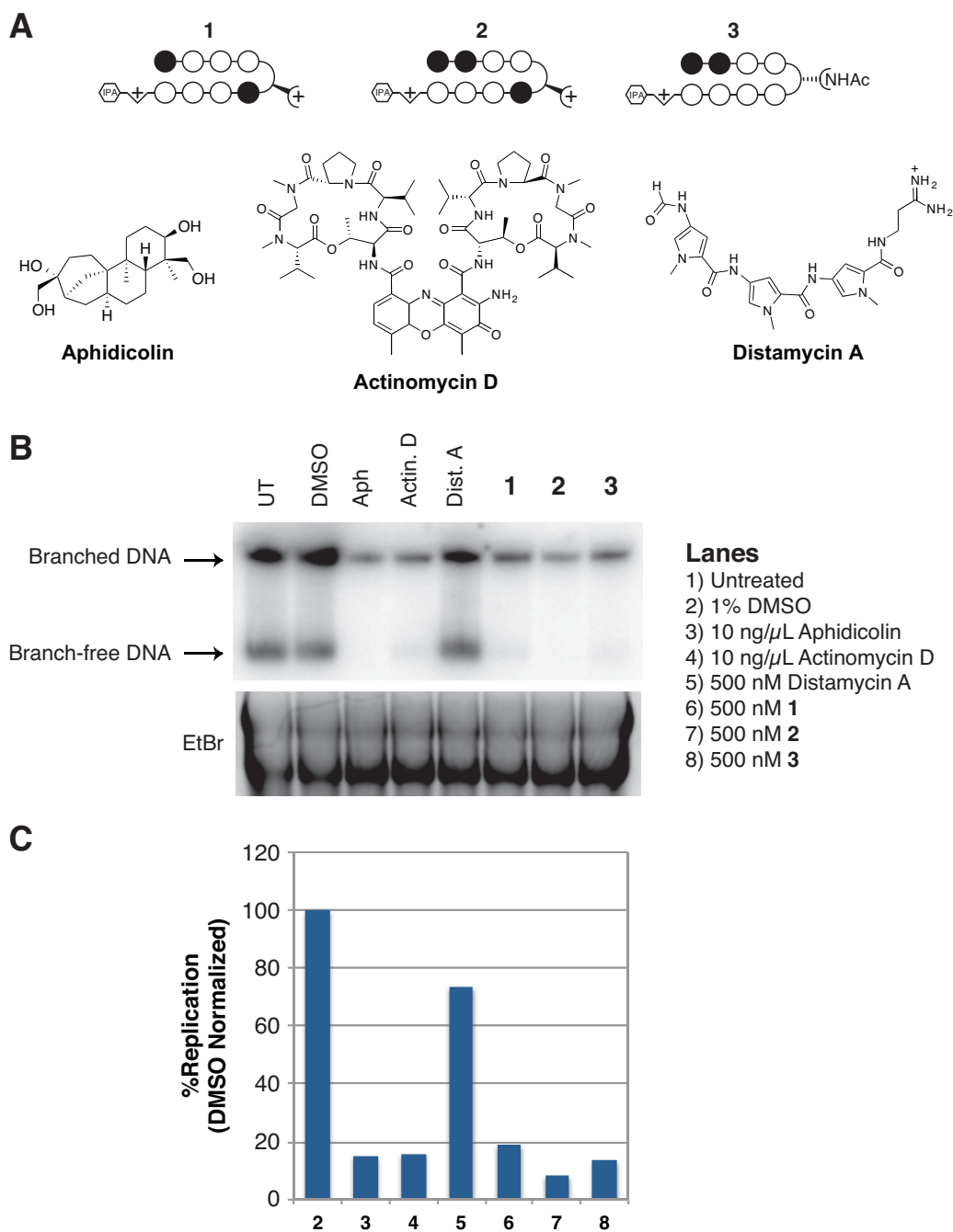


Figure 3.2 Py-Im Polyamides targeted to different DNA sequences equally inhibit DNA replication in *Xenopus* oocyte extracts. **(A)** Ball-and-stick representations of polyamides and chemical structures of other inhibitors used in this experiment. **(B)** Depiction of the extent of [α - 32 P]-dATP incorporation from egg extracts treated with a variety DNA-binding small molecules, including aphidicolin (Aph), actinomycin D (Actin D), distamycin A (Dist A), and polyamides 1-3. **(C)** The percent of DNA replication completed was estimated by measuring the band intensity for the entire lane and shown in the bar graphs in the bottom panel. At the concentrations tested, DNA replication was significantly inhibited by all of the tested small molecules except distamycin A. Data is representative of two replicates.

preventing downstream loading of Cdc45, was also tested. Extracts treated with p27 showed loading of Orc2 and MCM2, but not Cdc45 (lane 5). Aphidicolin-treated extracts were included as a representative inhibitor of active DNA replication that induces replication fork stalling and ssDNA accumulation. These extracts showed loading of MCM2, as well as weak loading of Cdc45 and Orc2 (lane 4). In addition, aphidicolin treatment induced significant loading of RPA70, confirming ssDNA accumulation. Extracts treated with 1 μ M **1** showed significant loading of Orc2, Cdc45, and MCM2, but not RPA70 (lane 3). Extracts treated with DMSO showed similar results (lane 2). Therefore, no aspect of pre-RC loading was affected by polyamide treatment. In addition, polyamide treatment did not cause significant ssDNA formation as observed under treatment with aphidicolin.

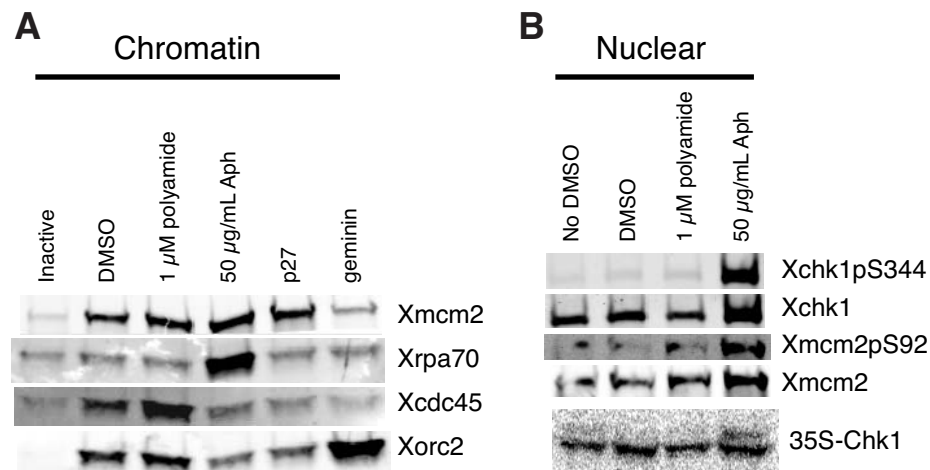


Figure 3.3 Polyamide **1** does not inhibit loading of pre-RC factors or activate ATR checkpoint signaling. **(A)** Chromatin loading of representative pre-RC factors Orc2 and MCM2, as well as the helicase component Cdc45 and the large subunit of ssDNA-binding protein RPA70 were probed by immunoblot. Extracts were untreated or treated with 1% DMSO, or **1**, as well as aphidicolin, p27, and geminin for comparison. Polyamide treatment did not inhibit pre-RC loading or result in the accumulation of ssDNA. **(B)** Nuclear lysates were prepared from untreated extracts and extracts treated with DMSO, **1**, or aphidicolin and probed for phosphorylation of Chk1 and MCM2 by immunoblot. Only treatment with aphidicolin resulted in phosphorylation of MCM2 and Chk1, and therefore **1** does not activate ATR checkpoint signaling. Blots are representative of two replicates.

Py-Im Polyamide treatment does not induce phosphorylation of ATR targets.

The previous experiment showed that loading of pre-RC factors was not inhibited by polyamide treatment. We next investigated whether polyamide treatment affected active replication. In order to test this, we probed for the activation of the ATR-checkpoint pathway given that partial activation of the pathway was observed in response to polyamide treatment in DU145 cells (Chapter 2). Chk1 S344 (corresponds to human Chk1 S345) and MCM2 S92 (corresponds to human MCM2 S108) phosphorylation were chosen as representative targets of ATR. Chk1 phosphorylation was readily observed in extracts treated with aphidicolin, but not polyamide **1** (Figure 3.3B). This result was consistent with observations in DU145 cells (Chapter 2). The lack of Chk1 phosphorylation was also confirmed using 35S-Chk1. A slower migrating band representing the heavier phosphorylated form of the protein was only observed in extracts treated with aphidicolin. Interestingly, MCM2 S92 was also not phosphorylated in response to polyamide treatment, despite being phosphorylated in DU145 cells. Given the lack of phosphorylation observed for both targets, it is unlikely that polyamide treatment induces ATR activation. Therefore, polyamide-induced inhibition of replication likely acts through a different mechanism than in DU145 cells.

Py-Im polyamide treatment inhibits chromatin decondensation.

Inhibition of DNA replication without affecting loading of the pre-RC complex or activating the ATR checkpoint pathway, suggested that a process prior to these steps might be inhibited by polyamide treatment. Sperm chromatin from male frogs used for this system is initially in a condensed form. Upon activation of the extracts, the DNA

undergoes decondensation via a rapid nucleoplasmin-dependent step and a slower nuclear membrane-dependent step (5). Only after DNA decondensation and formation of a functional nuclear membrane can replication begin. Previous studies on polyamide:DNA binding showed that these molecules can bind to DNA wrapped around in histones in a nucleosome core particle, demonstrating the potential for polyamides to interact with condensed DNA (6). Therefore, we investigated whether polyamide **1** was inhibiting sperm chromatin decondensation.

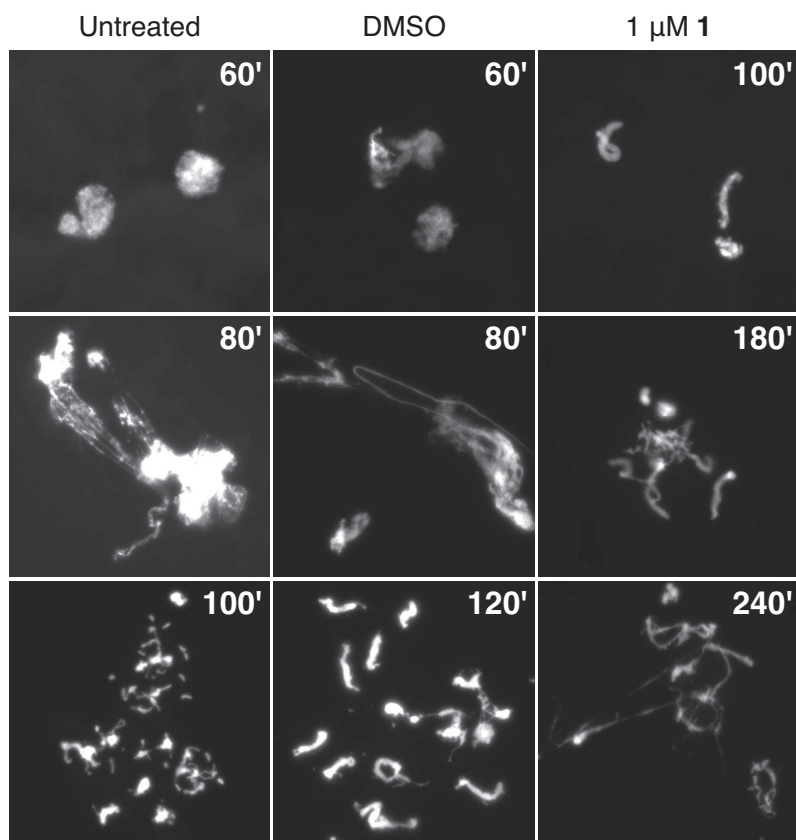


Figure 3.4 Polyamide **1** inhibits decondensation of sperm chromatin. Aliquots of activated untreated extracts and extracts treated with 1% DMSO or **1** were taken at the indicated time point at the DNA stained with Hoechst 33258. The cell cycle was completed by 100 min in untreated lysates, which is consistent with previous studies. DMSO slowed down the cell cycle slightly; however, there was no obvious defects. Treatment with polyamide **1** results in inhibition of sperm chromatin decondensation, which dramatically slowed down the cell cycle. Images are representative of two replicates.

In order to monitor this step, extracts are activated as in other experiments, but aliquots are removed at regular time intervals for visualization by staining with Hoechst 33258. After 60 min incubation, nearly all chromatin in the untreated extract is decondensed and contained in fully formed nuclei. By 80 min, the DNA in untreated cells entered telophase (Figure 3.4). Finally, at 100 min nuclear envelope breakdown had occurred and DNA condensed into chromosomes, ready for another cycle. DMSO-treated extracts completed all of the same steps, though 120 min was required to complete a single cell cycle. Extracts treated with 1 μ M polyamide **1**, however, showed striking differences from the untreated and DMSO-treated extracts. The sperm chromatin in extracts treated with **1** remained in a condensed state even after 100 min. By 180 min, some DNA appeared to be in a decondensed state similar to telophase. Finally, at 240 min, most of the DNA was decondensed but it had not recondensed as expected at the completion of the cell cycle. These results demonstrated that polyamide treatment prevents proper decondensation of sperm chromatin, which can prevent replication from ever initiating.

Previous efforts investigating plausible mechanisms for replication inhibition *in vitro* demonstrated that polyamides are capable of inhibiting DNA helicase activity. However, polyamide-induced inhibition of sperm chromatin decondensation occurs prior to DNA replication initiation, and therefore it is unclear whether polyamides can inhibit active replication forks. In order to test this hypothesis using the low speed supernatant extracts, polyamides need to be dosed at times after release from CSF arrest in order to bypass the initial chromatin decondensation and nuclear membrane formation steps. For

this experiment, extracts mixed with sperm chromatin were activated with CaCl_2 followed by the addition of polyamide **1** 15 or 30 min later in order to allow time for nuclei to form and DNA to decondense. Reduced incorporation of $[\alpha\text{-}^{32}\text{P}]\text{-dATP}$ was observed at both time points, though the effect was much weaker when polyamide was added after 30 min compared to 15 min or when the compound is added prior to release from CSF-arrest (Figure 3.5). These results suggest that it is likely that polyamides can inhibit actively replicating forks, albeit weakly. However, under these conditions, the total incubation time of polyamide with DNA is sufficiently short that the polyamide and DNA were not fully equilibrated.

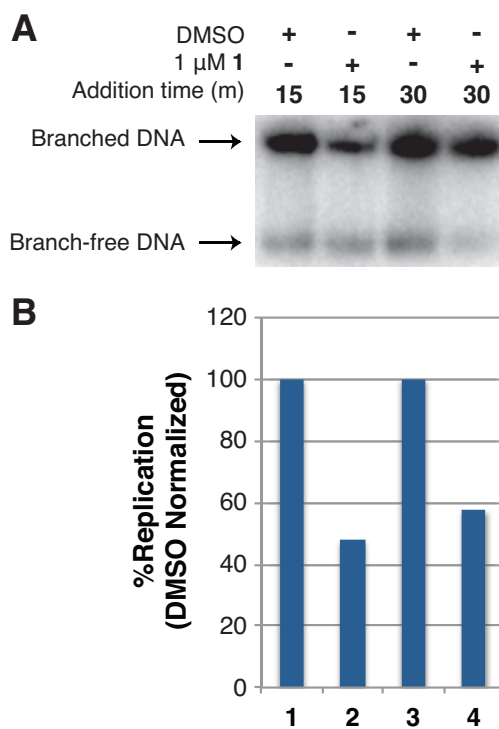


Figure 3.5 Polyamide **1** inhibits DNA replication when dosed after DNA decondensation step. (A) Depiction of the extent of $[\alpha\text{-}^{32}\text{P}]\text{-dATP}$ incorporation from egg extracts treated with DMSO or 1 μM **1** either 15 or 30 min after release from CSF arrest by CaCl_2 . (B) Bar graphs showing the extent of nucleotide incorporation. At the time points tested, DNA replication was inhibited by polyamide **1**, although the effect observed was less than when polyamide was dosed prior to the addition of CaCl_2 . Data is representative of two replicates.

3.3 Discussion

In this study we demonstrated that Py-Im polyamides targeted to a variety of 6 base pair DNA sequences are all equally capable of inhibiting DNA replication in the cell-free *Xenopus* oocyte extract system. Polyamide treatment did not cause activation of the ATR checkpoint or preclude binding of pre-RC factors. However, polyamide treatment did disrupt sperm chromatin decondensation, thus preventing initiation of DNA replication. Inhibition this early in the cell cycle in this model system limits its use in understanding how polyamides might inhibit active replication; however, inhibition of decondensation is an interesting result and may provide new insight into the mechanistic effects of polyamides.

Inhibition of chromatin decondensation in frog egg extracts has been shown to occur in response to many DNA-binding small molecules, including ethidium bromide, doxorubicin, and echinomycin (7,8). Sperm chromatin in extracts treated with ethidium bromide failed to fully decondense even after 90 minutes, though it is noticeably expanded in size compared to its initial size (8). This study concluded that modification to the DNA topology by ethidium led to inhibition of nuclear membrane formation and lamina assembly, which is necessary for the second phase of proper chromatin decondensation. Ethidium bromide treated extracts were also assessed for loading of pre-RC factors; the MCMs, PCNA, and RPA were all loaded despite a lack of nuclear membrane formation. This result is similar to our observations of polyamide treatment, except for significant loading of RPA. However, Krasinska et al. used GFP-fused proteins to assess DNA loading as opposed to chromatin fractionation. Inhibition of

decondensation by ethidium bromide was also accompanied with inhibition of nucleotide incorporation but no activation of the DNA checkpoints, consistent with the effects observed by polyamide treatment. Given that a variety of DNA-binding small molecules similarly inhibit DNA decondensation, there must be a common mechanism related to distortion of the structure of DNA causing this effect.

Py-Im polyamides are unique compared to other DNA-binding small molecules because they can be designed in a modular fashion in order to target specific sequences of DNA. However, this study shows that they still share many of the same effects as other DNA-binding molecules despite each having different binding modes with the DNA; ethidium bromide is an intercalator, doxorubicin has a mixture of intercalation and minor groove interactions, echinomycin is a bis-intercalator with minor groove interactions, and polyamides bind in the minor groove. Interestingly, The parent molecule of Py-Im polyamides, the minor groove binder distamycin A, has been shown to alter the structure of soluble chromatin resulting in compaction of chromatin (9). Majumder *et al.* show by electron microscopy that individual nucleosomes in di- and tri-nucleosomes are pulled close together under treatment with distamycin. This result may explain how polyamide binding inhibits decondensation of sperm chromatin in egg extracts. In a separate study, distamycin has also been shown to induce remodeling of a chromatosome by eviction of the linker histone H1 (10). This effect is also suggested to be due to torsional stress induced by distamycin binding to DNA and might provide insight into the phenomenon caused by polyamides in egg extracts. Similar investigations into the effects of Py-Im polyamides on chromatin structure and DNA topology would likely prove useful in

explaining how chromatin decondensation is inhibited and perhaps even how DNA replication and transcription are inhibited generally.

While the CSF arrested extracts were not suitable as a model to test whether polyamides can inhibit the progression of replication forks, *Xenopus* oocyte extracts can be prepared in a different manner that allows for the replication of exogenous plasmids without the need for nuclear formation. In this system, egg extracts are prepared by high speed ultracentrifugation and mixed with a concentrated nucleoplasmic extract (NPE) (11). The ability to use exogenous plasmids for the DNA template bypasses the DNA decondensation step and also allows for the DNA sequence to be controlled such that any number of polyamide match sites can be incorporated in order to test for sequence dependence.

Another method to bypass the chromatin decondensation and nuclear membrane formation steps would be to use a hybrid *Xenopus*-mammalian cell system. This method uses the nuclei from G1 synchronized mammalian cells, which have not yet initiated DNA replication, and incubates these with frog egg extracts. May *et al.* use this technique to demonstrate that echinomycin inhibits the DNA replication of human chromosomes after failing to proceed past the decondensation step using frog sperm chromatin (7). Cell culture studies in DU145 cells or other cell lines can also provide more insight into polyamide effects on the cell cycle by employing synchronization. Through a variety of means (Figure 3.6), cells can be synchronized at each phase of the cell cycle and then dosed with polyamides to determine what effects are caused relative to

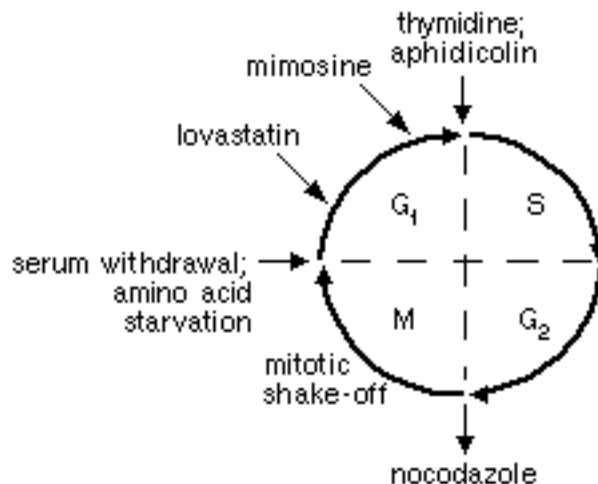


Figure 3.6 Methods of synchronizing mammalian cells at different stages of the cell cycle (12).

each phase (12). Future studies employing these methods will be invaluable for understanding how Py-Im polyamides induce replication stress and potentially cell death or reduced tumor growth in animal models.

3.4 Materials and Methods

Chemicals and reagents.

Hairpin Py-Im polyamides were synthesized on solid phase Kaiser oxime resin using previously published protocols (13). Aphidicolin, actinomycin D, and distamycin A were purchased from Sigma-Aldrich, as were all other reagents unless otherwise noted. Anti-Chk1 antibody was purchased from Santa Cruz Biotech. Anti-Chk1 pS345 (cross-reacts with Xchk1 pS344) was purchased from Cell Signaling Technology.

*Preparation of *X. laevis* oocyte extracts.*

Female frogs were primed with pregnant mare serum gonadotropin (PMSG) 3 days prior to induction with human chorionic gonadotropin (HCG, Sigma) as described in

(14). Cytostatic factor-arrested low speed supernatant extracts from healthy unactivated *Xenopus* eggs and demembrated sperm chromatin were prepared as also described in (14). Interphase egg extracts were prepared by addition of CaCl_2 (0.4 mM). Egg extracts used for the preparation of nuclear and chromatin fractions were also incubated with 100 $\mu\text{g}/\text{mL}$ cycloheximide to inhibit cyclin synthesis and subsequent entries into mitosis. The *Xenopus* Chk1 protein was radiolabeled *in vitro* with the TnT system (Promega, Madison, WI) in the presence of TRAN35S-LABEL (MP Biomedicals, Santa Ana, CA).

Measuring DNA replication by the incorporation of [α - ^{32}P]-dATP.

The replication was run similarly to (15). Freshly prepared extract was mixed with 3,000 nuclei/ μL and polyamide dissolved in DMSO at the indicated dose. The final DMSO concentration was 1%. 0.02 μCi of radiolabelled [α - ^{32}P]-dATP was also added to each reaction for continuous labeling of DNA replication. The cell cycle was activated with the addition of 0.4 mM CaCl_2 and allowed to incubate for 100 min. When the reaction was complete, 10 μL was removed and mixed with 10 μL sample buffer (80 mM Tris HCl, pH 8.0, 8 mM EDTA, 0.13% phosphoric acid, 10% Ficoll, 5% sodium dodecyl sulfate, and 0.2% bromophenol blue) to quench the reaction. Samples were then treated with 1 mg proteinase K per mL for 1 h at 37°C prior to gel electrophoresis on a 1% agarose gel. The gel was then dried and exposed on a storage phosphor screen for 1 h, followed by scanning on a Molecular Dynamics Storm 840.

Assessment of checkpoint activation and replication complex formation by immunoblots.

Fractionation of egg extracts into total nuclear and chromatin portions was performed as in (16). Nuclear and chromatin fractions from egg extracts were boiled in Laemmli buffer, and total protein was separated by sodium dodecyl sulphate-polyacrylamide gel electrophoresis (SDS-PAGE) on 4–15% gradient polyacrylamide gels (Bio-Rad). After transfer to the Immobilon-LF PVDF membrane (Millipore) and blocking with Odyssey Blocking Buffer (Li-Cor), primary antibodies were incubated overnight at 4°C. After washing the membrane three times in PBST, 1:3000 donkey anti-rabbit or donkey anti-mouse 800CW IR dye-conjugated secondary antibody (Li-Cor) was added for 1 h at room temperature and the bands were visualized on an Odyssey infrared imager (Li-Cor).

3.5 Acknowledgments

The authors would like to thank members of the Dunphy lab for helpful discussions, assistance with preparation of egg extracts, and access to animals, in addition to the animal protocol. We would also like to thank the Dunphy lab for antibodies targeting *Xenopus* MCM2 S92, MCM2, Orc2, and RPA70. The authors thank J.A. Raskatov and J.O. Szablowski for contribution of polyamides used in these experiments.

3.6 References

1. Martinez, T.F., Phillips, J.W., Karanja, K.K., Polaczek, P., Wang, C.M., Li, B.C., Campbell, J.L. and Dervan, P.B. (2014) Replication stress by Py-Im polyamides induces a non-canonical ATR-dependent checkpoint response. *Nucleic Acids Res*, 42, 11546-11559.
2. Lemaitre, J.M., Vassetzky, Y. and Mechali, M. (2001) Analysis of Chromatin Assembly, Chromatin Domains, and DNA Replication Using *Xenopus* Systems. *Mapping Protein/DNA Interactions by Cross-Linking*.
3. Sonnevile, R., Querenet, M., Craig, A., Gartner, A. and Blow, J.J. (2012) The dynamics of replication licensing in live *Caenorhabditis elegans* embryos. *J Cell Biol*, 196, 233-246.
4. Luo, L., Uerlings, Y., Happel, N., Asli, N.S., Knoetgen, H. and Kessel, M. (2007) Regulation of geminin functions by cell cycle-dependent nuclear-cytoplasmic shuttling. *Mol Cell Biol*, 27, 4737-4744.
5. Philpott, A., Leno, G.H. and Laskey, R.A. (1991) Sperm decondensation in *Xenopus* egg cytoplasm is mediated by nucleoplasmin. *Cell*, 65, 569-578.
6. Suto, R.K., Edayathumangalam, R.S., White, C.L., Melander, C., Gottesfeld, J.M., Dervan, P.B. and Luger, K. (2003) Crystal structures of nucleosome core particles in complex with minor groove DNA-binding ligands. *J Mol Biol*, 326, 371-380.
7. May, L.G., Madine, M.A. and Waring, M.J. (2004) Echinomycin inhibits chromosomal DNA replication and embryonic development in vertebrates. *Nucleic Acids Res*, 32, 65-72.
8. Krasinska, L. and Fisher, D. (2009) Replication initiation complex formation in the absence of nuclear function in *Xenopus*. *Nucleic Acids Res*, 37, 2238-2248.
9. Majumder, P. and Dasgupta, D. (2011) Effect of DNA groove binder distamycin A upon chromatin structure. *PLoS One*, 6, e26486.
10. Majumder, P., Banerjee, A., Shandilya, J., Senapati, P., Chatterjee, S., Kundu, T.K. and Dasgupta, D. (2013) Minor groove binder distamycin remodels chromatin but inhibits transcription. *PLoS One*, 8, e57693.
11. Lebofsky, R., Takahashi, T. and Walter, J.C. (2009) DNA replication in nucleus-free *Xenopus* egg extracts. *Methods Mol Biol*, 521, 229-252.
12. Jackman, J. and O'Connor, P.M. (2001) Methods for synchronizing cells at specific stages of the cell cycle. *Curr Protoc Cell Biol*, Chapter 8, Unit 8 3.

13. Belitsky, J.M., Nguyen, D.H., Wurtz, N.R. and Dervan, P.B. (2002) Solid-phase synthesis of DNA binding polyamides on oxime resin. *Bioorg Med Chem*, 10, 2767-2774.
14. Murray, A.W. (1991) Cell cycle extracts. *Methods Cell Biol*, 36, 581-605.
15. Kornbluth, S., Smythe, C. and Newport, J.W. (1992) In vitro cell cycle arrest induced by using artificial DNA templates. *Mol Cell Biol*, 12, 3216-3223.
16. Lee, J., Kumagai, A. and Dunphy, W.G. (2003) Claspin, a Chk1-regulatory protein, monitors DNA replication on chromatin independently of RPA, ATR, and Rad17. *Mol Cell*, 11, 329-340.

Chapter 4

DNA-binding Py-Im Polyamides Targeted to the AR-ERG Signaling Axis in VCaP Prostate Cancer Cells

The text of this chapter was taken in part from a manuscript draft co-authored with Amanda E. Hargrove, Alissa A. Hare, Jerzy O. Szablowski, and Peter B. Dervan (California Institute of Technology); Sudha Sud (University of Michigan) and Kenneth J. Pienta (Johns Hopkins University).

Abstract

ETS-gene fusions are now recognized as critically important in prostate cancer diagnosis and progression. Specifically, the *TMPRSS2-ERG* fusion results in androgen receptor (AR)-driven overexpression of the ERG protein, a transcription factor which then participates in several oncogenic mechanisms. DNA-binding pyrrole-imidazole (Py-Im) polyamides inhibit transcription factor-DNA interfaces and were thus designed to target the AR-ERG signaling axis through interactions to both AR- and ERG-DNA binding sites. Cell culture studies in VCaP cells, an immortalized cell line harboring the *TMPRSS2-ERG* gene fusion, identified both ARE (AR response element)- and ERG-targeted Py-Im polyamides that significantly downregulate gene expression associated with each respective pathway. Contrary to many DNA-binding small molecule therapeutics, Py-Im polyamides reduced the high levels of double stranded DNA breaks in VCaP cells. Similar cell culture results were observed in the PC3-ERG cell model. Finally, significant reductions in tumor growth were observed in VCaP cell xenografts upon weekly treatment with an ARE-targeted polyamide. These studies support the therapeutic potential of Py-Im polyamides to target ERG-positive prostate cancers without leading to genotoxic stress.

4.1 Introduction

Gene fusions are increasingly recognized as a critical component of prostate cancer progression, in particular fusions involving the E-twenty six (ETS) family of transcription factors (1). Among this family, the *TMPRSS2-ERG* fusion has garnered particular attention due to its prevalence in prostate cancer patient samples (~50%) (2) and its association with aggressive prostate cancers (3,4). The fusion of the 3'-untranslated region of *TMPRSS2*, an androgen receptor (AR) driven gene, and the 5'-translated region of *ERG*, an ETS transcription factor, leads to overexpression of a truncated ERG protein (5). Increased levels of ERG have been associated with a number of oncogenic pathways, including those involved in invasion (6) and DNA damage (7). Furthermore, aberrant ERG expression is sufficient to drive aggressive prostate cancer phenotypes in mouse models when combined with alterations in the pten/PI3K/Akt pathway (8,9).

Pyrrrole-imidazole (Py-Im) polyamides bind the minor groove of DNA sequence specifically (Figure 4.1) (10,11), leading to compression of the major groove (12) and offering a unique opportunity to target transcription factor activity. Several oncogenic pathways have been targeted with Py-Im polyamides, and both genotypic and phenotypic responses have been observed in cell culture (13-17) and animal studies (18-20). We recently reported reduction in tumor growth of an LNCaP prostate cancer xenograft upon treatment with a Py-Im polyamide (21). Toxicity studies have revealed a dependence on polyamide architecture in hairpin vs. cyclic polyamides (22) as well as a dependence on differences in hairpin modifications (23,24), allowing for the identification of hairpin

structures demonstrating xenograft growth inhibition but no observed toxicity at 10 mg/kg doses in mice (24). In this study, we show that this technology could be utilized to inhibit both AR signaling, including transcription of the *TMPRSS2-ERG* fusion, and downstream ERG activity in ERG-positive prostate cancer models.

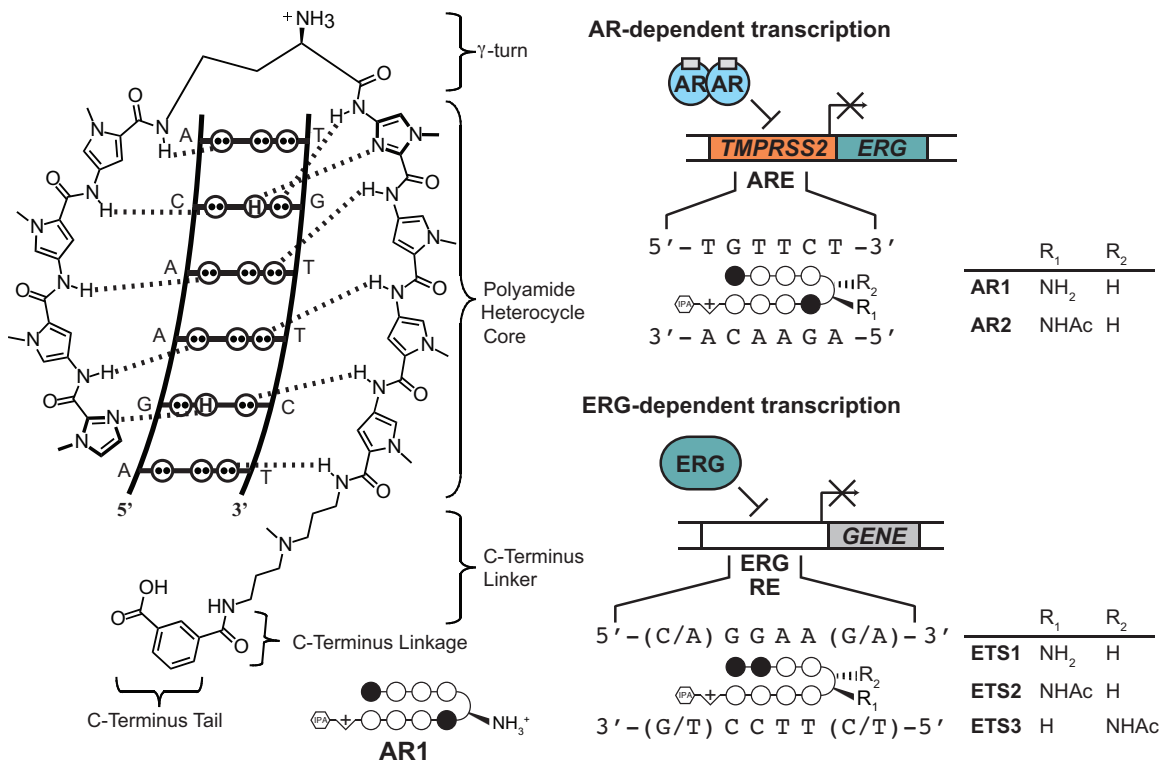


Figure 4.1 Diagrams of targeting AR- and ERG-DNA interfaces by Py-Im polyamides. **(Left)** Model of hairpin Py-Im polyamide recognition of the DNA minor groove in which the Py-Py pair recognizes A·T or T·A base pairs while the Im-Py pair recognizes the G·C base pair. The circle and stick representation (**AR1**) is the shorthand polyamide depiction (code: closed circles, Im; open circles, Py; diamonds, β -alanine; IPA, isophthalic acid). **(Right)** Five Py-Im polyamides used in this study to target prostate cancer cells containing the *TMPRSS2-ERG* gene fusion.

4.2 Results

Design and DNA-binding ability of Py-Im polyamides targeted to the AR-ERG signaling axis.

The two-pronged AR-ERG approach first utilized previously reported Py-Im polyamides **AR1** and **AR2**, which are known to bind the AR response element (ARE) half-site (5'-TGTTCT-3') and effect dihydrotestosterone (DHT)-induced expression profiles (14,24), (Table 4.1A). Secondly, a series of Py-Im polyamides was designed to target the ETS-DNA consensus sequence (5'-(C/A)GGAA(G/A)-3'), namely **ETS1**, **ETS2**, and **ETS3** (Figure 4.1). Initial experiments confirmed the ability of the latter set

A

Sequence		5'-TGTTCT-3'	
Polyamide		T _m (°C)	ΔT _m (°C)
—		61.8 (±0.5)	—
AR1		74.1 (±0.3)	12.3
AR2		70.1 (±0.2)	8.3

B

Sequence	5'-AGGAAA-3'	5'-AGGAAG-3'	5'-CGGAAG-3'	5'-CGGAAA-3'	
T _m (°C)	57.7 (±0.2)	60.1 (±0.4)	58.8 (±0.6)	58.2 (±0.2)	
Polyamide	ΔT _m (°C)				
ETS1		8.8 (±0.3)	1.0 (±0.3)	5.9 (±0.2)	7.8 (±0.6)
ETS2		6.6 (±1.0)	0.8 (±0.3)	5.4 (±0.2)	1.6 (±0.6)
ETS3		10.9 (±0.5)	3.7 (±0.4)	7.9 (±0.4)	7.7 (±0.3)

Table 4.1 Analysis of DNA thermal stabilization by binding of Py-Im polyamides. **(A)** Melting temperature analysis for **AR1** and **AR2** binding to match sequence DNA. ΔT_m denotes the shift in melting temperature following the addition of polyamide to the given DNA sequence of the pattern 5'-TTGC-NNNNN-GCAA-3'. Assays were performed at 2 μM DNA (15 b.p.) with or without 3 μM polyamide in a buffer solution consisting of 10 mM sodium cacodylate, 10 mM KCl, 10 mM MgCl₂, and 5 mM CaCl₂ at pH 7.0. ΔT_m results for **AR1** and **AR2** are taken from (24). **(B)** Melting temperature analysis for **ETS1-3** binding to match sequence DNA. ΔT_m denotes the shift in melting temperature following polyamide treatment for the given DNA sequence 5'-TGAAA-NNNNN-TGAG-3'.

to bind a variety of potential ERG-DNA binding sequences through thermal denaturation analysis (Table 4.1B).

ARE-targeted Py-Im polyamides mitigate AR-driven TMPRSS2-ERG expression under DHT-induction.

To examine the effect of Py-Im polyamides on AR-driven pathways in ERG-positive cells, the activity of polyamides **AR1** and **AR2** were studied in VCaP cells, the only immortalized cell line known to harbor the *TMPRSS2-ERG* gene fusion. Dosage

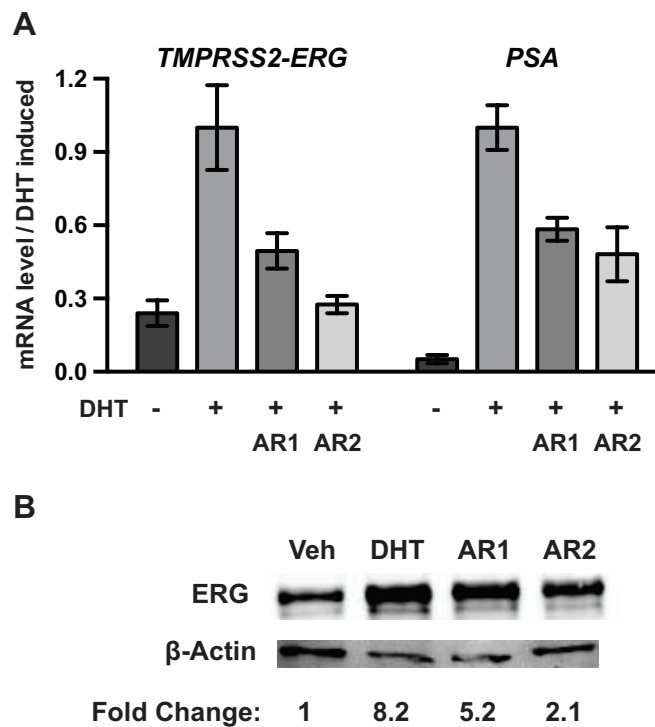


Figure 4.2 Representative expression data for VCaP cells treated with **AR1** and **AR2** followed by DHT-induction. VCaP cells plated at 31k/cm² were treated with medium containing 0.1% DMSO (with or without 10 μ M polyamide) and 10% charcoal-treated FBS (CT-FBS) for 72 h followed by induction with 1 nM dihydrotestosterone (DHT) or vehicle for an additional 24 h. **(A)** mRNA expression levels of representative androgen driven genes, *TMPRSS2-ERG* and *PSA*, were measured by qPCR, referenced to *GUSB*, and the polyamide effects compared to vehicle treatment. **(B)** ERG protein levels were measured by immunoblot, referenced to beta-actin, and the polyamide effects compared to vehicle treatment. Gel image has been cropped for clarity.

Treatment	Conc.	DHT	TMP2:ERG	AR	FKBP5	PSA	SLC45A3
Vehicle	-	-	0.23 ± 0.06	2.12 ± 0.19	0.01 ± 0.004	0.07 ± 0.02	0.12 ± 0.04
AR1	10 µM	+	0.50 ± 0.06	0.52 ± 0.13	0.62 ± 0.12	0.63 ± 0.08	0.69 ± 0.18
AR2	1 µM	+	0.68 ± 0.04	0.81 ± 0.17	0.85 ± 0.14	0.77 ± 0.06	0.82 ± 0.34
AR2	10 µM	+	0.30 ± 0.05	0.43 ± 0.08	0.46 ± 0.06	0.47 ± 0.05	0.48 ± 0.13

Treatment	Conc.	DHT	EZH2	MYC	PLAT
Vehicle	-	-	1.08 ± 0.19	12.4 ± 4.06	Unmeasurable
AR1	10 µM	+	1.79 ± 0.46	1.40 ± 0.13	Unmeasurable

Table 4.2 Gene expression data for VCaP cells treated with **AR1** and **AR2** followed by induction with DHT. Data shown are average of the fold changes (normalized to DHT-induced conditions) for three or more biological replicates +/- standard error.

concentrations were chosen based on previous reports of polyamide gene expression effects in the LNCaP prostate cancer cell line (14,24). Both polyamides **AR1** and **AR2** were found to reduce the DHT-induced expression of the *TMPRSS2-ERG* fusion as well as other AR target genes, including *PSA*, in VCaP cells (Figure 4.2, Table 4.2). Decreased expression of ERG protein was confirmed by Western blot (Figure 4.2).

Py-Im polyamides decrease ERG-driven signaling in non-induced VCaP cells.

Polyamides **ETS1**, **ETS2**, and **ETS3** were screened for their effect on ERG-dependent gene expression in VCaP cell culture under non-induced conditions (Figure 4.3, Table 4.3). Notably, all ERG-targeted Py-Im polyamides were observed to downregulate *PLAT*, a well-characterized ERG-driven gene (25), as well as the *MYC* oncogene. While minimal effects were observed on *EZH2* expression, **ETS2** and **ETS3** were found to increase expression levels of *SLC45A3*, a gene reported to be repressed by ERG-DNA binding (26). Due to their ability to inhibit ERG-activated genes and de-inhibit ERG-repressed genes, **ETS2** and **ETS3** were chosen for further phenotypic studies.

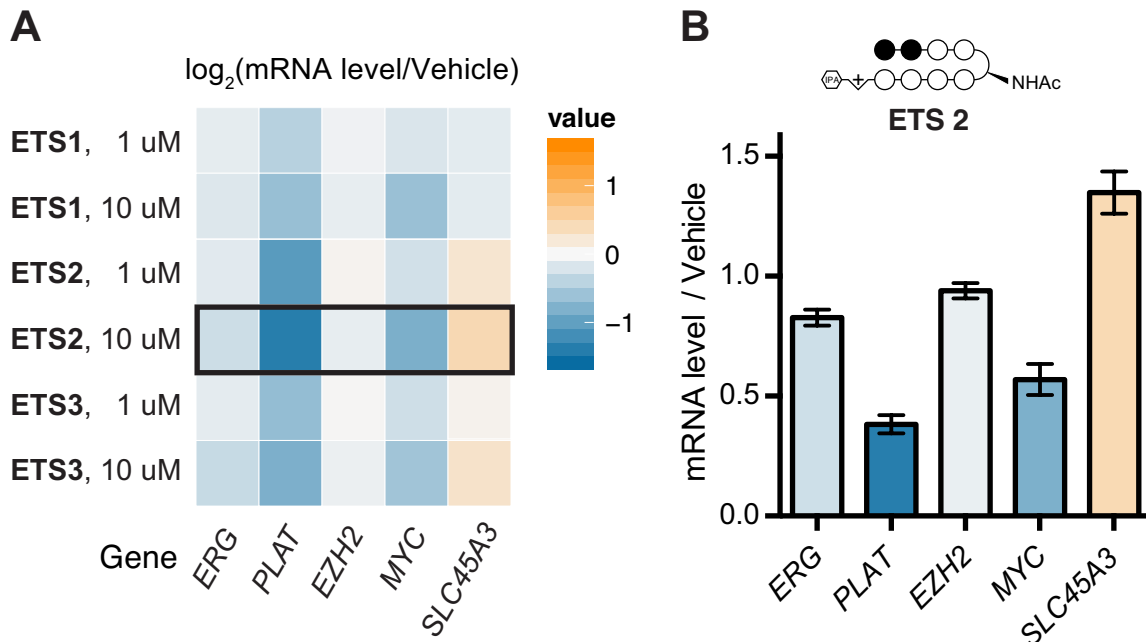


Figure 4.3 Representative expression data for VCaP cells treated with **ETS1-3**. (A) VCaP cells plated at 31k/cm² were treated with medium containing 0.1% DMSO vehicle (with or without polyamide) and 10% FBS for 72 h. mRNA levels were measured by qPCR, referenced to GUSB, and the polyamide effects compared to vehicle treated samples. log₂ conversions of treated/untreated values are reported as a heat map to allow comparison of multiple conditions. (B) Representative data from samples treated with 10 μ M **ETS2**. Bars represent average fold-change of three or more biological replicates +/- standard error.

We also measured the effects of **AR1** and **AR2** on TMPRSS2-ERG expression and downstream targets in VCaP cells under basal conditions. VCaP cells grown in media containing FBS without the addition of DHT. In the absence of DHT-induction, both **AR1** and **AR2** reduced ERG expression, although the effect was less pronounced compared to the effect observed under DHT-induction (Table 4.3). In addition, expression of the ERG-activated genes PLAT and c-Myc were also reduced under treatment with **AR1**.

Polyamide	Conc.	ERG	PLAT	EZH2	MYC	SLC45A3	TMPRSS2-ERG
ETS-1	1 μ M	0.93 \pm 0.02	0.75 \pm 0.10	0.98 \pm 0.05	0.88 \pm 0.02	0.92 \pm 0.02	0.92 \pm 0.04
	10 μ M	0.89 \pm 0.03	0.65 \pm 0.05	0.94 \pm 0.03	0.66 \pm 0.03	0.92 \pm 0.02	0.88 \pm 0.04
ETS-2	1 μ M	0.91 \pm 0.06	0.48 \pm 0.06	1.03 \pm 0.06	0.85 \pm 0.03	1.18 \pm 0.02	0.86 \pm 0.08
	10 μ M	0.83 \pm 0.03	0.38 \pm 0.04	0.94 \pm 0.03	0.57 \pm 0.07	1.35 \pm 0.09	0.80 \pm 0.05
ETS-3	1 μ M	0.93 \pm 0.02	0.64 \pm 0.07	1.01 \pm 0.05	0.83 \pm 0.03	1.04 \pm 0.09	0.94 \pm 0.02
	10 μ M	0.80 \pm 0.03	0.57 \pm 0.05	0.96 \pm 0.05	0.68 \pm 0.06	1.21 \pm 0.10	0.89 \pm 0.05
AR-1	1 μ M	0.84 \pm 0.07	0.67 \pm 0.06	1.00 \pm 0.10	0.70 \pm 0.04	0.98 \pm 0.10	1.02 \pm 0.08
	10 μ M	0.86 \pm 0.05	0.42 \pm 0.11	0.93 \pm 0.03	0.49 \pm 0.05	0.78 \pm 0.07	0.91 \pm 0.05
AR-2	1 μ M	0.67 \pm 0.06	0.68 \pm 0.09	1.03 \pm 0.07	0.66 \pm 0.06	0.56 \pm 0.06	0.66 \pm 0.06
	10 μ M	0.49 \pm 0.04	0.46 \pm 0.02	0.89 \pm 0.03	0.32 \pm 0.02	0.29 \pm 0.03	0.50 \pm 0.04

Polyamide	Conc.	AR	PSA	FKBP5
AR-1	1 μ M	0.96 \pm 0.04	0.81 \pm 0.09	0.93 \pm 0.09
	10 μ M	1.09 \pm 0.08	0.68 \pm 0.08	0.83 \pm 0.04
AR-2	1 μ M	0.87 \pm 0.04	0.66 \pm 0.02	0.81 \pm 0.02
	10 μ M	0.75 \pm 0.05	0.49 \pm 0.07	0.46 \pm 0.03

Table 4.3 Gene expression data for VCaP cells treated with ETS-targeting and AR-targeting polyamides. Data shown are average of the fold changes (normalized to DHT-induced conditions) for three or more biological replicates \pm standard error.

Cytotoxicity and nuclear uptake of Py-Im polyamides.

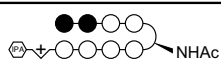
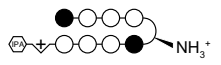
The four lead molecules, **ETS2**, **ETS3**, **AR1**, and **AR2**, were further examined for effects on proliferation of VCaP cells using the WST-1 assay under conditions similar to the gene expression experiment. After a 72 h incubation with polyamide, an IC_{50} value of $12 \pm 2 \mu$ M was determined for **AR2** but the remaining molecules did not reach a 50% reduction in signal at concentrations below 30 μ M, above which polyamide aggregation began to be observed (Figure 4.4). In contrast, **AR1** has been found to have an IC_{50} of $7 \pm 3 \mu$ M under similar conditions in LNCaP cells (21). When incubated for 96 h, however, **AR** was found to have an IC_{50} of $6.5 \pm 0.3 \mu$ M. To test differences in uptake, FITC-labeled derivatives of each lead molecule were prepared and incubated with VCaP cells prior to imaging by confocal microscopy (Figure 4.5,4.6). All intracellular polyamide signal was observed to be localized in the nucleus, with **ETS3-FITC** and **AR1-FITC**

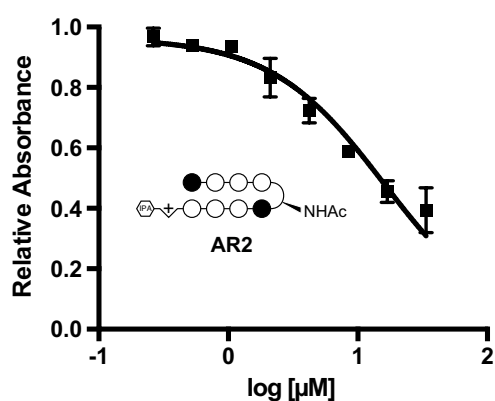
also showing significant membrane binding. In line with the cytotoxicity results, **AR2-FITC** displayed the strongest nuclear uptake. The overall level of uptake in VCaP cells was found to be qualitatively less than that in LNCaP cells (24).

Reduction of DNA damage in VCaP cells upon treatment with Py-Im polyamides.

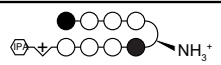
The effect of DNA-binding polyamides on the high level of extant DNA damage in VCaP cells was also investigated. After incubation with polyamide, VCaP cells were submitted to the neutral Comet assay, which allows visualization of double-strand breaks

A

Py-Im Polyamide	IC ₅₀ (WST-1)
ETS2 	> 30 μM
ETS3 	> 30 μM
AR1 	> 30 μM
AR2 	12 ± 3 μM



B

Py-Im Polyamide	IC ₅₀ (WST-1)
AR1 	6.5 ± 0.3 μM

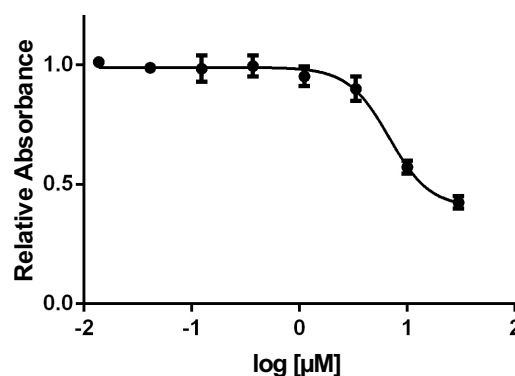


Figure 4.4 AR1 and AR2 are cytotoxic in VCaP cells. (A) Cytotoxicity (IC₅₀) values were determined using the WST-1 assay after 72 h incubation of VCaP cells with Py-Im polyamide. The conversion of WST-1 to formazan was measured by the absorbance at 450 nm referenced to 650 nm in treated cells and compared to that of vehicle (0.1% DMSO) treated cells. Top: Values are reported as the average ± SEM of three or more biological replicates where applicable. Bottom: Representative data from a single replicate using polyamide **AR2**. (B) WST-1 assay results after 96 h incubation of VCaP cells with **AR1**.

through single cell electrophoresis (Figure 4.7). The percentage of DNA in the “tail” of the comets was then compared using two-way ANOVA statistical analysis. A significant reduction in DNA damage ($p < 0.001$) was observed with **ETS2**, **ETS3**, and **AR1** over the vehicle control. No significant difference was observed upon treatment with **AR2**, possibly due to competing effects of toxicity. Interestingly, treatment with **ETS3** led to notably reduced damage relative to the other polyamides tested ($p < 0.001$ vs **ETS2** and

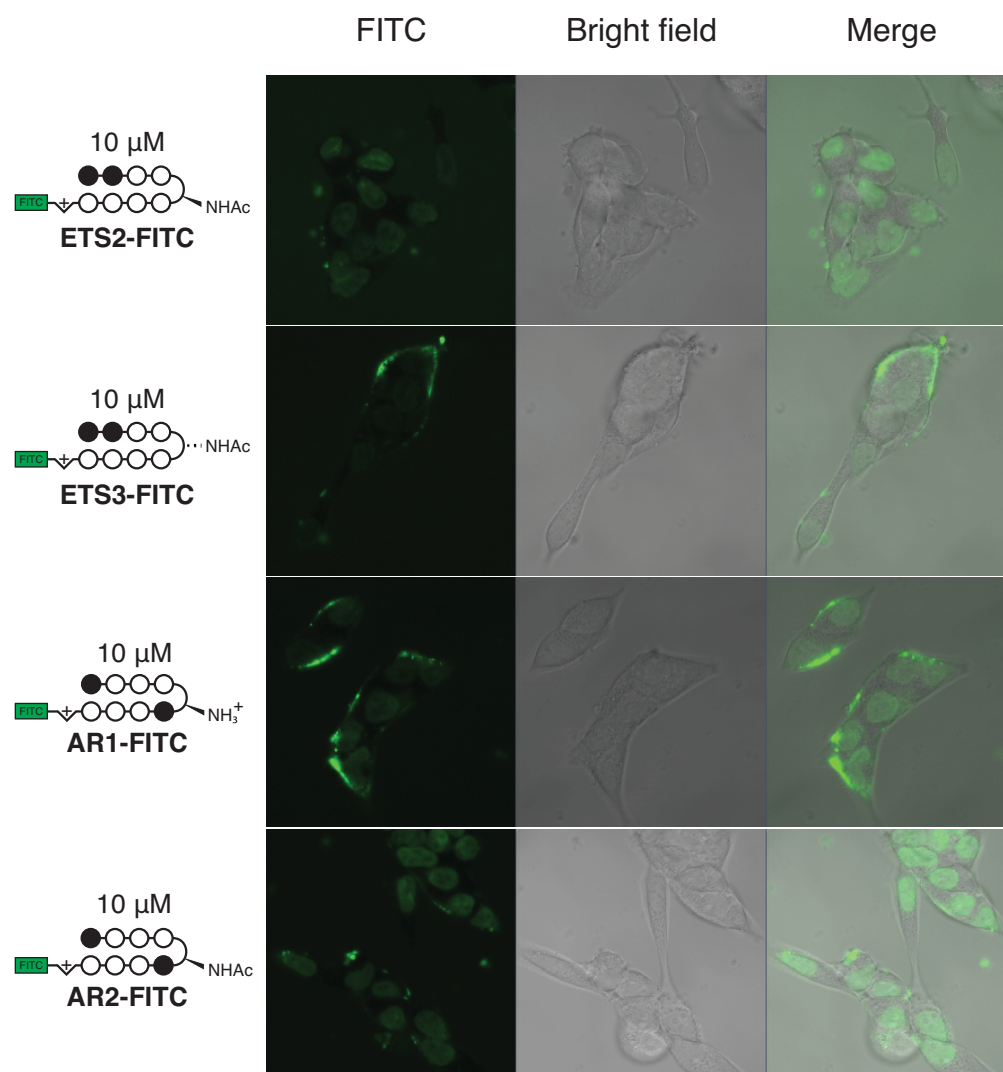


Figure 4.5 Nuclear uptake of FITC-analog polyamides in VCaP cells after 24 h. VCaP cells seeded at a density of 300,000/mL were incubated with FITC-labeled polyamides for 24 h before visualization by confocal microscopy. **ETS2** and **AR2** show significant nuclear uptake, while other compounds tested showed significant membrane binding but relatively low nuclear uptake.

AR1, respectively), despite the modest level of cellular uptake observed with the FITC-derivative (Figure 4.5,4.6) and the weaker effects on ERG-related gene expression compared to **ETS2** (Figure 4.3). At the same time, **ETS3** did stabilize the cognate ERG-DNA binding sequence to a greater extent than **ETS2** (Table 4.1), which may indicate a dependence on DNA stabilization in the reduction of double stranded breaks.

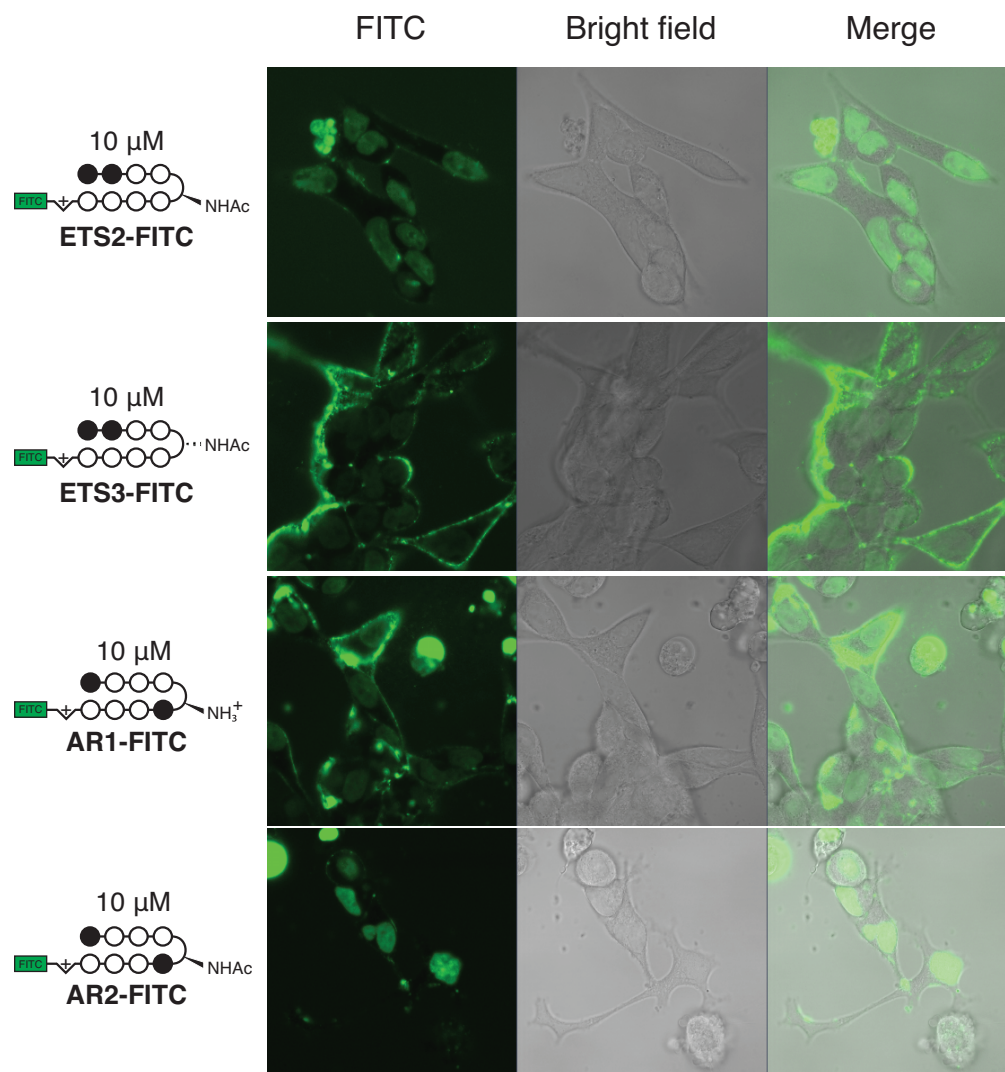


Figure 4.6 Nuclear uptake of FITC-analog polyamides in VCaP cells after 48 h. VCaP cells seeded at a density of 300,000/mL were incubated with FITC-labeled polyamides for 48 h before visualization by confocal microscopy. **ETS2** and **AR2** show significant nuclear uptake, while other compounds tested showed significant membrane binding but relatively low nuclear uptake.

Py-Im polyamide activity in PC3 cells overexpressing ERG.

Polyamide effects were further studied in the PC3-ERG cell line, which was derived from the AR- and ERG-negative PC3 prostate cancer line (7,27). Comparing PC3-ERG to the direct parent cell line, PC3-Luc, the strongest differences in expression were observed in the upregulation of *PLAT* and downregulation of *SLC45A3* (Figure 4.8, 4.9). Polyamides **ETS2** and **ETS3**, as well as control polyamide **AR1**, were chosen for comparison due to their observed lack of toxicity in VCaP cells. Treatment with all three polyamides resulted in expression levels of *PLAT* and *SLC45A3* near the parent levels, with **AR1** demonstrating the strongest activity. Significant reductions in DNA damage were also observed in Comet assays of PC3-ERG cells upon treatment with **ETS3** and **AR1** ($p < 0.001$). Notably, **AR1** decreased overall *ERG* expression nearly 2-fold, an

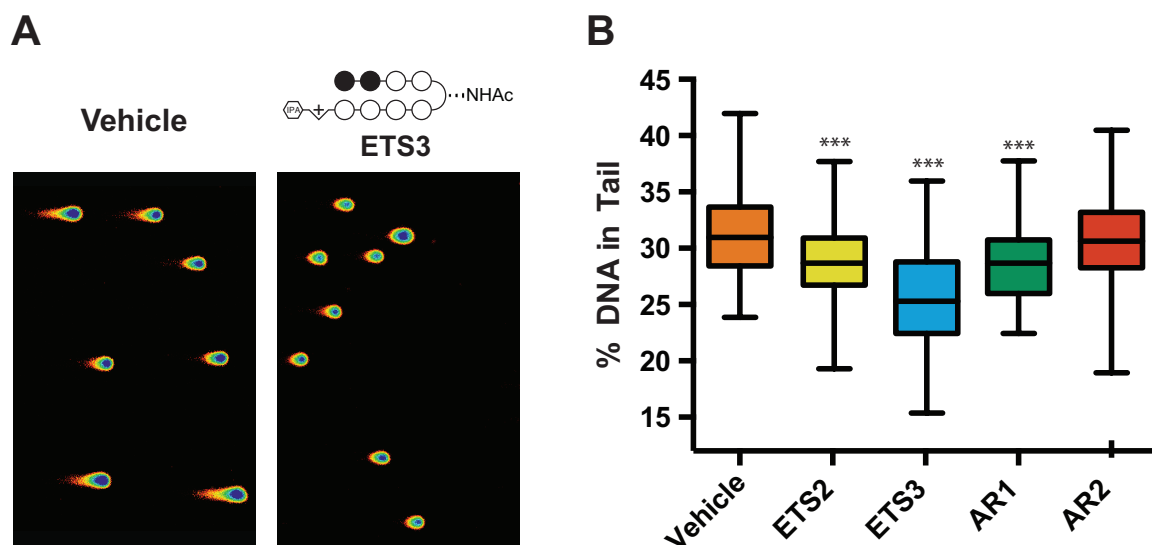


Figure 4.7 Analysis of DNA damage by neutral comet assay. (A) The extent of DNA damage in untreated and treated VCaP cells was measured using the neutral COMET assay after 72 h incubation with 0.1% DMSO (vehicle) with or without 10 μ M Py-Im polyamide as indicated. Comets were analyzed using Comet Assay IV software (Perceptive). Statistical significance was determined using two-way ANOVA analysis (Prism) where *** = $p < 0.001$ relative to vehicle. Boxes are bounded by the upper and lower quartile, while whiskers represent the 1st and 99th percentile. (B) Representative images taken for vehicle and ETS2 treated cells.

unexpected effect given the CMV promoter driving its overexpression. The significant effects of **AR1** on *PLAT* and *SLC45A3* expression (Figure 4.9) as well as the reduction in DNA damage levels in PC3-ERG cells suggest a general rather than ERG-specific mechanism for this molecule.

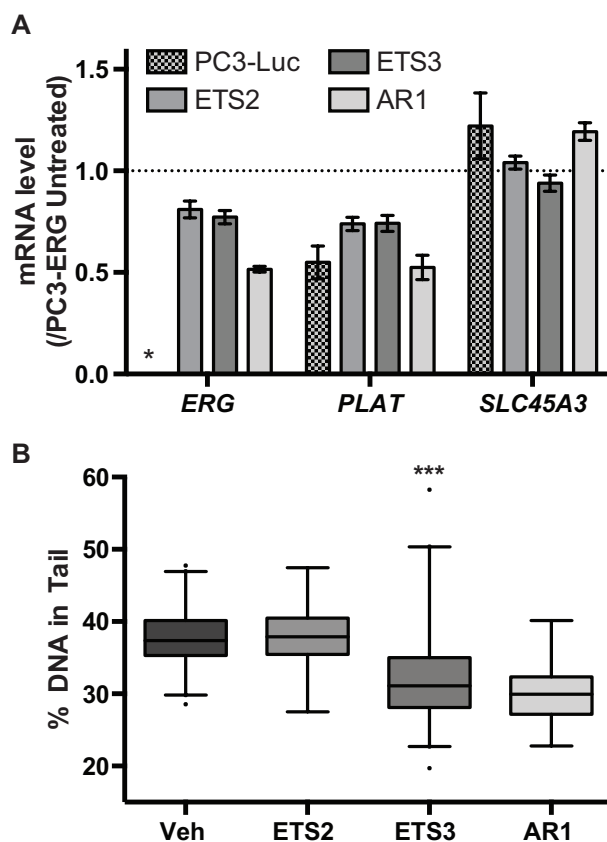


Figure 4.8 Py-Im polyamides mediate ERG-driven expression in PC3-ERG cells and reduce extant DNA damage. **(A)** PC3-ERG cells were treated with 0.1% DMSO (with or without 10 μ M polyamide) for 72 h. mRNA levels were measured by qPCR and referenced to GUSB. *ERG mRNA levels were too low to be measured in PC3-Luc cells. **(B)** The extent of DNA damage in untreated and treated PC3-ERG cells was measured using the neutral COMET assay. Comets were analyzed using Comet Assay IV software (Perceptive). Statistical significance was determined using two-way ANOVA analysis (Prism) where *** = $p < 0.001$ relative to vehicle. Boxes are bounded by the upper and lower quartile, while whiskers represent the 1st and 99th percentile, and outliers are indicated by single points.

Tube formation studies in a healthy cell line model.

Preliminary investigations of polyamide effects on ERG-activity in healthy cells involved the study of tube formation in human umbilical vein endothelial cells (HUVEC) as this process has been reported to be driven by ERG (28). After incubation with polyamide, **ETS2**, **ETS3**, and **AR1** demonstrated no significant effects on tube formation. Treatment with **AR3**, however, led to a nearly 2-fold reduction in observable branching points (Figure 4.10). The reduction observed upon treatment with **AR2** was unexpected and inhibition of angiogenesis will be investigated as a potential side effect of **AR2** treatment.

	PLAT	PLAU	SLC45A3	ERG	EZH2	MYC
PC3-Luc (control)	0.55 ± 0.05	1.24 ± 0.02	1.22 ± 0.09	0.00 ± 0.30	0.99 ± 0.04	1.32 ± 0.06
ETS2	0.74 ± 0.03	0.88 ± 0.03	1.04 ± 0.03	0.81 ± 0.04	1.01 ± 0.02	0.94 ± 0.04
ETS3	0.74 ± 0.04	0.79 ± 0.02	0.94 ± 0.04	0.77 ± 0.03	0.99 ± 0.02	0.96 ± 0.04
AR1	0.52 ± 0.06	0.53 ± 0.05	1.19 ± 0.04	0.52 ± 0.01	1.08 ± 0.04	1.32 ± 0.05

Figure 4.9 Gene expression data for PC3-ERG cells treated with ETS-targeting and AR-targeting polyamides for 72 h. Data shown are average of the fold changes (normalized to expression levels in PC3-ERG cells) for three or more biological replicates +/- standard error.

Diminished growth in VCaP xenografts upon polyamide treatment.

Initial xenograft experiments were conducted with **AR1** and **ETS3** in male SCID mice bearing subcutaneous VCaP cell xenografts. Treatments were started after tumor sizes in each group of mice reached $\sim 100 \text{ mm}^3$ and were administered three times per week for a total of 10 injections through subcutaneous injection in DMSO vehicle. Dose-dependent retardation of tumor growth was observed in mice treated with **AR1** (Figure 4.11). After 5 weeks, tumors treated with vehicle grew to approximately 6-fold the initial volume of that group while tumors treated with **AR1** at 5.0 mg/kg grew to approximately 1.6-fold the initial volume of that cohort. Equivalent treatment with **ETS3**, however, did not exhibit this effect.

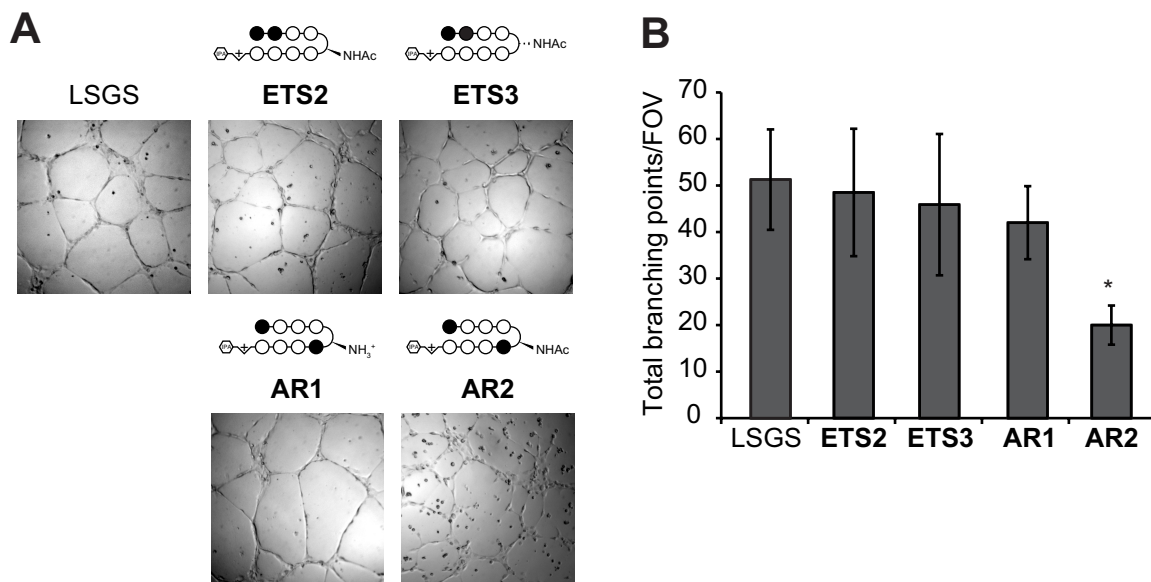


Figure 4.10 AR2 inhibits HUVEC tube formation *in vitro*. (A) Representative images showing effects of Py-Im polyamides (10 μ M) on the formation of tubes by HUVEC cells after 72 h incubation. Only AR2 demonstrated perturbed tube formation resulting in a fragmented network. (B) Quantitative analysis of branching points show that AR2 significantly inhibited tube formation in this assay * = $p < 5e-4$. A total of 8 fields of view, split between 4 different wells were been used in this data. Error bars represent 95% CI.

4.3 Discussion

This study evaluated the ability of Py-Im polyamides to target oncogenic pathways in advanced prostate cancer, specifically the AR-ERG signaling axis. Effects on gene expression, DNA damage levels, and *in vivo* tumor growth were observed VCaP cells, which express high levels of AR and the *TMPRSS2-ERG* gene fusion, as well as PC3-ERG cells, which is derived from PC3 prostate cancer cells that are natively AR- and ERG. The activity of Py-Im polyamides AR1 and AR2 targeting the ARE, had been previously studied in LNCaP cells, a model of castration-resistant prostate cancer that is AR-positive but ERG-negative (14,24). Polyamides were designed to target the ERG-DNA consensus sequence following the traditional Py-Im pairing rules (Figure 4.1). Substitution at the turn position was varied based on reports of its importance to cell

culture activity and *in vivo* toxicity (24). **ETS1** and **ETS3** have been previously studied in A549 cells for effects on the NF- κ B pathway (17,18) while **ETS2** is a novel molecule. The ability of these molecules to bind potential ERG-DNA binding sites was confirmed through thermal denaturation analysis prior to cell culture work (Table 4.1B).

Initial cell culture experiments determined that ARE-targeted polyamides **AR1** and **AR2** were able to disrupt DHT-induced signaling in VCaP cells, in line with previous studies in LNCaP cells (Figure 4.2, Table 4.2) (14,24). Decreased levels of the *TMPRSS2-ERG* fusion transcript were observed after polyamide treatment as well as reduced levels of ERG protein expression by Western blot (Figure 4.2). We also observed downregulation of other known AR targets, *PSA* and *FKBP5* (Table 4.2). Interestingly, **AR1** and **AR2** still had a small effect on *ERG* expression and the downstream targets *PLAT* and *c-Myc* under non-DHT-induced conditions (Table 4.3). Given the decrease in transcription by polyamides, as polyamide treatment has been shown to cause RNA pol II

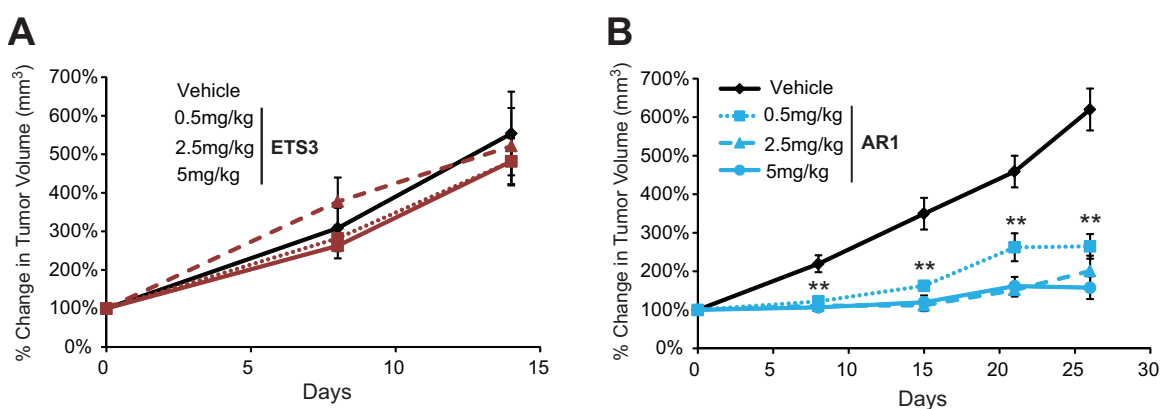


Figure 4.11 **AR1** but not **ETS3** reduces the growth of VCaP tumors in SCID mice. VCaP tumors were measured by caliper and treatment began when the tumor size reached 100 mm³. All mice were treated subcutaneously with vehicle (DMSO) or (A) **ETS3** or (B) **AR1** as reported (3 times per week, 10 total injections). Tumor growth was followed weekly by caliper measurements. All data points were measured in groups of 6-10 mice except for the week 4 data point of ETS3 treatment in which all but 2 mice had to be euthanized due to large tumor size.

ERG expression is fairly low, this result may reflect a non-specific or general effect on degradation previously (21). Furthermore, Py-Im polyamides targeted to the *ERG*-DNA binding site reversed the effects of *ERG* overexpression on select genes (Figure 4.3), despite the modest uptake in VCaP cells observed with the FITC-conjugates (Figure 4.5,4.6). These studies confirmed that Py-Im polyamides have the potential to affect the AR-*ERG* signaling axis in prostate cancers natively expressing the gene fusion.

Given the positive results observed on gene expression, we wanted to probe for polyamide effects on *ERG*-driven phenotypes. *ETS* gene fusions in prostate cancer are thought to be formed by double stranded DNA breaks at transcription factor-targeted loci (29) and overexpression of *ETS* proteins has been observed to increase the prevalence of double stranded DNA breaks (7,27). While these breaks ultimately result in cancer cell death, increases in the number of DNA breaks may also lead to higher mutational rates in prostate cancer (1). Consistent with the downregulation of *ERG* expression and downstream targets, treatment with **ETS2**, **ETS3**, and **AR1** caused a reduction in double stranded DNA breaks in VCaP cells (Figure 4.7). This result is in contrast to other DNA-binding therapeutics, such as the TOP2B inhibitors etoposide and doxorubicin, which lead to increased levels of DNA breaks. While these breaks ultimately result in cancer cell death, increases in the number DNA breaks may also lead to higher mutational rates in prostate cancer (1). Py-Im polyamides, which participate in non-covalent interactions with DNA, may thus present a unique route to therapeutically target DNA without increasing, and in some cases decreasing, levels of double stranded DNA breaks in cancer cells. Investigations are underway to determine the underlying cause of this

decreased DNA damage, specifically whether it is the result of disrupted ERG-DNA interactions or a combination with more general mechanisms of polyamide activity.

Genotypic and phenotypic effects were also observed in the PC3-ERG cell line, created as an isogenic cell line to PC3 cells, which do not express AR or ERG. Specifically, polyamides **ETS2**, **ETS3**, and **AR1** demonstrated significant decreases in ERG-driven gene expression, and a reduction in DNA damage was also observed with **ETS3** and **AR1** (Figure 4.8,4.9). Though formally targeted to the ARE, **AR1** was found to be the most effective at reversing ERG-related effects on mRNA levels. The strong decrease in DNA damage by **AR1** in PC3-ERG cells was also unexpected. In this system, **AR1** is as effective as **ETS3** in reduction of DNA damage, though **ETS3** was found to be more effective than all other polyamides in VCaP cells. These results are consistent with an overall decrease in ERG protein levels by **AR1**, a hypothesis supported by the strong downregulation of *ERG* mRNA levels after **AR1** treatment. This downregulation may indicate binding of **AR1** to the CMV promoter rather than native transcription factor binding sites or general inhibition of transcription.

We also investigated the effect of polyamides on another ERG-driven phenotype, tube formation in human umbilical vein endothelial cells (HUVECs). **ETS2**, **ETS3**, and **AR1** showed no effect on the ability of HUVECs, a model of healthy cells, to undergo tube formation (Figure 4.10). These results suggest that the ERG-targeting polyamides may not have significant effects in healthy cells, which would be an advantage as a potential therapeutic. Interestingly, treatment with **AR2** inhibited tube formation in

HUVECs, despite the ERG coding region not being fused to the AR-driven promoter of TMPRSS2 as in VCaP cells. Inhibition of tube formation only occurring in response to **AR2** is also consistent with the high potency observed in gene expression and cytotoxicity assays, and suggests that this compound might act non-specifically.

To further investigate the therapeutic potential of Py-Im polyamides against ERG-positive prostate cancer, **AR1** and **ETS3** were tested for efficacy against VCaP xenografts in SCID mice. Weekly treatment with **AR1** at 5.0 mg/kg resulted in a notable reduction in tumor growth relative to vehicle treated controls (Figure 4.11) with no observable signs of toxicity. A similar reduction in tumor growth was not observed in **ETS3** treated mice. This result is consistent with the cytotoxicity of **AR1** observed in cell culture and the downregulation of ERG and downstream targets given that ERG is a driver of cell proliferation in VCaP cells (30). It is possible, however, that general effects on transcription or replication by **AR1** may also contribute to the observed reduction in tumor growth (21,31). Reduced tumor growth and the observed reduction in expression of ERG targets in both the presence and absence of DHT-induction also suggest that **AR1** can be effective even when circulating levels of androgens are low. Why **ETS3** showed no effect is unclear, though this molecule also failed to reduce the growth of A549 xenografts in SCID mice despite showing toxicity in cell culture (32). Therefore, there is likely a confounding variable that contributes to the efficacy of polyamides against mouse xenografts, such as uptake into engrafted cells (33), that is not captured by cell culture studies. Subsequent studies will focus on higher doses of these molecules to

determine the therapeutic window as well as examination of the *in vivo* activity of second-generation compounds **AR2** and **ETS2**.

In conclusion, these studies indicate that select Py-Im polyamides can be used to reverse many of the negative effects of AR and ERG related signaling in prostate cancer, including oncogenic expression pathways and DNA damage, while also slowing tumor growth in an AR- and ERG-positive prostate cancer xenograft. Future work will focus on detailed mechanistic studies as well as non-rodent toxicity studies as we push to determine the utility of this class of molecules in human therapeutics.

4.4 Materials and Methods

Synthesis and quantitation of Py-Im polyamides.

All synthesis was performed using previously reported procedures as indicated (34,35). Chemicals were obtained from Sigma Aldrich or Fisher Scientific unless otherwise noted. Briefly, polyamides were synthesized by microwave-assisted solid phases synthesis on Kaiser oxime resin (Nova Biochem) (34) and then cleaved from the resin with neat 3,3'-diamino-*N*-methyldipropylamine. The triamine-conjugated polyamides were purified by reverse phase HPLC and subsequently modified at the C-terminus with isophthalic acid (IPA) or fluorescein-5-isothiocyanate (FITC isomer I, Invitrogen) (35). The α - or β -amine substituents of the γ -aminobutyric acid (GABA) turn units of the polyamides were deprotected using either trifluoroacetic acid (Boc) or 9:1 trifluoroacetic acid/triflic acid (CBz), respectively (36,37). For polyamides **AR2**, **ETS2**, and **ETS3**, the primary amine on the turn unit was acetylated using excess acetic

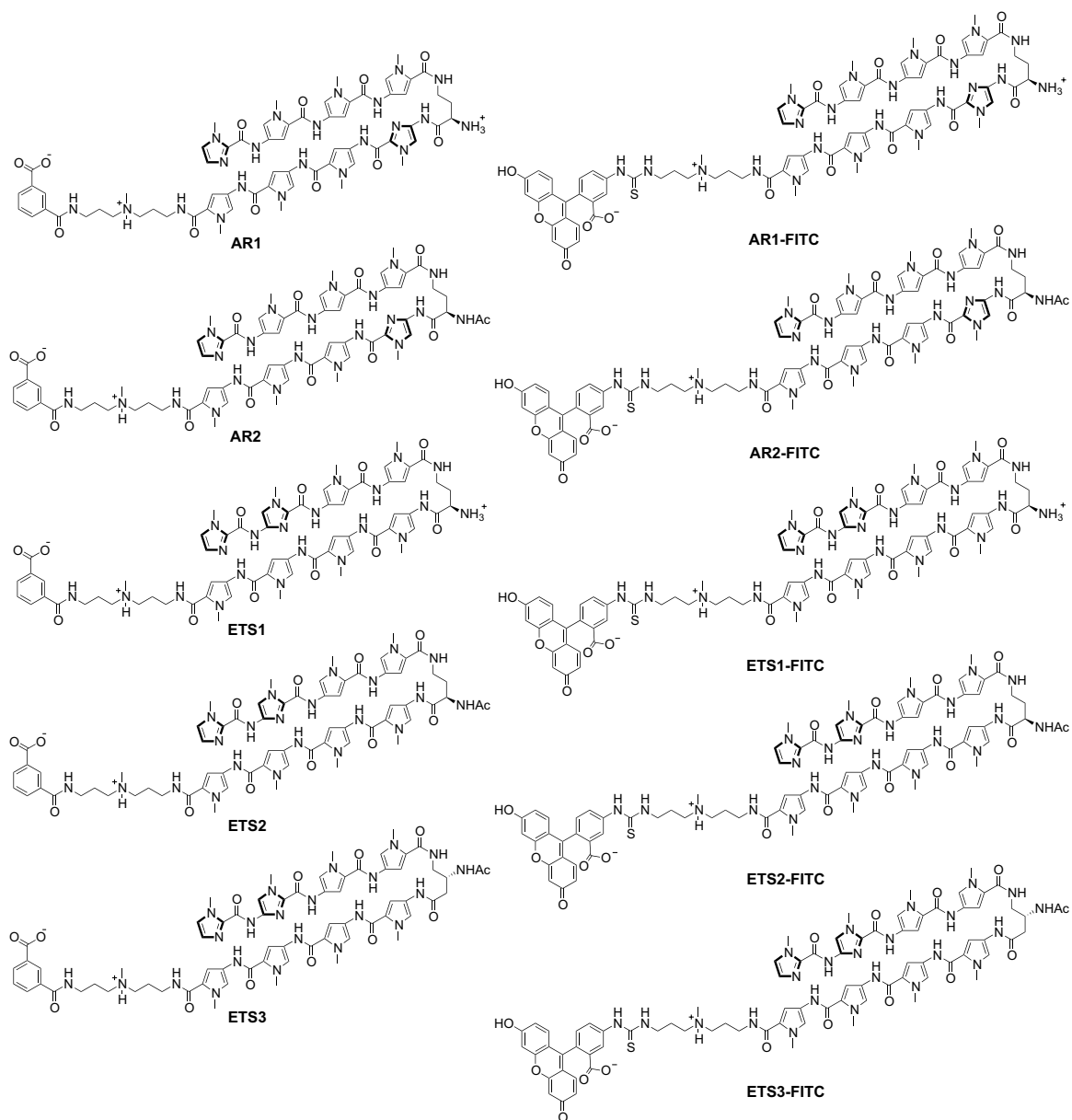


Figure 4.12 Chemical structures of Py-Im polyamides studied.

anhydride under basic conditions (38). The final polyamides were purified by reverse phase HPLC, lyophilized to dryness, and stored at -20°C . The identity and purity of the final compounds were confirmed by matrix-assisted, LASER desorption/ionization time-of-flight (MALDI-TOF) spectrometry and analytical HPLC. Chemical structures are represented in Figure 4.12.

Py-Im polyamides were dissolved in sterile DMSO (ATCC) and quantitated by UV spectroscopy in either 4:1 0.1% TFA (aqueous):acetonitrile ($\epsilon(310\text{nm}) = 69,500 \text{ M}^{-1}\text{cm}^{-1}$) or 9:1 water:DMSO ($\epsilon(310\text{nm}) = 107,100 \text{ M}^{-1}\text{cm}^{-1}$) as dictated by solubility. Polyamides were added to cell culture solutions at 10x concentration to give 0.1% DMSO solutions.

Thermal denaturation analysis.

Melting temperature analysis was carried out using a Varian Cary 100 spectrophotometer with a thermocontrolled cell holder and a cell path length of 1 cm. The analysis buffer used was a degassed aqueous solution of 10 mM sodium cacodylate, 10 mM KCl, 10 mM MgCl_2 , and 5 mM CaCl_2 at pH 7.0. Oligonucleotides were purchased from Integrated DNA technologies (HPLC purified) and were added as a 200 μM solution in Ultrapure Distilled Water (Gibco). DNA duplexes and polyamides were mixed to a final concentration of 2 μM and 3 μM , respectively, in 1 mL of analysis buffer just prior to each experiment. The samples were initially heated to 90°C and then cooled to 25°C. The denaturation profiles were recorded at $\lambda = 260 \text{ nm}$ from 25°C to 90°C with a heating rate of 0.5°C/min. The melting temperatures were defined as the maximum of the first derivative of the denaturation profile.

Cell culture.

All cell lines were obtained from the laboratories of Dr. Kenneth J. Pienta and Dr. Arul M. Chinnaiyan at the University of Michigan Department of Pathology. VCaP cells

were received at passage 19 and cultured in DMEM (Gibco 10313-039) with 4 mM glutamine (Invitrogen) and fetal bovine serum (Omega Scientific) on Corning CellBind flasks. All experiments were performed below passage 30. PC3 cells expressing luciferase (PC3-Luc) or expressing luciferase and the *TMPRSS2-ERG* gene fusion (PC3-ERG) have been previously described (7,27) and were cultured in RPMI medium (Gibco, 21870-092).

Gene expression analysis by quantitative RT-PCR (qPCR).

For dihydrotestosterone (DHT) induction experiments, VCaP cells were plated in 6-well plates coated with poly-L-lysine (BD BioCoat) in charcoal-treated FBS containing media at a density of 31k/cm² (3x10⁵ cells per well). The cells were allowed to adhere for 24 h and then dosed with 0.1% DMSO with or without polyamide for 72 h followed by the addition of 0.01% ethanol in PBS with or without dihydrotestosterone (1 nM final concentration). Cells were harvested after additional 24 h incubation. For native expression experiments, VCaP cells were plated as above but using standard FBS media and harvested after 72 h of treatment. PC3-Luc and PC3-ERG cells were plated in 6-well plates without poly-L-lysine at 2.5x10⁴ cells per well and allowed to adhere for 24 h before treatment with 0.1% DMSO, with or without polyamide, for 72 h. For all experiments, the mRNA was extracted using the QIAGEN® RNeasy mini kit following the standard purification protocol. Samples were submitted to DNase treatment using the TURBO DNA-free Kit (Ambion), and the mRNA was reverse-transcribed by using the Transcriptor First Strand cDNA Synthesis Kit (Roche). Quantitative PCR was performed by using the FastStart Universal SYBR Green Master (Rox) (Roche) on an ABI 7300

qPCR (mRNA)	Sequence	Reference
AR-f	CAGTGGATGGGCTGAAAAAT	Yu JD, et al. Cancer Cell. 2010;17:443-54.
AR-r	GGAGCTTGGTGAGCTGGTAG	
cMYC-f	AGCGGGCGGGCACTTTGC	*
cMYC-r	GCGGGAGGCTGCTGGTTTTTC	
ERG_ALL-f	CGCAGAGTTATCGTGCCAGCAGAT	Tomlins SA, et al. Science. 2005;310:644-8.
ERG_ALL-r	CCATATTCTTTACCGCCCACTCC	
EZH2-f	TGCAGTTGCTTCAGTACCCATAAT	Yu JD, et al. Cancer Cell. 2010;17:443-54.
EZH2-r	ATCCCCGTGTACTTTCCATCATAAT	
FKBP5-F	CGG AAA GGA GAG GGA TAT TCA	Meier JL, et al. Nucleic Acids Res. 2011;40:2345-56.
FKBP5-R	CCA CAT CTC TGC AGT CAA ACA	
GUSB-f	CTCATT TGGAATTTGCCGATT	Jacobs CS, et al. J Med Chem. 2009;52:7380-8.
GUSB-r	CCGAGTGAAGATCCCCCTTTTA	
KLK3-f	TCTGCGGCGGTGTTCTG	Jacobs CS, et al. J Med Chem. 2009;52:7380-8.
KLK3-r	GCCGACCCAGCAAGATCA	
PLAT-f	GCAGAGCCCTCTCTTCATTG	*
PLAT-r	CTGGAGAGAAAACCTCTGCG	
PLAU-f	CCAGCTCACAATTCCAGTCA	*
PLAU-r	TGACCCACAGTGGAAAACAG	
SLC45A3-f	TCGTGGGCGAGGGGCTGTA	Lin C, et al. Cell. 2009;139:1069-83.
SLC45A3-r	CATCCGAACGCCTTCATCATAGTGT	
TMPRSS2-ERG-f	TAGGCGCGAGCTAAGCAGGAG	Tomlins SA, et al. Science. 2005;310:644-8.
TMPRSS2-ERG-r	GTAGGCACACTCAAACAACGACTGG	

Figure 4.13 Primer sequences for qPCR analysis. Sequences for mRNA analysis without a listed reference (*) were designed using qPrimerDepot (primerdepot.nci.nih.gov), and the single amplification products verified by agarose gel electrophoresis against the 1.1 kB NEB ladder.

Real Time PCR System. Gene expression was normalized against GUSB. Primers used are referenced in Figure 4.13.

Immunoblot of ERG protein levels.

For assessment of ERG and beta-actin protein levels, 3×10^6 VCaP cells were plated in 10 cm diameter dishes with charcoal-treated FBS containing media for 24 h before treatment with 0.1% DMSO vehicle with or without **AR1** or **AR2** for an additional 72 h. Ethanol (0.01%) in PBS with or without dihydrotestosterone (1 nM final concentration) was then added. After 24 h incubation, cells were lysed in TBS-Tx buffer (50 mM Tris-HCl pH 7.4, 150 mM NaCl, 1 mM EDTA, 1% Triton X100) containing fresh 1 mM PMSF and protease inhibitors (Roche). The samples were quantified by Bradford assay, denatured by boiling in Laemmli buffer, and total protein was separated

by SDS-PAGE. After transfer to the PVDF membrane (Bio-Rad) and blocking with Odyssey Blocking Buffer (LI-COR), primary antibodies were incubated overnight at 4°C. Rabbit monoclonal anti-ERG antibody (Epitomics 2805-1) and rabbit polyclonal anti-actin antibody (Sigma A2066) were used. Goat anti-rabbit near-IR conjugated secondary antibody (LI-COR) was added and the bands were visualized on an Odyssey infrared imager (LI-COR). The experiment was conducted in duplicate and the data are representative of both trials.

Cellular uptake studies.

For visualization of uptake using FITC-analog polyamides, VCaP cells were plated in 35-mm optical dishes (MatTek) at 7.5×10^4 cells per dish and allowed to adhere for 48 h. Media was then changed and cells were treated with 0.1% DMSO with polyamide for 24 or 48 h. Cells were then imaged at the Caltech Beckman Imaging Center using a Zeiss LSM 5 Exciter inverted laser scanning microscope equipped with a 63x oil immersion lens as previously described (39).

WST-1 proliferation assay.

VCaP cells were plated at 1×10^3 per well in 96-well plates coated with poly-L-lysine (BD BioCoat). After 24 h, an additional volume of medium containing vehicle or polyamide was added to each well. All medium was removed following 72 h of polyamide incubation and replaced with one volume of WST-1 reagent (Roche) in medium according to manufacturer protocol. After 4 h of incubation at 37°C, the absorbance was measured on a FlexStation3 plate reader (Molecular Devices). The value

of $A(450\text{nm})-A(630\text{nm})$ of treated cells was referenced to vehicle treated cells. Non-linear regression analysis (Prism software, Graphpad) was performed to determine IC_{50} values.

HUVEC tube formation.

HUVEC cells were plated at a density of 2×10^5 cells per 75 cm flask in 200 PRF medium (Gibco) supplemented with Low Serum Growth Supplement (LSGS, Invitrogen). After 36 h, polyamides were added to a concentration of 10 μM , and the cells were incubated for 72 h. The cells were then trypsinized and 8×10^4 cells/well were plated in 12-well plates coated with 100 μL of solidified Geltrex reduced growth factor basement membrane (Invitrogen). After 6 h the wells were imaged on an inverted microscope equipped with a 5x objective by selecting four random fields of view between two wells per treatment condition. Data was analyzed by manually counting the number of sprouts in each field of view.

Single cell electrophoresis (COMET) assay.

VCaP cells (3×10^6 cells) were plated in 10 cm cell culture dishes and allowed to adhere for 24 h before addition of DMSO vehicle or polyamide stock in DMSO. After 72 h incubation, cells were washed with warm PBS (37°C), gently scraped, and counted. Samples were centrifuged, resuspended at 1×10^5 cells/mL, and treated according to manufacturer protocol (Trevigen) for neutral electrophoresis. Slides were stained with SybrGreen (Trevigen) and imaged at the Caltech Beckman Imaging Center using a Zeiss LSM 5 Pascal inverted laser scanning microscope equipped with a 5x air objective lens.

Overlaid fluorescence and bright field images were obtained using standard filter sets for fluorescein. Images were analyzed using COMET IV software (Perceptive Instruments Ltd) with 200-600 comets measured per sample. A random sampling of 200 comets per condition was used for two-way ANOVA analysis (Prism software, GraphPad) of three biological replicates.

Xenograft assays.

SCID mice (4-6 weeks old) were injected above the right flank with 1×10^6 VCaP cells (10 mice per dose group). Tumor was measured by caliper until the tumor size reached 100 mm^3 . All mice were treated subcutaneously with control (DMSO) or with doses of polyamides as reported (3 times per week, 10 total injections). Tumor growth was followed weekly by caliper measurements (40).

4.5 Acknowledgments

The authors would like to thank Prof. Arul M. Chinnaiyan (University of Michigan) for the VCaP cell line, and J. Chad Brenner (University of Michigan) for helpful discussions.

4.6 References

1. Rubin, M.A. (2012) ETS rearrangements in prostate cancer. *Asian J Androl*, 14, 393-399.
2. Perner, S., Demichelis, F., Beroukhim, R., Schmidt, F.H., Mosquera, J.M., Setlur, S., Tchinda, J., Tomlins, S.A., Hofer, M.D., Pienta, K.G. *et al.* (2006) TMPRSS2:ERG fusion-associated deletions provide insight into the heterogeneity of prostate cancer. *Cancer research*, 66, 8337-8341.
3. Demichelis, F., Fall, K., Perner, S., Andren, O., Schmidt, F., Setlur, S.R., Hoshida, Y., Mosquera, J.M., Pawitan, Y., Lee, C. *et al.* (2007) TMPRSS2:ERG gene fusion associated with lethal prostate cancer in a watchful waiting cohort. *Oncogene*, 26, 4596-4599.
4. Attard, G., Clark, J., Ambrosine, L., Fisher, G., Kovacs, G., Flohr, P., Berney, D., Foster, C.S., Fletcher, A., Gerald, W.L. *et al.* (2008) Duplication of the fusion of TMPRSS2 to ERG sequences identifies fatal human prostate cancer. *Oncogene*, 27, 253-263.
5. Tomlins, S.A., Rhodes, D.R., Perner, S., Dhanasekaran, S.M., Mehra, R., Sun, X.W., Varambally, S., Cao, X., Tchinda, J., Kuefer, R. *et al.* (2005) Recurrent fusion of TMPRSS2 and ETS transcription factor genes in prostate cancer. *Science (New York, N.Y.)*, 310, 644-648.
6. Perner, S., Mosquera, J.M., Demichelis, F., Hofer, M.D., Paris, P.L., Simko, J., Collins, C., Bismar, T.A., Chinnaiyan, A.M., De Marzo, A.M. *et al.* (2007) TMPRSS2-ERG fusion prostate cancer: an early molecular event associated with invasion. *The American journal of surgical pathology*, 31, 882-888.
7. Brenner, J.C., Ateeq, B., Li, Y., Yocum, A.K., Cao, Q., Asangani, I.A., Patel, S., Wang, X., Liang, H., Yu, J. *et al.* (2011) Mechanistic Rationale for Inhibition of Poly(ADP-Ribose) Polymerase in ETS Gene Fusion-Positive Prostate Cancer. *Cancer Cell*, 19, 664-678.
8. Carver, B.S., Tran, J., Gopalan, A., Chen, Z., Shaikh, S., Carracedo, A., Alimonti, A., Nardella, C., Varmeh, S., Scardino, P.T. *et al.* (2009) Aberrant ERG expression cooperates with loss of PTEN to promote cancer progression in the prostate. *Nature genetics*, 41, 619-624.
9. King, J.C., Xu, J., Wongvipat, J., Hieronymus, H., Carver, B.S., Leung, D.H., Taylor, B.S., Sander, C., Cardiff, R.D., Couto, S.S. *et al.* (2009) Cooperativity of TMPRSS2-ERG with PI3-kinase pathway activation in prostate oncogenesis. *Nature genetics*, 41, 524-526.
10. Dervan, P.B. (2001) Molecular recognition of DNA by small molecules. *Bioorgan Med Chem*, 9, 2215-2235.

11. Dervan, P.B. and Edelson, B.S. (2003) Recognition of the DNA minor groove by pyrrole-imidazole polyamides. *Current Opinion in Structural Biology*, 13, 284-299.
12. Chenoweth, D.M. and Dervan, P.B. (2010) Structural Basis for Cyclic Py-Im Polyamide Allosteric Inhibition of Nuclear Receptor Binding. *J Am Chem Soc*, 132, 14521-14529.
13. Olenyuk, B.Z., Zhang, G.-J., Klco, J.M., Nickols, N.G., Kaelin, W.G., Jr. and Dervan, P.B. (2004) Inhibition of vascular endothelial growth factor with a sequence-specific hypoxia response element antagonist. *Proceedings of the National Academy of Sciences of the United States of America*, 101, 16768-16773.
14. Nickols, N.G. and Dervan, P.B. (2007) Suppression of androgen receptor-mediated gene expression by a sequence-specific DNA-binding polyamide. *Proceedings of the National Academy of Sciences of the United States of America*, 104, 10418-10423.
15. Nickols, N.G., Jacobs, C.S., Farkas, M.E. and Dervan, P.B. (2007) Modulating hypoxia-inducible transcription by disrupting the HIF-1-DNA interface. *ACS Chemical Biology*, 2, 561-571.
16. Muzikar, K.A., Nickols, N.G. and Dervan, P.B. (2009) Repression of DNA-binding dependent glucocorticoid receptor-mediated gene expression. *Proceedings of the National Academy of Sciences of the United States of America*, 106, 16598-16603, S16598/16591-S16598/16596.
17. Raskatov, J.A., Meier, J.L., Puckett, J.W., Yang, F., Ramakrishnan, P. and Dervan, P.B. (2012) Modulation of NF-kappaB-dependent gene transcription using programmable DNA minor groove binders. *Proceedings of the National Academy of Sciences of the United States of America*, 109, 1023-1028.
18. Raskatov, J.A., Nickols, N.G., Hargrove, A.E., Marinov, G.K., Wold, B. and Dervan, P.B. (2012) Gene expression changes in a tumor xenograft by a pyrrole-imidazole polyamide. *Proceedings of the National Academy of Sciences of the United States of America*, 109, 16041-16045.
19. Nickols, N.G., Szablowski, J.O., Hargrove, A.E., Li, B.C., Raskatov, J.A. and Dervan, P.B. (2013) Activity of a py-im polyamide targeted to the estrogen response element. *Molecular cancer therapeutics*, 12, 675-684.
20. Wang, X., Nagase, H., Watanabe, T., Nobusue, H., Suzuki, T., Asami, Y., Shinojima, Y., Kawashima, H., Takagi, K., Mishra, R. *et al.* (2010) Inhibition of MMP-9 transcription and suppression of tumor metastasis by pyrrole-imidazole polyamide. *Cancer science*, 101, 759-766.

21. Yang, F., Nickols, N.G., Li, B.C., Marinov, G.K., Said, J.W. and Dervan, P.B. (2013) Antitumor activity of a pyrrole-imidazole polyamide. *Proc Natl Acad Sci U S A*, 110, 1863-1868.
22. Raskatov, J.A., Hargrove, A.E., So, A.Y. and Dervan, P.B. (2012) Pharmacokinetics of Py-Im Polyamides Depend on Architecture: Cyclic versus Linear. *J Am Chem Soc*, 134, 7995-7999.
23. Synold, T.W., Xi, B., Wu, J., Yen, Y., Li, B.C., Yang, F., Phillips, J.W., Nickols, N.G. and Dervan, P.B. (2012) Single-dose pharmacokinetic and toxicity analysis of pyrrole-imidazole polyamides in mice. *Cancer chemotherapy and pharmacology*, 70, 617-625.
24. Yang, F., Nickols, N.G., Li, B.C., Szablowski, J.O., Hamilton, S.R., Meier, J.L., Wang, C.M. and Dervan, P.B. (2013) Animal toxicity of hairpin pyrrole-imidazole polyamides varies with the turn unit. *J Med Chem*, 56, 7449-7457.
25. Tomlins, S.A., Laxman, B., Varambally, S., Cao, X., Yu, J., Helgeson, B.E., Cao, Q., Prensner, J.R., Rubin, M.A., Shah, R.B. *et al.* (2008) Role of the TMPRSS2-ERG gene fusion in prostate cancer. *Neoplasia*, 10, 177-188.
26. Yu, J.D., Yu, J.J., Mani, R.S., Cao, Q., Brenner, C.J., Cao, X.H., Wang, X.J., Wu, L.T., Li, J., Hu, M. *et al.* (2010) An Integrated Network of Androgen Receptor, Polycomb, and TMPRSS2-ERG Gene Fusions in Prostate Cancer Progression. *Cancer Cell*, 17, 443-454.
27. Brenner, J.C., Feng, F.Y., Han, S., Patel, S., Goyal, S.V., Bou-Maroun, L.M., Liu, M., Lonigro, R., Prensner, J.R., Tomlins, S.A. *et al.* (2012) PARP-1 inhibition as a targeted strategy to treat Ewing's sarcoma. *Cancer research*, 72, 1608-1613.
28. Birdsey, G.M., Dryden, N.H., Amsellem, V., Gebhardt, F., Sahnun, K., Haskard, D.O., Dejana, E., Mason, J.C. and Randi, A.M. (2008) Transcription factor Erg regulates angiogenesis and endothelial apoptosis through VE-cadherin. *Blood*, 111, 3498-3506.
29. Berger, M.F., Lawrence, M.S., Demichelis, F., Drier, Y., Cibulskis, K., Sivachenko, A.Y., Sboner, A., Esgueva, R., Pflueger, D., Sougnez, C. *et al.* (2011) The genomic complexity of primary human prostate cancer. *Nature*, 470, 214-220.
30. Mounir, Z., Lin, F., Lin, V.G., Korn, J.M., Yu, Y., Valdez, R., Aina, O.H., Buchwalter, G., Jaffe, A.B., Korpai, M. *et al.* (2014) TMPRSS2:ERG blocks neuroendocrine and luminal cell differentiation to maintain prostate cancer proliferation. *Oncogene*.
31. Martinez, T.F., Phillips, J.W., Karanja, K.K., Polaczek, P., Wang, C.M., Li, B.C., Campbell, J.L. and Dervan, P.B. (2014) Replication stress by Py-Im polyamides

- induces a non-canonical ATR-dependent checkpoint response. *Nucleic Acids Res*, 42, 11546-11559.
32. Raskatov, J.A., Nickols, N.G., Hargrove, A.E., Marinov, G.K., Wold, B. and Dervan, P.B. (2012) Gene expression changes in a tumor xenograft by a pyrrole-imidazole polyamide. *Proc Natl Acad Sci U S A*, 109, 16041-16045.
 33. Raskatov, J.A., Szablowski, J.O. and Dervan, P.B. (2014) Tumor xenograft uptake of a pyrrole-imidazole (Py-Im) polyamide varies as a function of cell line grafted. *J Med Chem*, 57, 8471-8476.
 34. Puckett, J.W., Green, J.T. and Dervan, P.B. (2012) Microwave Assisted Synthesis of Py-Im Polyamides. *Org. Lett.*, 14, 2774-2777.
 35. Nickols, N.G., Jacobs, C.S., Farkas, M.E. and Dervan, P.B. (2007) Improved nuclear localization of DNA-binding polyamides. *Nucleic Acids Research*, 35, 363-370.
 36. Dose, C., Farkas, M.E., Chenoweth, D.M. and Dervan, P.B. (2008) Next Generation Hairpin Polyamides with (R)-3,4-Diaminobutyric Acid Turn Unit. *J Am Chem Soc*, 130, 6859-6866.
 37. Li, B.C., Montgomery, D.C., Puckett, J.W. and Dervan, P.B. (2013) Synthesis of cyclic Py-Im polyamide libraries. *The Journal of organic chemistry*, 78, 124-133.
 38. Meier, J.L., Montgomery, D.C. and Dervan, P.B. (2011) Enhancing the cellular uptake of Py-Im polyamides through next-generation aryl turns. *Nucleic Acids Research*, 40, 2345-2356.
 39. Best, T.P., Edelson, B.S., Nickols, N.G. and Dervan, P.B. (2003) Nuclear localization of pyrrole-imidazole polyamide-fluorescein conjugates in cell culture. *Proceedings of the National Academy of Sciences of the United States of America*, 100, 12063-12068.
 40. McGregor, N., Patel, L., Craig, M., Weidner, S., Wang, S. and Pienta, K.J. (2010) AT-101 (R-(-)-gossypol acetic acid) enhances the effectiveness of androgen deprivation therapy in the VCaP prostate cancer model. *J. Cell. Biochem.*, 110, 1187-1194.

Appendix A

Investigations of anti-BrdU Antibody Staining of Py-Im Polyamide Treated Cells

This research was conducted in collaboration with Peter B. Dervan (California Institute of Technology).

A.1 Background

A long-standing problem in the field of DNA-binding Py-Im polyamides is to map the location of bound polyamides throughout the genome. Recently, attempts have been made to pull down biotin-conjugated polyamides that are crosslinked to chromatin via streptavidin beads. This strategy proved to be unsuccessful for mapping polyamide binding sites throughout the genome of cancer cells (1,2); however, it was successfully retooled for use with the Bind-N-Seq platform (3). While analogs of the standard 8-ring hairpin polyamides with chemical handles such as biotin substituted for the C-terminus isophthalic acid are effective, there is always the concern as to whether or not the analog behaves in exactly the same manner as the parent compound. This same problem arises when using FITC-substituted polyamides as a means of inferring whether or not the parent molecule is able to traffic to the nucleus in live cells. In animal studies, the issue of monitoring tissue distribution without the use of a dye-conjugated molecule was solved by using a ^{14}C -labeled analog of the parent molecule; the substitution of a single C atom with a radioactive isotope provided a means for sensitive detection of the polyamide with little chance of altering the behavior of the molecule (4,5). If there were a means of recognizing an 8-ring hairpin polyamide without the use of substituting the isophthalic acid for a chemical handle, it would provide a more accurate means of mapping polyamide binding and perhaps another method for staining polyamides in nuclei. One possible method would be through the use of an antibody that can recognize an 8-ring hairpin Py-Im polyamide.

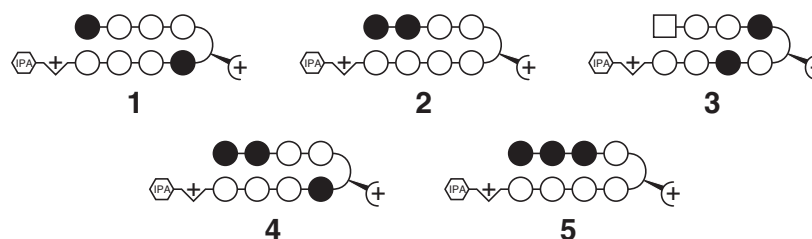


Figure A.1 Ball-and-stick representations of Py-Im polyamides used in this study. Polyamide **1** targets the sequence 5'-WGWWCW-3', polyamide **2** targets the sequence 5'-WGGWWW-3', polyamide **3** targets 5'-WTWCGW-3', polyamide **4** targets 5'-WGGWCW-3', and polyamide **5** targets 5'-WGGGWW-3'.

While attempting to stain for Py-Im polyamide-induced ssDNA foci by detection of incorporated 5-bromo-2'-deoxyuridine (BrdU) via immunocytochemistry (Chapter 2), it was observed that the mouse monoclonal anti-BrdU antibody MoBU-1 resulted in polyamide-dependent intranuclear punctate staining in the absence of BrdU. This result spurred the investigation as to what the antibody was recognizing in polyamide treated DU145 cells, and whether different polyamides cause the same effect (Figure A.1). In this chapter, we report the early studies into MoBU-1 staining and suggest future experiments for this study.

A.2 Results

Mouse monoclonal antibody MoBU-1 stains nuclear foci in Py-Im polyamide treated DU145 cells.

In order to stain BrdU in DU145 cells by immunocytochemistry for detection of ssDNA cells were treated with 50 μ M BrdU for 12 h followed by treatment with DMSO vehicle, 10 or 30 μ M Py-Im polyamide **1** for 36 h (Figure A.2), or 4 mM HU for 2 h. The cells were then washed three times with ice cold PBS (pH 7.4) and then fixed with fresh 3:1 methanol:acetic acid (MeOH:AcOH) for 20 min at -20°C . No denaturation step was

used afterward. Next, fixed cells were washed with a solution of .05% Tween 20 in PBS and then blocked using 2% normal goat serum for 30 min in a 37°C incubator. Immunostaining was carried out overnight at 4°C with MoBU-1 (Life Technologies) diluted 1:100 in blocking buffer. The next day, cells were washed three times with .05% Tween 20 in PBS before staining with the secondary antibody, Alexa Fluor® 488-conjugated donkey anti-mouse. Finally, cells were mounted using Prolong Gold Antifade

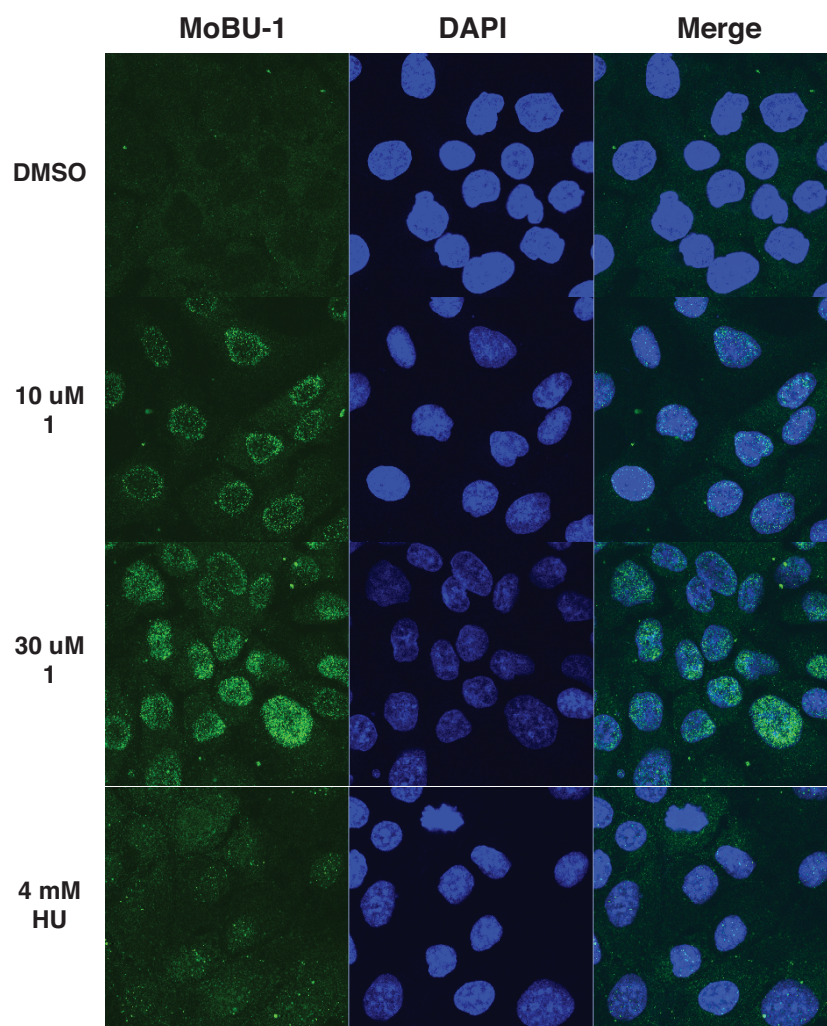


Figure A.2 MoBU-1 immunocytochemistry shows punctate staining in DU145 cells treated with BrdU followed by polyamide **1**. DU145 cells were pre-treated with 50 μ M BrdU for 12 h prior to incubation with 10 μ M or 30 mM **1** for 36 h. Cells were then fixed with MeOH:AcOH and incubated with MoBU-1 (1:100) and Alexa Fluor® 488 anti-mouse antibody (1:500). Significant punctate staining localized to the nucleus of polyamide treated cells. Only marginal staining was observed in cells treated with 4 mM hydroxyurea (HU) for 2 h.

with DAPI mounting solution for counterstaining of the nuclei. Imaging by confocal fluorescence microscopy (LSM 5 Exciter, 63x oil objective) showed significant nuclear staining in polyamide treated cells, but not in DMSO treated cells. However, cells treated with 4 mM hydroxyurea (HU) showed significantly less staining, which was unexpected given results from other experiments, such as the absence of Chk1 phosphorylation, which suggested that polyamide-induced replication stress was weaker than 4 mM HU-induced stress. Therefore, we tested whether the staining observed in response to polyamide treatment was a false positive.

In order to test whether MoBU-1 may be reacting to an antigen other than incorporated BrdU, the experiment was re-run in the absence of BrdU. Compared to DU145 cells treated with BrdU prior to incubation with **1**, polyamide **1** treated cells lacking BrdU showed equivalent nuclear punctate staining (Figure A.3). Next, we tested whether the fluorophore-conjugated secondary antibody might be reacting non-specifically and thus resulting in punctate staining. To test this possibility, polyamide **1** treated cells were stained using only the Alexa Fluor® 488 anti-mouse antibody. Under these conditions, no foci were observed. These results demonstrated that the nuclear staining observed in cells treated with **1** is dependent upon MoBU-1 but not BrdU.

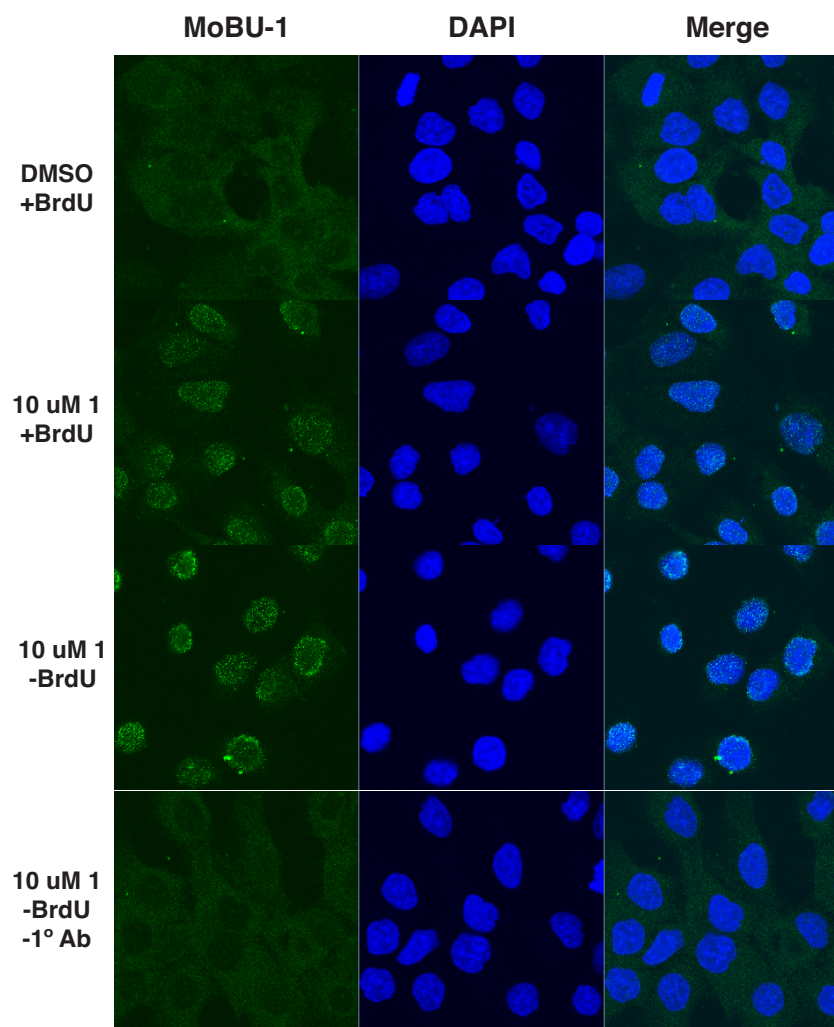


Figure A.3 MoBU-1 stains polyamide **1** treated DU145 cells in the absence of BrdU. DU145 cells were pre-treated with 50 μ M BrdU or PBS for 12 h prior to incubation with 10 μ M **1** for 36 h. Cells were then fixed with MeOH:AcOH and incubated with MoBU-1 (1:100) or blocking solution and Alexa Fluor® 488 anti-mouse antibody (1:500). Punctate staining is still observed in polyamide treated cells in the absence of **1**, but not when MoBU-1 is also removed.

*MoBU-1 staining of polyamide **1** treated cells is not dependent on MeOH:AcOH fixation.*

The previous results demonstrated that the anti-BrdU antibody MoBU-1 reacts with an unknown antigen in DU145 cells treated with **1** to form punctae. In order to determine whether the antibody is recognizing **1** directly, or whether it can at least be useful as a means of detecting polyamides in cells indirectly, we tested what other dependencies the MoBU-1 reaction might have. Different cell or tissue fixation methods

have been shown alter the structure of chromatin and shape of nuclei (6). Fixation by MeOH:AcOH works by dehydrating cells and does not preserve the 3D structure of chromatin, while fixation by formaldehyde results in protein crosslinking and does preserve the 3D structure of chromatin. Therefore, we next tested if the MoBU-1 staining observed in cells treated with **1** was dependent upon alterations to the chromatin induced by dehydration with MeOH:AcOH.

Polyamide treated cells fixed with MeOH:AcOH were compared to cells fixed with 2% formaldehyde (Figure A.4). For formaldehyde fixation, fresh 2% formaldehyde was prepared by dilution of 16% formaldehyde (10 mL ampule, Ted Pella, Inc.) into PBS. Cells were fixed in formaldehyde for 5 min at room temperature. Next, cells were washed three times with PBS at room temperature and then permeabilized with 0.2% Triton X-100 in PBS. Following permeabilization, cells were blocked with 3% normal goat serum with 0.1% Triton X-100 in PBS for 45 min at room temperature. Immunostaining by MoBU-1 and Alexa Fluor® 488-anti-mouse antibody was carried out as before. Despite the difference in fixation method, robust staining by MoBU-1 in cells treated with 10 μ M **1** but no BrdU. However, the staining in formaldehyde fixed cells was uniform throughout the nuclei and did not appear to be punctate as in MeOH:AcOH fixed cells. This difference was also observed in the DAPI stain, which suggests that the difference in staining appearance is likely due to the change in chromatin structure resulting from fixation.

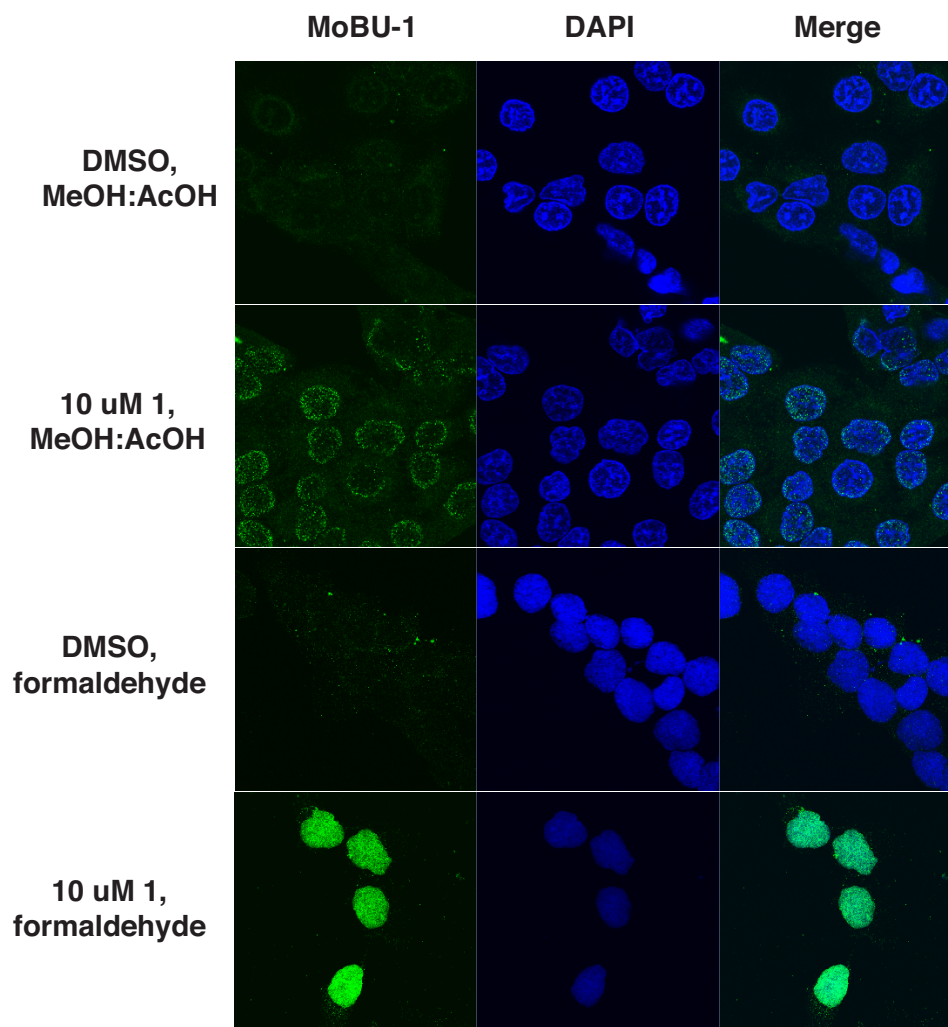


Figure A.4 MoBU-1 stains polyamide **1** treated DU145 cells when fixed with MeOH:AcOH or 2% formaldehyde. DU145 cells were treated with DMSO or 10 μ M **1** for 24 h. Cells were then fixed with MeOH:AcOH or 2% formaldehyde and incubated with MoBU-1 (1:100) and Alexa Fluor® 488 anti-mouse antibody (1:500). Significant nuclear staining was observed under both fixation conditions. Staining in formaldehyde fixed cells is more uniform throughout the nucleus.

These results clearly show that MoBU-1 staining is not dependent upon the fixation method. In addition, the appearance of the stain changing with the structure of the chromatin under different fixation conditions suggests that the MoBU-1 reaction occurs at the DNA level. Formaldehyde also has benefits over methanol:acetic acid. If MoBU-1 is reacting directly with polyamide or polyamide:DNA, it is important that the

reaction is not inhibited by formaldehyde used in pulldown studies to crosslink the small molecule to DNA. Formaldehyde fixation is also compatible with immunocytochemistry of nuclear proteins, such as PCNA (Chapter 2) and γ -H2AX. Furthermore methanol fixation will also permeabilize cells (7) and has been shown to alter the subcellular localization of dye-conjugated polyamides (8).

MoBU-1 staining in DU145 cells occurs in response to multiple Py-Im polyamides.

Staining of DU145 cells treated with polyamide **1** by MoBU-1 appeared to be robust, so we next tested how general the phenomenon was among a small library of polyamides targeted to different DNA sequences (Figure A.1). The five polyamides chosen were all 8-ring hairpin motifs with the isophthalic acid conjugated C-terminus and alpha amine substituted turn. These polyamides were chosen because they have been shown to be effective in targeting a variety of gene regulation pathways in previous studies (9-13). All polyamides were dosed at 10 μ M for 24 h and fixed with formaldehyde prior to immunostaining. Strong staining by MoBU-1 was observed in response to treatment with **1**, **3**, and **5**, while only marginal staining was observed in response to **2** and **4** (Figure A.5). Interestingly, staining in cells treated with **1** and **3** was localized to the nucleus but staining in cells treated with **5** was exclusively outside the nucleus. A cytoplasmic or membrane counterstain was not used; therefore, specific localization cannot be determined. However, it is plausible the staining occurs only on the cell surface. This result is interesting, because it suggests that if MoBU-1 is reacting directly with polyamides, it is not necessary for the polyamide to be DNA-bound.

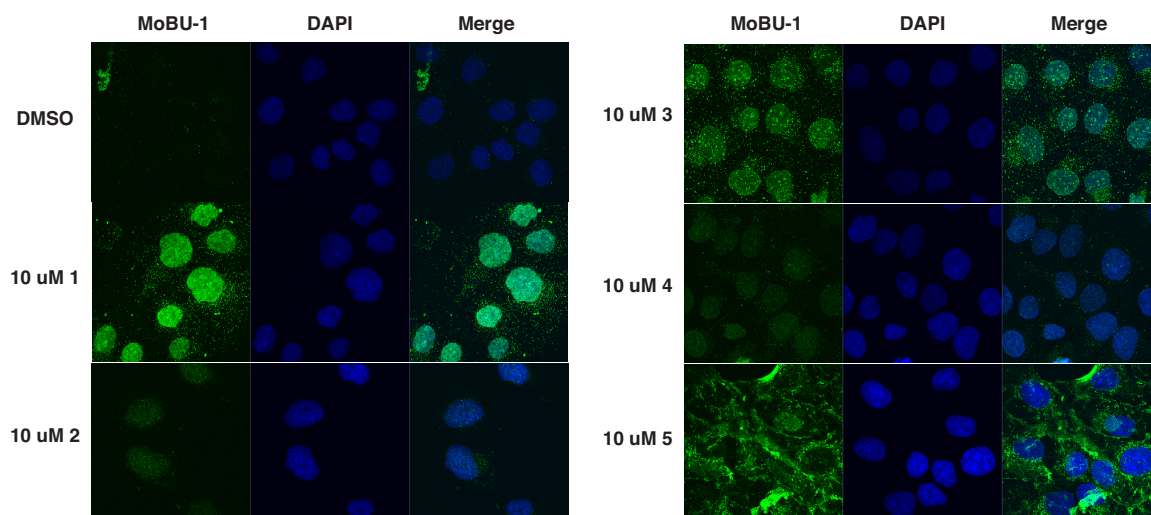


Figure A.5 MoBU-1 staining in response to a small library of polyamides. DU145 cells were treated with DMSO or 10 μ M **1-5** for 24 h. Cells were then fixed with 2% formaldehyde and incubated with MoBU-1 (1:100) and Alexa Fluor® 488 anti-mouse antibody (1:500). Significant nuclear staining was observed in response to **1**, **3**, and **5**. Staining in cells treated with **5** was observed outside the nucleus.

In order to get a more detailed look at the staining observed in response to **5**, several image slices were acquired by confocal microscopy through the Z-axis and combined to create a “3D” rendered Z-stack (Figure A.6). This Z-stack image clearly shows that MoBU-1 staining in response to **5** is almost exclusively outside the nucleus, while staining observed in response to **1** is predominantly localized to the nucleus.

Next, staining of polyamides **3** and **5** were also tested for dependence upon MoBU-1 and not non-specific binding of the secondary antibody. Just as with polyamide **1**, removal of MoBU-1 from the procedure did not result in immunostaining of cells treated with **3** or **5** (Figure A.7).

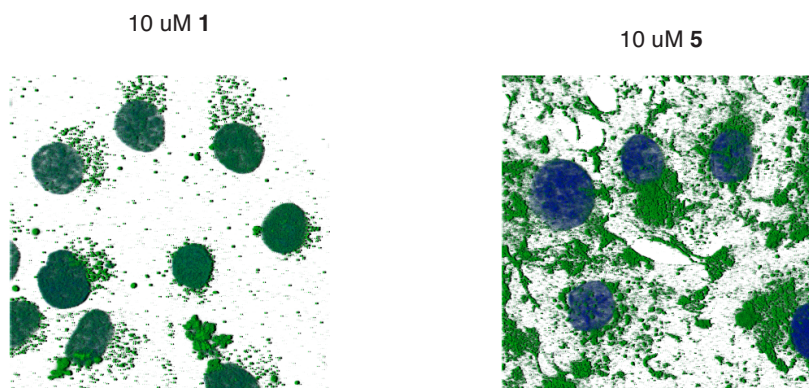


Figure A.6 Z-stack of MoBU-1 stained DU145 cells treated with polyamide **1** or **5**. The 3D rendered image of representative cells treated with **1** or **5** shows differences in localization of the staining.

MoBU-1 staining did not improve when polyamide was dosed after fixation and permeabilization.

If MoBU-1 is reacting directly with polyamide or polyamide:DNA, then the differences in staining observed in response to MoBU-1 might be a result of differences in uptake of polyamides into live cells. Therefore, if polyamides are dosed after fixation and permeabilization of cells, then uptake potential should be roughly equal and all polyamides can be recognized by MoBU-1. It is also possible, however, that MoBU-1 is reacting with an endogenous factor/complex that forms in response to polyamide treatment. If this model is correct, then dosing cells after fixation and permeabilization should prevent this endogenous factor from forming to react with MoBU-1 and no staining would be observed. These hypotheses were tested by fixing untreated cells with formaldehyde and then permeabilizing as before. Next, cells were treated with DMSO or polyamide for 24 h diluted in PBS. Afterward, cells were washed three times with PBS, blocked with goat serum, and then incubated with antibodies. When dosed after fixation,

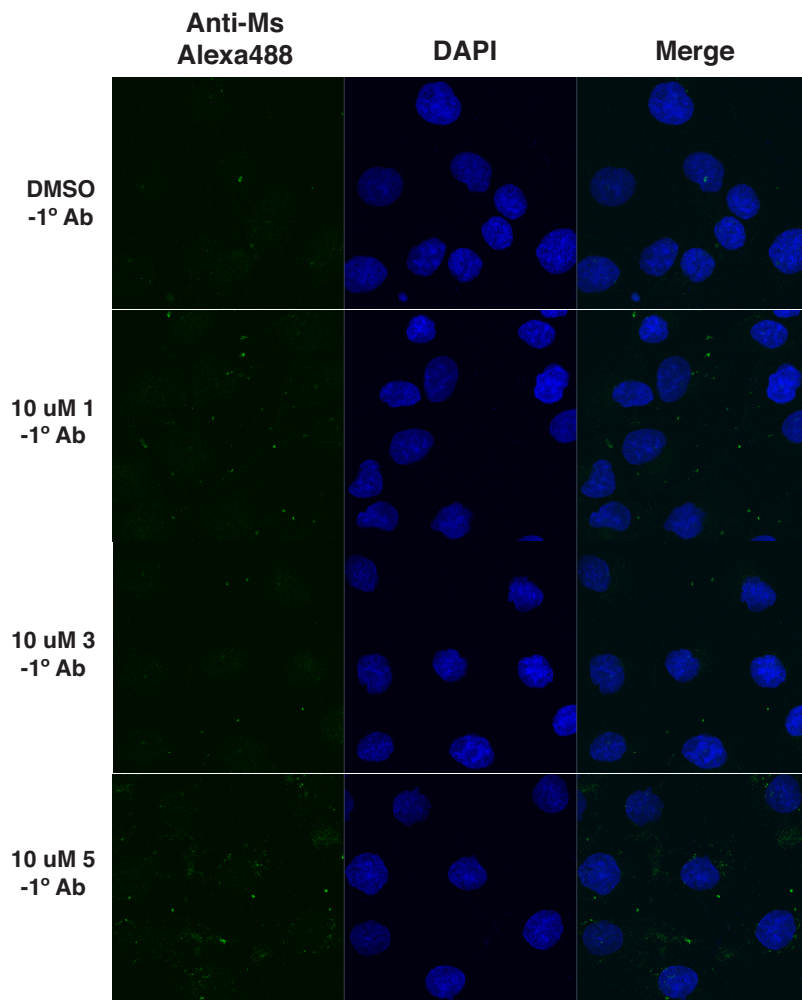


Figure A.7 Staining of polyamide treated cells is dependent upon MoBU-1. DU145 cells treated with 10 μ M polyamide followed by fixation and incubation with Alexa Fluor® 488 secondary antibodies showed no staining, proving the dependence on MoBU-1 across all polyamide tested.

cells treated with polyamides **1** and **3** still showed strong nuclear staining by MoBU-1 (Figure A.8). These results demonstrated that the MoBU-1 antigen is not an endogenous factor that forms in response to polyamide treatment. However, polyamide **2** treated cells showed increased staining, but significantly less than observed for **1** and **3**. This is puzzling given uptake should be the same for all polyamides, but may perhaps be due instead to unanticipated differences in binding affinity to chromatin. Interestingly, cells treated with polyamide **5** showed significantly less staining when dosed after fixation.

This result suggests that the MoBU-1 response to polyamide **5** treatment might actually be dependent on a cellular process or protein. One such possibility is if **5** normally interacts with a cell surface protein, which is significantly altered by formaldehyde fixation and Triton X-100 permeabilization, and that this complex is no longer able to form.

At least one other anti-BrdU antibody is capable of staining Py-Im polyamide treated DU145 cells.

The reaction of the mouse monoclonal anti-BrdU antibody MoBU-1 with an unknown antigen in polyamide treated cells showed some generality and potential utility as means of detecting which cells receive polyamides, and possibly even where the polyamide is localized. Before this antibody can be used for these purposes, however, it is critical to understand what the antibody is reacting with and how. One means of inferring what the antibody might react with, is to test whether there is a strong similarity between the intended antigen, BrdU-incorporated ssDNA, and the antigen in polyamide treated cells. If other anti-BrdU antibodies demonstrate this same effect, then the antigen in polyamide treated cells must be structurally and electronically similar to BrdU-incorporated ssDNA. If the phenomenon is truly unique to MoBU-1, then the effect might be understood by investigating the difference in the antigen binding site of MoBU-1 from other anti-BrdU antibodies. We know at least one other anti-BrdU antibody is not capable of this phenomenon, as we were able to use the rat monoclonal anti-BrdU antibody ICR1 (Santa Cruz Biotech) to recognize CldU incorporation without observing non-specific effects in polyamide-treated cells (Chapter 2). To test whether a third anti-

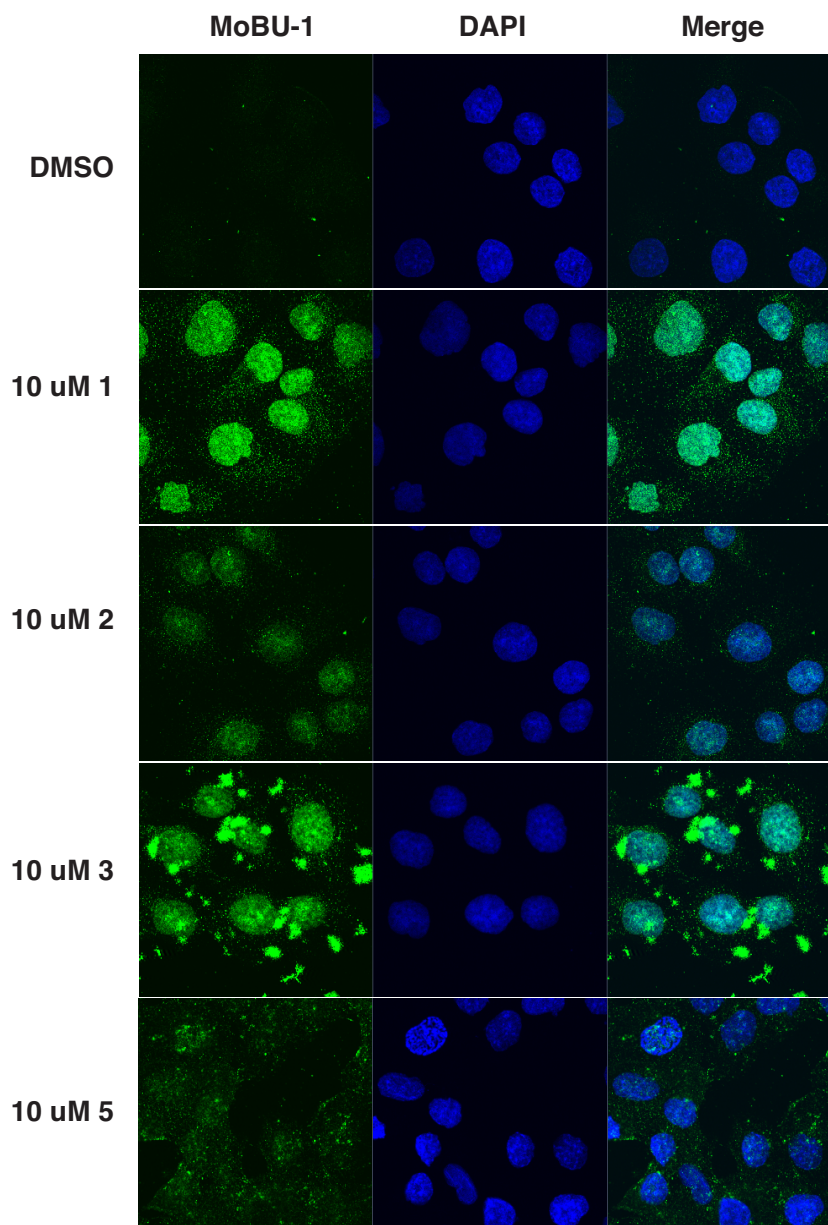


Figure A.8 MoBU-1 staining in DU145 cells treated with Py-Im polyamides after fixation with formaldehyde. Untreated DU145 cells were fixed and permeabilized prior to dosing with 10 μ M polyamide for 24 h. Then, cells were blocked with 3% goat serum and incubated with MoBU-1 and Alexa Fluor® 488 secondary antibody. Dosing cells after fixation did not affect staining of cells treated with 1-3. However, staining in response to 5 was significantly reduced.

BrdU antibody might also show the same phenomenon as MoBU-1, we repeated the staining experiment using ZBU30 (Life Technologies), which is also a mouse monoclonal antibody (Figure A.9). Live DU145 cells treated with 10 μ M 1 for 24 h and

then incubated with ZBU30 and Alexa Fluor® 488 anti-mouse secondary antibody showed significant staining of the nucleus, which was comparable to cells stained with MoBU-1 (Figure A.8). Cells treated with DMSO and incubated with ZBU30 showed weak non-specific staining but only outside of the nucleus. Cells treated with **1** and incubated with ICR1 and Alexa Fluor® anti-rat secondary antibody did not result in staining, as expected.

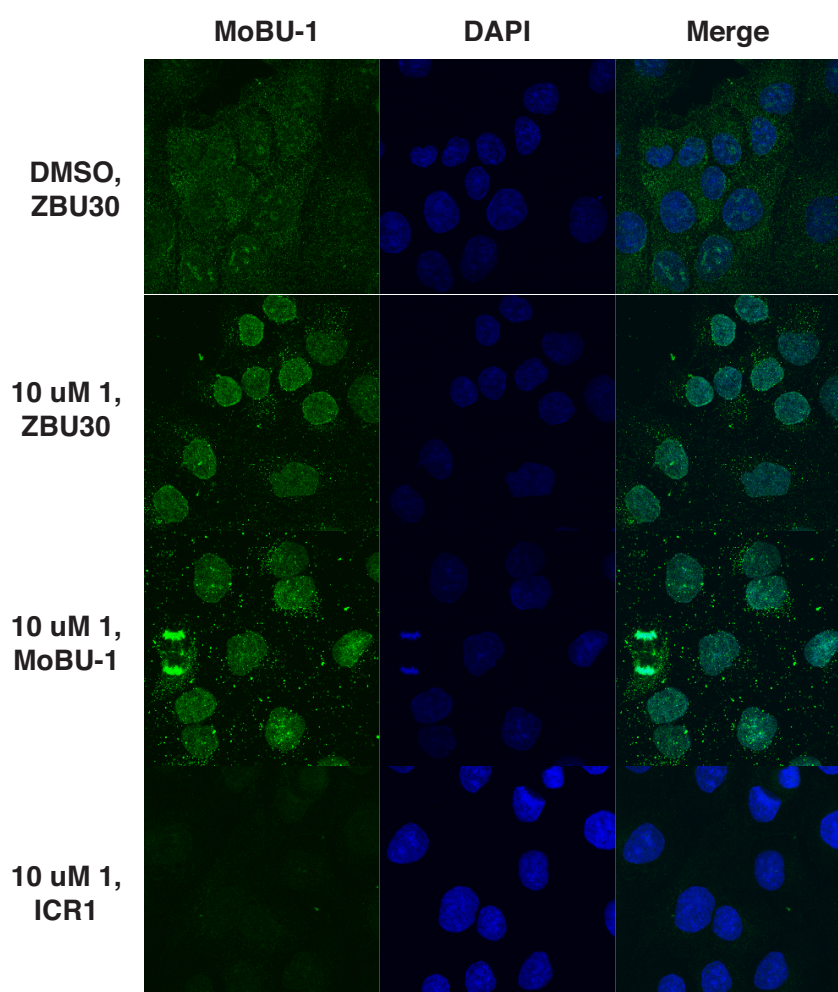


Figure A.9 Anti-BrdU antibody ZBU30 but not ICR1 stains polyamide treated DU145 cells. DU145 cells were treated with DMSO or 10 μ M **1** for 24 h. Cells were then fixed with 2% formaldehyde and incubated with either MoBU-1 (1:100), ZBU30 (1:100), or ICR1 (1:10) and Alexa Fluor® 488 anti-mouse antibody (1:500) or anti-rat antibody (1:500). Similar staining was observed using ZBU30 as MoBU-1. ICR1 did result in staining of the cells.

These results demonstrate that there may in fact be a common structural feature between BrdU-incorporated ssDNA and the antigen reacting with MoBU-1 in polyamide treated cells. However, that ICR1 does not show the same effect despite also being capable of recognizing BrdU suggests that it may not be a strong similarity. The cross-reactivities of the three antibodies tested may provide further insight into why this difference exists. MoBU-1 is known to have high specificity for BrdU and not have cross-reactivity with 5-ethynyl-2'-deoxyuridine (EdU) or thymidine. ZBU30 is known to cross-react with 5-iodo-2'-deoxyuridine (IdU) and not thymidine. ICR1, however, is known to cross-react with 5-chloro-2'-dexoyuridine (CIdU) and not thymidine. Iodine is a larger halide than bromine while chlorine is smaller. Perhaps the same feature of the antigen binding site that allows for reaction with larger 2' halides in ZBU30 allows it recognize the unknown antigen in polyamide treated cells, while the ability to recognize smaller halides by ICR1 prevents the reaction in polyamide treated cells. It is also interesting to note that the immunogen used to raise MoBU-1 is BrdU conjugated to hemocyanin, an extracellular oxygen carrier protein found in arthropods. The specific immunogens used to raise ZBU30 and ICR1 are unknown.

Attempts to characterize the putative MoBU-1:polyamide:DNA complex by biophysical methods.

Investigations of the MoBU-1 staining phenomenon provided clues into the generality of the effect, but little evidence about its ability to recognize polyamides directly. As a direct means of answering this question, we employed an *in vitro* electrophoretic mobility shift assay (EMSA) to test whether MoBU-1 is capable of

forming a ternary complex with polyamide:DNA (Figure A.10). Polyamide **1** was incubated with 600 fmol Cy5-labeled duplex DNA containing a single match site for 1.5 h at room temperature in 1x TAEMg buffer (40 mM Tris pH 7.5, 1 mM EDTA, 12.5 mM Mg(OAc)₂, 20 mM acetic acid). The total reaction volume was 20 μ L. The DNA duplex and binding conditions were also used previously to demonstrate ternary complex formation of biotin-analog of **1** (1). Reactions were run on native 6% polyacrylamide gels in 1x TBE at 175 V for 1.5 h. DNA duplex incubated with 300 nM or 1 μ M **1** ran higher on the gel than DNA incubated with DMSO, representing the

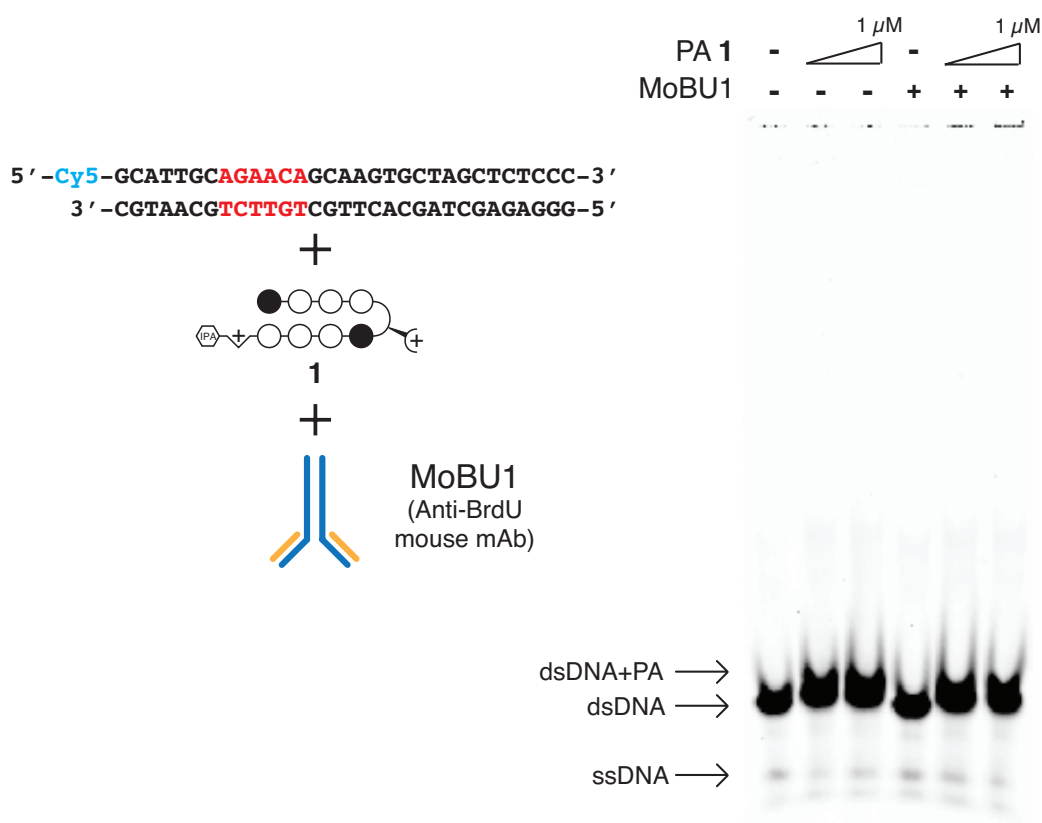


Figure A.10 Electrophoretic mobility shift assay (EMSA) of MoBU-1 and polyamide **1**:DNA. A shift of the Cy5-DNA duplex containing a match site for **1** was observed when incubated with 300 nM and 1 μ M **1** in 1x TAEMg. A further shift of this complex representing the ternary complex was not observed when the polyamide:DNA complex was incubated with 133 nM MoBU-1.

higher weight polyamide:DNA complex. When DNA and polyamide were also incubated with 133 nM MoBU-1, no higher shift was observed. These results show that MoBU-1 does not bind to polyamide:DNA directly under these conditions.

We also attempted to probe for MoBU-1 binding to polyamide **1** by surface plasmon resonance (SPR). SPR involves conjugating one of the molecules of interest, or ligand, to the surface of a gold-coated glass slide. The putative binding partner, or analyte, is flowed over the top of the surface-conjugated molecule, and if binding occurs the surface properties of the sensor chip are also altered. These alterations are detected as changes in the angle of incident light needed to induce SPR waves and are proportional to the amount of analyte bound. For this particular study we decided to use the antibody capture method to attach MoBU-1 to the surface of a CM5 Sensor Chip (14). The CM5 chip has an approximately 100 nm thick carboxymethylated dextran layer on top of the gold-coated glass slide, which provides a hydrophilic environment that is favorable to many biomolecular interactions. The negatively charged carboxyl groups also allows for covalent attachment of a variety of biomolecules, such as proteins by amine coupling (14). The antibody capturing method involves covalently coupling an anti-mouse IgG antibody to the surface of the chip by standard amine coupling conditions and then capturing the antibody of interest, MoBU-1, via its interaction with the anti-mouse antibody. For our experiment, we used AffiniPure Sheep anti-Ms IgG (Jackson ImmunoResearch) to conjugate to the surface of the CM5 chip. Conjugation was performed with 1 μ M antibody done in 10 mM acetate buffer, pH 5 at a flow rate of 1 μ L/min. Capture of MoBU-1 was performed using 100 nM MoBU-1 in 1x HBS-EP+ at

flow rate of 10 $\mu\text{L}/\text{min}$ for 120 s. Binding of polyamide **1** to MoBU-1 was investigated as a complex with DNA or alone. The same DNA duplex was used as in the EMSA experiment, except lacking the Cy5 dye. 1 μM polyamide **1**:DNA was used as the analyte and flowed over the chip at 10 $\mu\text{L}/\text{min}$ for 30 sec. No response was observed under these conditions relative to a flow cell conjugated with only the anti-mouse antibody. 10 μM **1** alone was also tested as the analyte and no response was observed relative to the control flow cell. ZBU30 was also captured to the chip and tested for binding to both polyamide:DNA and polyamide **1** alone, but no response was observed. Different binding conditions for SPR may be required to observe binding if possible. These results are consistent with the EMSA studies and suggest that the antigen recognized by MoBU-1 in cells might be more complex.

A.3 Conclusions

The mouse monoclonal anti-BrdU antibodies MoBU-1 and ZBU30 are robustly stain DU145 cells treated with multiple polyamides under both MeOH:AcOH and formaldehyde fixation conditions. Biophysical experiments did not show that MoBU-1 was capable of binding to polyamide **1** bound to DNA, but it is possible that these *in vitro* assays are not accurate models for polyamide bound chromatin in the nuclear environment or polyamide bound to other factors. Perhaps crystallography studies and molecular modeling can provide better insight into direct recognition of polyamides by MoBU-1.

If in the future it can be shown that MoBU-1 is reacting directly with polyamides, it would prove useful for genome-wide mapping studies. The ability of MoBU-1 to pull

down polyamide:DNA can be tested using the Bind-N-Seq methodology, though the *in vitro* studies suggest that this is unlikely to succeed (3). Another area where MoBU-1 can be tested for utility would be in the staining of tissue sections from treated animals. Currently, visualization of polyamides in tissue is done using FITC-analogs. If MoBU-1 is not sufficiently specific for these purposes, current results suggest that it might be possible to have an antibody specifically raised against Py-Im polyamides.

A.4 Acknowledgments

The authors would like to thank the Caltech Bioimaging Center for access to confocal fluorescent microscopes. We would also like to thank Dr. Jost Vielmetter at the Caltech Protein Expression Center for assistance with SPR experiments. Finally, we thank J.S. Kang, J.O. Szablowski, and A.A. Hare for contribution of polyamides used in this study.

A.5 References

1. Martinez, T.F. (2011), Candidacy Report, California Institute of Technology.
2. Meier, J.L. (2012), Postdoctoral Report, California Institute of Technology.
3. Meier, J.L., Yu, A.S., Korf, I., Segal, D.J. and Dervan, P.B. (2012) Guiding the design of synthetic DNA-binding molecules with massively parallel sequencing. *J Am Chem Soc*, 134, 17814-17822.
4. Raskatov, J.A., Puckett, J.W. and Dervan, P.B. (2014) A C-14 labeled Py-Im polyamide localizes to a subcutaneous prostate cancer tumor. *Bioorg Med Chem*, 22, 4371-4375.
5. Raskatov, J.A., Szablowski, J.O. and Dervan, P.B. (2014) Tumor xenograft uptake of a pyrrole-imidazole (Py-Im) polyamide varies as a function of cell line grafted. *J Med Chem*, 57, 8471-8476.
6. Kozubek, S., Lukasova, E., Amrichova, J., Kozubek, M., Liskova, A. and Slotova, J. (2000) Influence of cell fixation on chromatin topography. *Anal Biochem*, 282, 29-38.
7. Jamur, M.C. and Oliver, C. (2010) Permeabilization of cell membranes. *Methods Mol Biol*, 588, 63-66.
8. Belitsky, J.M., Leslie, S.J., Arora, P.S., Beerman, T.A. and Dervan, P.B. (2002) Cellular uptake of N-methylpyrrole/N-methylimidazole polyamide-dye conjugates. *Bioorg Med Chem*, 10, 3313-3318.
9. Yang, F., Nickols, N.G., Li, B.C., Marinov, G.K., Said, J.W. and Dervan, P.B. (2013) Antitumor activity of a pyrrole-imidazole polyamide. *Proc Natl Acad Sci U S A*, 110, 1863-1868.
10. Nickols, N.G., Szablowski, J.O., Hargrove, A.E., Li, B.C., Raskatov, J.A. and Dervan, P.B. (2013) Activity of a Py-Im polyamide targeted to the estrogen response element. *Mol Cancer Ther*, 12, 675-684.
11. Raskatov, J.A., Meier, J.L., Puckett, J.W., Yang, F., Ramakrishnan, P. and Dervan, P.B. (2012) Modulation of NF-kappaB-dependent gene transcription using programmable DNA minor groove binders. *Proc Natl Acad Sci U S A*, 109, 1023-1028.
12. Nickols, N.G., Jacobs, C.S., Farkas, M.E. and Dervan, P.B. (2007) Modulating hypoxia-inducible transcription by disrupting the HIF-1-DNA interface. *ACS Chem Biol*, 2, 561-571.
13. Kang, J.S. and Dervan, P.B. (2015), *Unpublished*.

14. (2008) Online Manual: Biacore Sensor Surface Handbook BR-1005-71 Edition
AB. *GE Lifesciences*.